NASA Contractor Report 3912

Advanced Integrated Power and Attitude Control System (IPACS) Study

Ronald E. Oglevie
and David B. Eisenhaure

CONTRACT NAS1-17633
NOVEMBER 1985

NASA

NASA Contractor Report 3912

Advanced Integrated Power and Attitude Control System (IPACS) Study

Ronald E. Oglevie
Rockwell International Corporation
Downey, California

David B. Eisenhaure
Charles Stark Draper Laboratory, Inc.
Cambridge, Massachusetts

Prepared for
Langley Research Center
under Contract NAS1-17633

National Aeronautics
and Space Administration

Scientific and Technical
Information Branch

1985

1. Report No.	2. Government Accession No.	3. Recipient's Catalog No.
NASA CR-3912		

4. Title and Subtitle	5. Report Date
Advanced Integrated Power and Attitude Control System (IPACS) Study	November 1985
	6. Performing Organization Code
7. Author(s)	8. Performing Organization Report No.
Ronald E. Oglevie*and David B. Eisenhaure**	SSS85-0025
	10. Work Unit No.
9. Performing Organization Name and Address	11. Contract or Grant No.
*Rockwell International 12214 Lakewood Blvd. Downey, CA 90241 **Charles Stark Draper Laboratory, Inc. 555 Technology Square Cambridge, MA 02139	NAS1-17633
	13. Type of Report and Period Covered
12. Sponsoring Agency Name and Address	Contractor Report
National Aeronautics and Space Administration Washington, DC 20546	14. Sponsoring Agency Code
	506-64-13-01

15. Supplementary Notes

Langley Technical Monitors: James L. Williams and Claude R. Keckler
Appendix A and B by Patricia A. Burdick; Appendix C by James R. Downer; Appendix D by Richard L. Hockney and Laura Larkin; Appendix E by Stephen R. O'Dea; Appendix F by Ronald E. Oglevie.

16. Abstract

Integrated Power and Attitude Control System (IPACS) studies performed over a decade ago established the feasibility of simultaneously satisfying the demands of energy storage and attitude control through the use of rotating flywheels. It was demonstrated that, for a wide spectrum of applications, such a system possessed many advantages over contemporary energy storage and attitude control approaches. More recent technology advances in composite material rotors, magnetic suspension systems, and power control electronics have triggered new optimism regarding the applicability and merits of this concept. This study was undertaken to define an advanced IPACS and to evaluate its merits for a Space Station application. System and component designs are developed to establish the performance of this concept and system trade studies conducted to examine the viability of this approach relative to conventional candidate systems. It is clearly demonstrated that an advanced IPACS concept is not only feasible, but also offers substantial savings in mass and life-cycle cost for the Space Station mission.

17. Key Words (Suggested by Author(s))	18. Distribution Statement
Flywheels, Energy storage, Attitude control, Mass and cost savings, Space Station	Unclassified-Unlimited Subject Category 20

19. Security Classif. (of this report)	20. Security Classif. (of this page)	21. No. of Pages	22. Price
Unclassified	Unclassified	174	A08

For sale by the National Technical Information Service, Springfield, Virginia 22161

FOREWORD

This report was prepared by the Space Station Systems Division of Rockwell International and the Charles Stark Draper Laboratory for the National Aeronautics and Space Administration's Langley Research Center in accordance with the requirements of Exhibit A of Contract NAS1-17633. The contract directed a 12-month study of an Integrated Power and Attitude Control System (IPACS) concept employing composite rotors and magnetic bearings as a potential solution to the shortcomings of systems employing isotropic rotor materials and ball bearings. The future Space Station was the specified application.

The IPACS system-level design analysis and trade studies were performed by the Rockwell International team under the direction of Mr. Ronald E. Oglevie. The IPACS component-level design analysis and trade studies were performed by the Charles Stark Draper Laboratory under the direction of Mr. David B. Eisenhaure, and under subcontract to Rockwell International. Acknowledgement is given to the following study team members as well as many others who offered valuable suggestions and comments:

Rockwell International

- IPACS configuration definition and system-level trade study—Ronald Oglevie
- Electrical power systems definition and sizing—Rex Moses
- Electrical power systems definition and sizing—John Q. Le
- Life-cycle cost analysis—Russell Morrissey
- Thermal control system—Fotis Georgatsos

Charles Stark Draper Laboratory

- Component system engineering and trades—David Eisenhaure
- System engineering and trades—Stephen O'Dea
- Composite rotor design analysis and trades—Patricia Burdick
- Magnetic bearings—James Downer
- Motor/generator and power electronics—Richard Hockney
- Motor/generator and power electronics—Laura Larkin
- Coordination, arrangements, and financial—Rhonda Mariano

In addition, the valuable comments and suggestions received from Messrs. James L. Williams, Nelson Groom, and Claude Keckler of the NASA/Langley Research Center are gratefully acknowledged. Pertinent information related to control moment gyro technology has been provided by the Sperry Flight Systems Division, and by the Bendix Guidance Systems Division.

Use of trademarks or names of manufacturers in this report does not constitute an official endorsement of such products or manufacturers, either expressed or implied, by the National Aeronautics and Space Administration.

SUMMARY OF STUDY RESULTS

The most fundamental requirement for an IPACS wheel configuration is that it be capable of simultaneously satisfying independent demands for energy (power) and momentum transfer (torque), and do so with negligible interaction between the respective outputs. Detailed trade studies for the Space Station application resulted in the system illustrated below. The system features five gimbaled IPACS units for the initial Space Station configuration, and nine units for the growth configuration. The number of wheel units was determined by the "fail-operational/fail-safe" (FO/FS) redundancy requirement. The system is sized to provide rated energy storage and momentum transfer capacity after one failure, and degraded performance after two failures (initial configuration only). The power demands are satisfied by increasing (or decreasing) the rotor speeds symmetrically. The attitude control torque demands are satisfied by gimbaling (precessing) the rotors. The "planar" array illustrated in the figure maximizes the momentum transfer perpendicular to the orbit plane, which is the axis with the largest momentum transfer requirement.

- FIVE GIMBALED WHEELS (IOC) IN PLANAR ARRAY (NINE WHEELS FOR GROWTH)
- RATED ENERGY STORAGE AND MOMENTUM CAPACITY WITH FOUR WHEELS, DEGRADED PERFORMANCE WITH THREE WHEELS

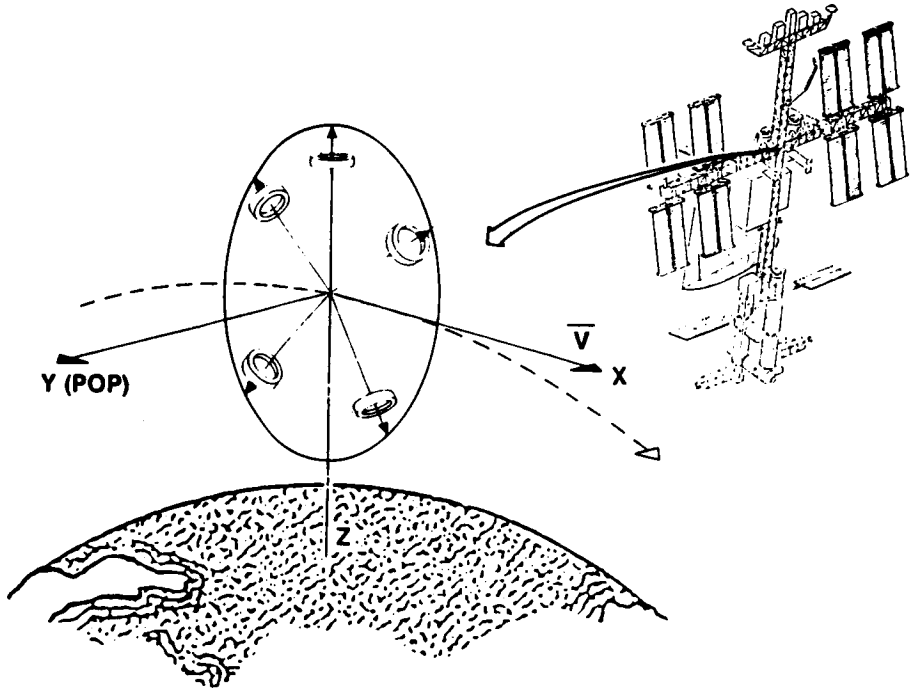

Summary of IPACS design features

The advanced IPACS component design concept that resulted from the study is shown below. This concept employs a composite rotor, very efficient motor/generator/electronics, and a new spherical large-angle magnetic bearing (LAMB). The rotor employs a filament-wound boron epoxy composite rotor with an annular shape and thin-wall design. This simple proven rotor design approach minimizes development risk and cost relative to more complex rotor shapes. A conservative fatigue life derating of one million cycles (200 years) and a safety factor of 1.56 have been employed in the rotor design to achieve hazard-free operation over the 20-year design lifetime. A system energy density (including all IPACS unique electronics) of 22 Wh/kg (10 Wh/lb) is achievable despite design conservatism. This energy density can potentially be doubled with the improvements in composite materials that are being tested today, and through less conservative stress derating that can be achieved through actual rotor design testing experience.

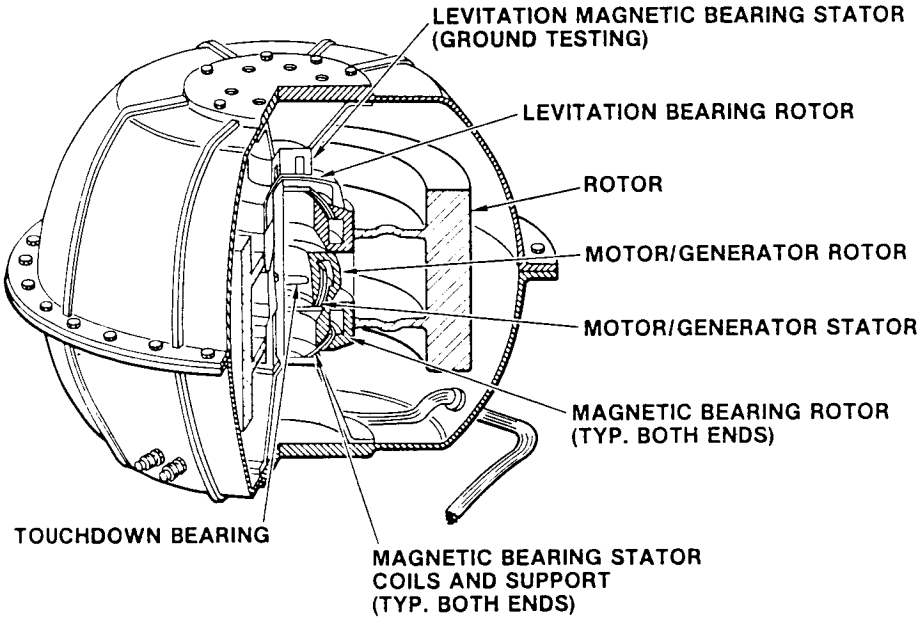

Advanced IPACS unit design concept

A roundtrip energy conversion efficiency of 85% has been validated with thorough analysis. This is achieved through the use of a permanent magnet rotating back-iron motor/generator and metal oxide semiconductor field effect transistor electronics.

The spherical LAMB is a new magnetic suspension approach that provides the dual functions of a magnetic bearing and rotor gimbal system. The additional bearing mass required to achieve the gimbaling function is quite small, particularly when compared to more conventional machine gimbal systems and single-axis torquers. The more conventional gimbals and torquers can produce a mass penalty that approaches the mass of the rotating element. The spherical LAMB can be gimbaled up to approximately 20 degrees with only a small mass penalty ($\approx$3% of rotating mass). This gimbal limitation constrains the momentum transfer capacity. However, the IPACS rotor has an abundance of momentum, and the

momentum transfer requirements in the Space Station application can be met with gimbal angles within this range. The spherical LAMB concept is quite attractive for other applications, such as an advanced momentum storage/transfer system for unmanned space platforms and other spacecraft. The LAMB technology development need not be tied to the IPACS technology development. However, the LAMB concept synergistically complements the thin-wall composite rotor technology in that it can be conveniently packaged within the rotor annulus, and permits appreciable mass and volume savings in this application.

A summary of the characteristics of a typical IPACS component for the five-wheel configuration is listed below. This particular design concept meets the rated momentum transfer requirement with only 9 degrees of gimbal travel, but requires that the IPACS components be physically realigned within the array to accommodate wheel failures.

SUMMARY OF ADVANCED IPACS UNIT CHARACTERISTICS

ROTOR

Annular ring material: boron/epoxy
Dimensions: O.D. = 1.148 m (3.77 ft); I.D. = 0.918 m (3.01 ft); height = 0.573 m (1.88 ft)
Spin axis inertia: 134 N-m-s^2 (98.8 ft-lb-s^2)
Operating speed: 5,000 to 10,000 rpm
Stress: maximum (yield) = 1,324 MPa; operational (10,000 rpm) = 410 MPa
(includes conservative deratings for fatigue life and safety factor = 1.56)
Cycle life: >10^5
Total energy capacity (75% DOD): 14.4 kWh
Momentum capacity (at half speed): 70K N-m-s (51.6K ft-lb-s)
Rotational element mass breakdown:
- Annular ring = 470 kg (1,036 lb)
- Rotor/suspension attachment structure = 45 kg (99.2 lb)
- Motor/generator rotor = 45 kg (99.2 lb)
- Magnetic bearing rotors = 60 kg (132 lb)
- Ground test bearing rotor = 12 kg (26.5 lb)

} These mass items are redundant to those given under "Motor/Generator," "Magnetic Spin Bearing," and "Ground Test Levitation Magnetic Bearing" below.

MOTOR/GENERATOR

Type: three-phase wye, permanent magnet synchronous, rotating back-iron
Materials:
- Magnet: samarium cobalt, 20 Mega-Oersted energy product
- Core: cold-rolled steel
- Stator: Litz wire and epoxy
Torque: 23.9 N-m (17.6 ft-lb)
Unit power rating: 11.5 kW (motoring); 15 kW (generating)
Size: spherical radius = 16.1 cm (6.34 in.); magnetic path gap = 0.500 cm (0.197 in.)
Mass: stator = 5.0 kg (11.0 lb); motor/generator rotor and support = 45 kg (99.2 lb)

MAGNETIC SPIN BEARING

Type: Lorentz force
Materials:
- Core: vanadium permendur
- Magnet: neodymium-iron-boron
Dimensions: spherical radius = 26.2 cm (10.3 in.); magnetic path gap = 1.3 cm (0.512 in.)
Maximum torque capacity: 300 N-m (221 ft-lb)
Operating angular range: ±9 degrees
Mass: stator = 13 kg (28.7 lb); rotor = 60 kg (132 lb)
Power consumption/unit: 83 W @ nominal precession torque; 402 W, maximum control torque

GROUND TEST LEVITATION MAGNETIC BEARING

Type: spherical-faced armature lifting electromagnet
Materials: cold-rolled carbon steel
Force capacity: rotating weight + 10%
Operating angular range: ±9 degrees
Mass: stator = 8 kg (17.6 lb); rotor = 12 kg (26.5 lb)

ELECTRONICS

Mass: 35 kg (77.2 lb)
Power consumption: 30 W, standby; 60 W, maximum motoring; 100 W, maximum generating
Circuit configuration:
- Motor/generator: three-phase, six-switch inverter/rectifier
- Spin bearings: 5-degree-of-freedom, servo-position control
- Ground test bearing: single-degree-of-freedom force control

IPACS COMPONENT PARAMETERS

Deliverable attitude control torque: 300 N-m (221 ft-lb)
Usable energy density (usable energy storage/total component mass):
- Study design concept (conservative design): 18.3 Wh/kg (8.3 Wh/lb)
- More optimal conservative design (extrapolation from study results): 22.0 Wh/kg (10 Wh/lb)
- Extrapolated results using new graphite-epoxy rotor material that became available late in study: 33 to 50 Wh/kg (15 to 23 Wh/lb)

Power losses: motor/generator = 39 W, motoring; 57 W, generating; spin bearing = 83 W (nominal precession); electronics = 30 W
Energy conversion efficiency: charge cycle = 0.933, discharge cycle = 0.911, charge/discharge cycle = 0.850
IPACS component total mass (5-wheel system): 788 kg (1,737 lb)
Mass of rotor vacuum housing: 95 kg (209 lb)

The system-level trade studies show that the IPACS approach has numerous advantages compared to the more contemporary nickel-hydrogen battery (NHB) and regenerative fuel cell (RFC) systems. These advantages include lower mass, complexity, cost, solar array drag makeup, and maintenance requirements. The single factor that should dominate in design decision-making of this type is life-cycle cost. Life-cycle cost data for the three energy storage systems that were traded in this study are tabulated below. These normalized cost data include all the significant interacting cost items including electrical power, attitude control (control moment gyros), thermal control, drag makeup propellant, transportation, and system maintenance over the assumed 20-year life cycle. The IPACS approach is seen to offer appreciably lower cost, both for the initial configuration and over the life cycle.

NORMALIZED COST DATA

CANDIDATE SYSTEM	INITIAL SYSTEM COST (IOC)	TOTAL LIFE-CYCLE COST (LCC)	
REGENERATIVE FUEL CELL	1.70	8.51	2.34
NICKEL-HYDROGEN BATTERY	1.26	5.43	1.49
IPACS	1.00	3.64	1.00
		NORMALIZED TO IPACS COST AT IOC	NORMALIZED TO IPACS LCC

The advanced IPACS technology development risks may be categorized as technical and schedule risks. The technical risks are deemed to be moderate and approximately equal to the RFC. The technology employed in all elements of the advanced IPACS unit has been demonstrated. The schedule risk for a Space Station application is very high because a technology development program for this purpose does not yet exist. The primary study recommendation is to undertake an IPACS technology development program that will make it available for future spacecraft.

CONTENTS

ILLUSTRATIONS

TABLES

INTRODUCTION

Integrated Power and Attitude Control System (IPACS) studies performed over a decade ago established the feasibility of simultaneously storing electrical energy in wheels and utilizing the resulting momentum for spacecraft attitude control. It was shown that such a system possessed many advantages over other contemporary energy storage and attitude control systems in many applications. More recent technology advances in composite rotors, magnetic bearings, and power control electronics have triggered new optimism regarding the feasibility and merits of such a system. The focus of the current study was to define an advanced IPACS and to evaluate its merits for the Space Station application. A system and component design concept is developed to establish the system performance capability. A system-level trade study, including life-cycle costing, is performed to define the merits of the system relative to two other candidate systems. It is concluded that an advanced IPACS concept is not only feasible, but offers substantial savings in mass and life-cycle cost.

The technical risks in developing the advanced IPACS technology presented herein are found to be acceptable. An IPACS technology develoment program of sufficient magnitude to meet the current Space Station technology readiness need date (1987) does not currently exist. The major recommendation of this study is that an IPACS technology development program be established that can provide technology readiness for the next generation of spacecraft.

Basic IPACS Concept

Most long-duration spacecraft rely on solar power generation methods such as photovoltaic solar arrays. It is generally convenient to provide energy storage elements, such as batteries, to accommodate peak power transients and periods of solar occultation. The Space Station, in its lowest orbital altitude (476 km), can be in the Earth's shadow up to 39% of the time. The IPACS concept is illustrated in figure 1. It provides for the storage of electrical energy as kinetic energy in mechanical rotors. Energy storage wheels can generally be made to provide higher energy density than most other secondary energy storage devices. When significant amounts of energy are stored in this fashion, angular momentum is available. This momentum may be utilized for the attitude control of the spacecraft. In order to accomplish this, the IPACS wheels are configured to satisfy simultaneous energy (power) and momentum (control torque) demands with negligible interaction between the two functions. This is accomplished with wheel arrays that are similar in nature to momentum wheel or control moment gyro attitude control systems. In a spacecraft electrical power system, the IPACS units replace the function of batteries or regenerative fuel cell energy storage devices.

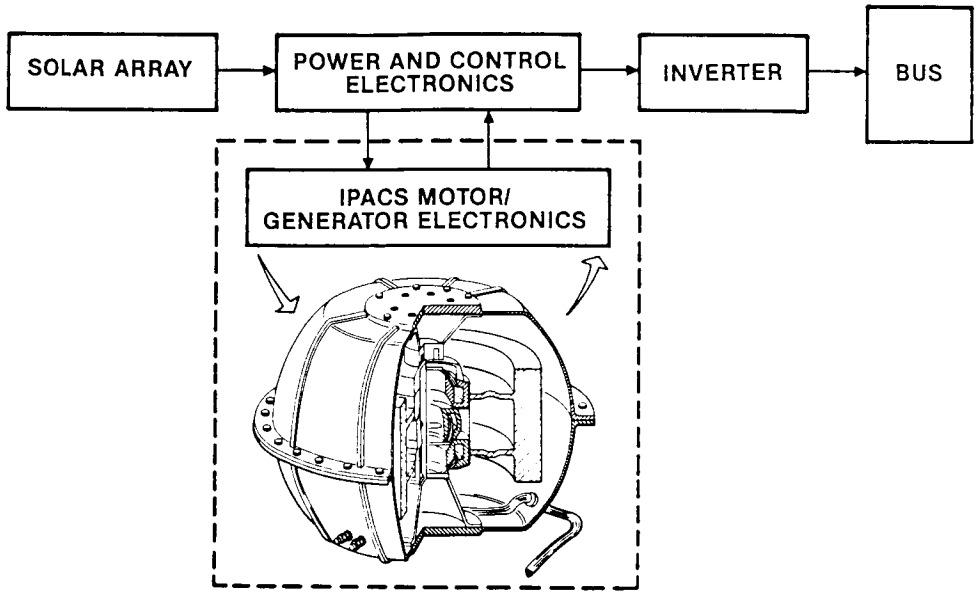

Figure 1.- Integrated power and attitude control system (IPACS) concept

Historical Background and Study Motivation

The energy storage wheel historical legacy is rich with focused and supporting technology developments that are applicable to the development of an advanced IPACS. This is particularly true for the advances in composite rotors, magnetic bearings, and motor/generator/circuitry technology that have occurred during the last 12 years. This section will review a small portion of that historical development, and why it results in improved expectations for the IPACS concept.

A number of pertinent IPACS historical developments is given in references 1 through 24. It is impossible to include all of the contributions made by many people, and apologies are offered for these omissions. The strongest body of spacecraft-oriented work was performed over a decade ago and is reflected in references 1 through 9. The most comprehensive spacecraft application study is given in references 4 and 5. A summary of the conclusions of this work is given in Table 1. The technical feasibility of the concept was established for a variety of spacecraft applications, as well as performance, weight, and cost advantages. The work led to the development of an engineering model of a ball bearing suspended titanium energy storage wheel for laboratory testing at the NASA Langley Research Center (ref. 7). The results of the subsequent laboratory testing are given in several of the references, including pages 5 through 21 of reference 15.

TABLE 1.-SUMMARY OF IPACS FEASIBILITY WORK (EARLY SEVENTIES)

- Design concepts developed for a variety of space applications: modular space station, TDRS, earth observation spacecraft, research and applications module, MJS planetary spacecraft, and extended-duration orbiter.
- Cost and weight advantages for most missions.
- Typical energy densities approximately twice that of NiCd batteries.
- Advantages increase with number of charge/discharge cycles.
- Readily adaptable to gimbaled and nongimbaled applications.
- Substantial performance improvement shown with conservative technology advances.
- Dynamic simulation of simultaneous energy management and attitude control; no significant performance or dynamic interaction problems.
- Detailed design approach established.
- Rotating assembly employing titanium rotor developed and successfully tested.
- Modified constant stress rotor shape utilized.
- Technical feasibility, performance and cost advantages established.
- Most applicable to spacecraft with larger energy and momentum storage requirements and long life.

Reference 10 presents a summary of an extensive amount of research oriented to the development of composite material energy storage wheel technology. This work was performed under the sponsorship of the Department of Energy (DOE) and focused on the achievement of high energy density for terrestrial applications. The research yielded a valuable legacy of composite rotor design techniques some of which are listed in the references of this document. The research included laboratory verification of many rotor designs.

The NASA Goddard Space Flight Center has also pursued the development of energy storage wheel technology for spacecraft as indicated in references 11, 12, and 14, and in the references of those documents.

Laboratory evidence of more recent advances in motor/generator/electronics efficiency is available in reference 13. Test results demonstrated that a round-trip charge/discharge cycle efficiency of 90% is feasible for a limited depth-of-discharge. This efficiency can be compared with the 60 to 65% that was achievable a decade ago, and is a major factor in reducing the size (and cost) of the overall spacecraft power system.

References 18 and 19 present descriptions of Combined Attitude, Reference, and Energy Storage Systems (CARES) employing magnetically suspended energy storage wheels that perform the attitude sensing function as well as energy storage and attitude control. Trade study results are presented that show

appreciable savings in overall system mass as well as complexity relative to other contemporary energy storage and attitude control systems concepts.

A recent study investigating the applicability of energy storage wheels in the Space Station application is given in reference 20. It presents a very knowledgeable and insightful treatment, particularly from an electrical power system point of view. It illustrates the appreciable effect of high charge/discharge cycle efficiency in reducing the overall electrical power system mass. The overall conclusion is drawn that flywheel energy storage has the potential to be superior to alkaline secondary batteries and regenerative fuel cells, and is in substantial agreement with the current study.

References 21 and 22 present a wealth of directly applicable IPAC technology. This NASA/OAST sponsored workshop (ref. 22) produced the focused concensus of 75 technologists regarding the current state of the energy storage wheel technology, the technology shortfalls, and a prioritization of the technology needs to rectify these shortfalls. This wealth of material and the strong support of the workshop by the various government agencies and industrial firms illustrate the strength of the IPACS technology base available in the United States today, and the conviction as to its applicability in the future. Reference 21 presents an abbreviated summary of this workshop.

Reference 23 is particularly pertinent to the current study, and presents trade study results of the IPACS application to the Space Station. The study concludes that the IPACS has weight and cost advantages relative to battery and regenerative fuel cell systems, both for the initial Space Station and its resupply. Reference 24 presents early results from the current study.

A summary of Annular Momentum Control Device (AMCD) references is presented in references 25 through 32. The AMCD is a momentum storage/transfer device, and consists of a magnetically suspended annular rotor of composite material. These references provide a valuable experience base, particularly in the area of magnetic bearing design and testing.

As discussed above, substantial technology advances have occurred during the last decade that have an appreciable impact on the IPACS performance and feasibility. The three basic technology areas that are the fundamental components of an advanced IPACS are listed on the left side of figure 2. Improvements in power processing circuitry, magnetic materials, and magnetic system design have increased the energy recovery efficiency (round-trip charge/discharge cycle efficiency) from approximately 60% to over 85%. In a spacecraft photovoltaic power system, this efficiency has a strong effect on the overall system sizing (including the solar array).

During the last decade, magnetic bearing technology has gone from an interesting laboratory curiosity to a proven technology with several flight applications having operated successfully in orbit, and many more applications proven in the laboratory. Notable among these are a Soviet flight experiment of a magnetically suspended reaction sphere, the flight of a rotating scanner with magnetic bearings by the Sperry Flight Systems Division, and the operational flight of European reaction wheels with magnetic bearings. Also, the

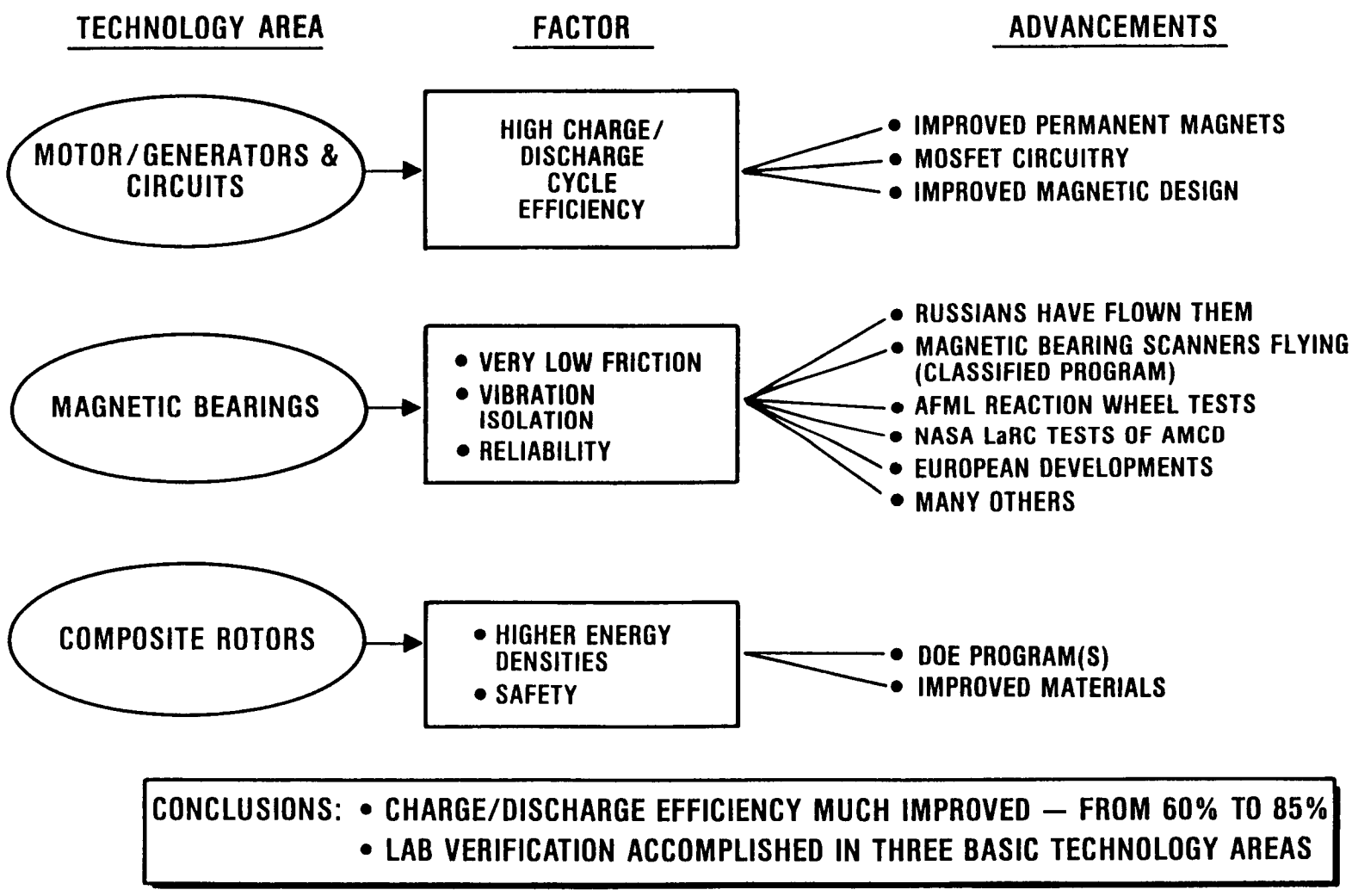

Figure 2.- Technology advances in the last decade

use of magnetic suspension for vibration isolation and high-accuracy pointing have been thoroughly studied and proven in the laboratory. The merits of very low friction losses, maintenance-free long life, and freedom from vibration disturbances, for example, are very attractive. These suggest "leap-frogging" past the use of ball bearings with the attendant problems of lifetime, vibration, maintenance, and the long-duration testing needed to validate bearing design.

The composite rotor technology is the key to achieving higher energy densities. The recent Department of Energy composite energy storage wheel development and testing programs have provided a valuable legacy that was not available a decade ago. Considerable data have been provided on various materials, rotor shapes, composite rotor fabrication, and testing techniques. In addition, advances in basic composite materials technology are continuing to be made at a high rate.

The advances in the three technology areas described above suggest that an advanced IPACS employing a composite structure rotor, magnetic bearings, and advanced motor/generator/electronics might be a feasible and cost-effective replacement for the systems used in the contemporary spacecraft of today.

Another factor was the emergence of the Space Station program. The Space Station was conceived to have power, energy storage, and momentum storage requirements that were approximately an order-of-magnitude greater than prior spacecraft. The NASA baseline "Power-Tower" Space Station configuration is illustrated in figure 3. During the Space Station Technology Workshop,

- ALTITUDE: 476 KM (257 NMI)
- INCLINATION: 28.5 DEGREES
- FLIGHT ORIENTATION:
  - TOWER AXIS LOCAL VERTICAL, SOLAR ARRAY BOOM AXIS PERPENDICULAR TO ORBIT PLANE
- POWER DELIVERED AT BUS (VALUES ASSUMED FOR STUDY)
  - INITIAL OPERATING CAPABILITY (IOC): 75 kW
  - GROWTH CAPABILITY: 150 kW

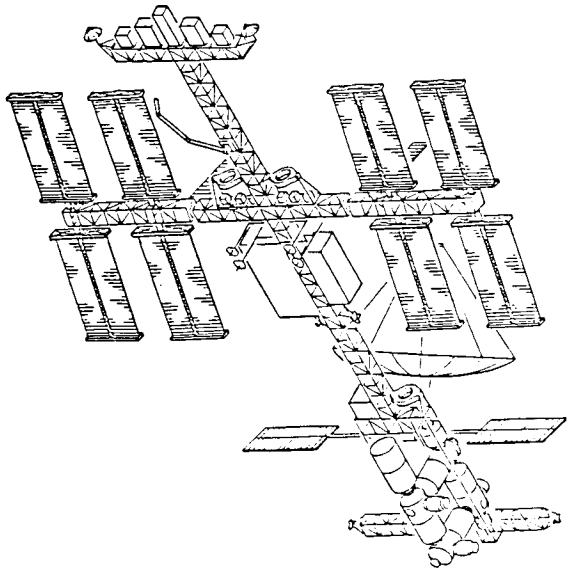

Figure 3.- Typical Space Station—
NASA "power tower" configuration

Williamsburg, Virginia, 28-31 March 1983, three different technology panels recommended energy storage wheel (or IPACS) technology development. These technology panels included: Systems Engineering, Guidance and Control, and Electrical Power Systems.

As a result of the motivational factors given above, the thrust of the current study was: the definition of an IPACS approach for Space Station, development of an advanced component design concept, and a definition of the merits of the resulting system relative to other competing energy storage and attitude control systems.

Study Objectives and Approach

The key factors that motivated the reconsideration of the IPACS concept were the strong advancements in the supporting technology and the emergence of the Space Station program which required an order-of-magnitude increase in electrical power and attitude control capacity relative to earlier spacecraft. Therefore, the major goal of the study was to investigate the incorporation of these technology advances into a system that would "leap-frog" across the limitations imposed by isotropic rotor materials, and ball-bearing technology through the use of composite materials and magnetic suspension. The major issues posed by this challenge were:

- What is the preferred rotor design? Would it be a hoop or a hub type design? What is the best approach for incorporating the magnetic suspension system?

- What is the preferred magnetic bearing approach?

- What are the preferred motor/generator/circuitry approaches to maximize charge/discharge cycle efficiency?

- What is the preferred design approach to provide acceptable safety?

- What is the preferred IPACS array to meet the requirements of Space Station?

- What are the preferred means of obtaining attitude control torques? Would it be an IPACS or would it separate the energy storage and attitude control functions? Should it employ gimbaled rotors or nongimbaled?, etc.

- What are the relative merits of an energy storage wheel approach relative to other contemporary energy systems, including nickel hydrogen battery and regenerative fuel cell systems?

The study approach that was selected to address these issues is presented in figure 4. The study inputs are given on the left side of the figure and the major study outputs are given on the right. The task titles correspond to those used in subsequent sections of this report.

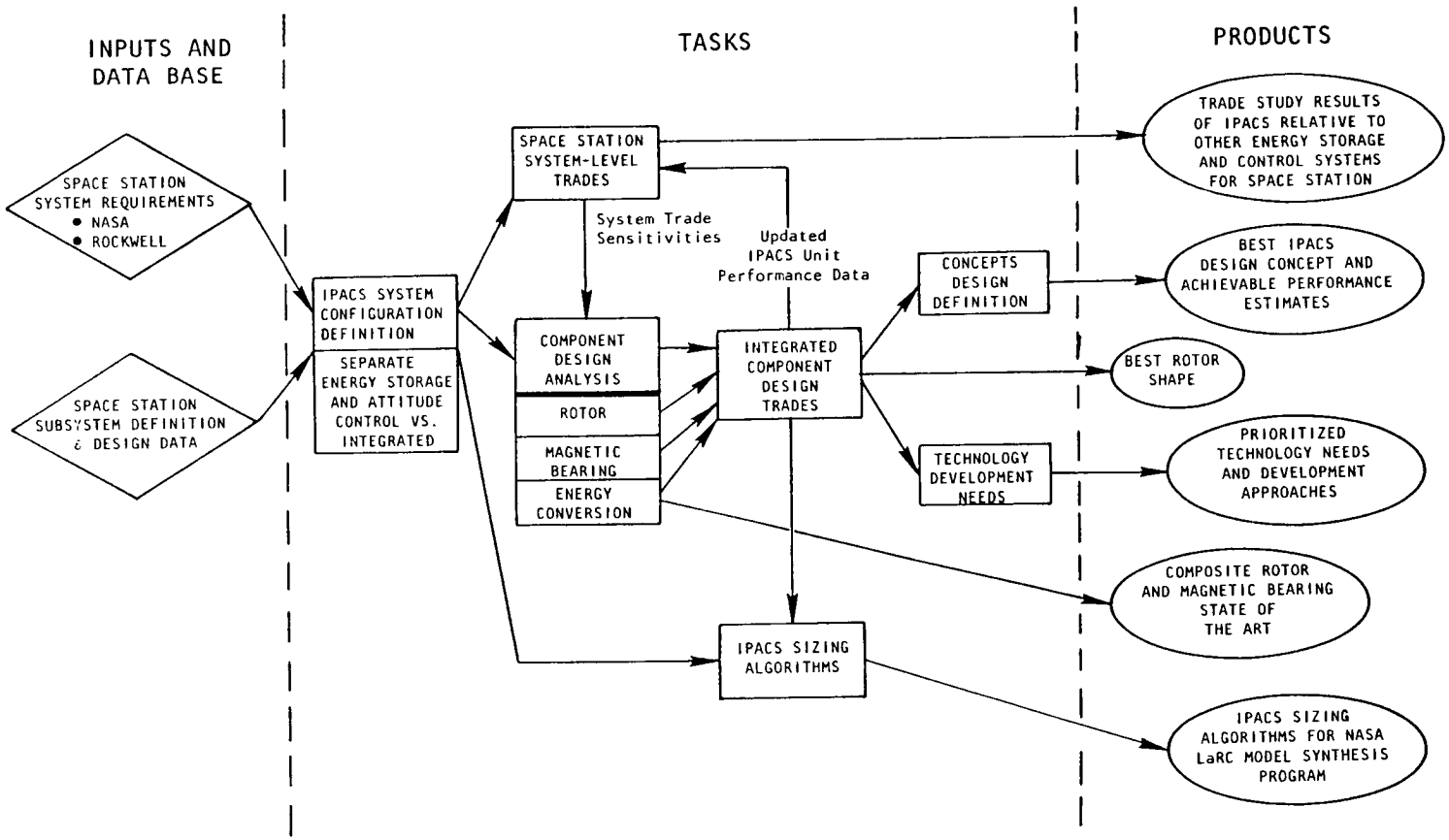

Figure 4.- Study logic, task interfaces, and study outputs

The IPACS Configuration Definition section develops the overall wheel array configuration for the Space Station application, and results in IPACS unit-level requirements. The Space Station System-Level Trades section develops and compares the IPACS approach with two other competing energy storage approaches (regenerative fuel cells and nickel-hydrogen batteries). System sizing and life-cycle cost data are developed for comparative analysis. Overall study results, conclusions and recommendations are summarized in the Conclusions and Recommendations section of this report.

The advanced IPACS component design concept is developed in the following manner. The Rotor (Appendices A and B by Patricia A. Burdick), Magnetic Bearing (Appendix C by James R. Downer), and Power Conversion (Appendix D by Richard L. Hockney and Laura Larkin) Design Analysis sections survey the current state of the art, perform trades, and develop parametric design data. The Integrated Component Design Trades section (Appendix E by Stephen R. O'Dea) examines the interactive trades between rotor, magnetic bearing, and power conversion elements to yield the proper design compromises and the IPACS design concept. Sizing algorithms, to aid the system designer in the development of spacecraft energy storage/attitude control systems, are presented in Appendix F by Ronald E. Oglevie.

IPACS CONFIGURATION DEFINITION

This section deals with the "system-level" considerations in developing an IPACS configuration for the Space Station. It includes the development of system requirements, wheel array configuration trades, wheel component-level requirements, and a trade study comparison of the IPACS approach with systems that employ separate energy storage and attitude control wheels. The system synthesis approach employed utilizes trade study methodology and is illustrated in figure 5.

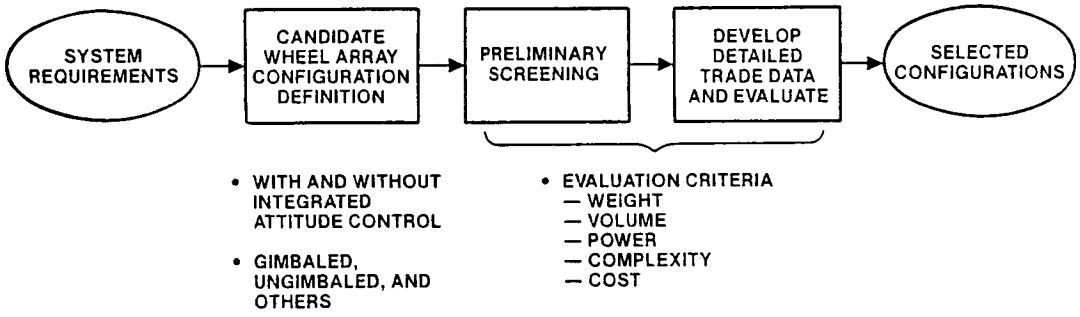

Figure 5.- IPACS configuration definition trade study logic

System Requirements Definition

The overall system requirements derived in this section are summarized in Table 2. They consist of a combination of given (study Request For Proposal) and derived requirements. During the course of the study the Space Station configurations and their related electrical power and attitude control system sizing parameters varied in a very volatile manner. The configuration selected as the reference for the requirements given in Table 2 is the "power tower" version (fig. 3) which evolved from NASA studies very late in the study. The bases for the derived requirements are presented in the material which follows.

Momentum Storage Requirements.-The momentum storage system (MSS) requirements are strongly related to the Space Station configuration, its orientation, and the functions ascribed to be performed by MSS. A wide variety of configurations evolved from the different design teams at several NASA centers and industrial firms (for example, see the first column of Table 3). Contributions to the MSS sizing budget can result from: aerodynamic and gravity-gradient disturbance torques, attitude maneuvering, docking/berthing operations, dynamic payload operations (such as manipulators moving a payload to or from the Shuttle payload bay to the Space Station), crew motion, "unwinding" solar array cables during orbital night, etc. Some of these functions may be ascribed to either the MSS or the reaction control system (RCS) depending on their magnitudes and frequency. References 33 and 34 present more detailed discussions of momentum storage sizing methodology.

TABLE 2.-SYSTEM REQUIREMENTS FOR SPACE STATION

- Energy storage capacity compatible with bus power levels of
  - Initial station (IOC), 75 kW
  - Final station, 150 kW (via modular growth)
- Energy Storage Wheel (ESW) depth of discharge: 75%
- Control torque capacity: 300 N-m/unit (220 ft-lb/unit)
- Momentum transfer capacity
  - Initial station, 36,600 N-m-sec (27,000 ft-lb-sec)
  - Final station, 73,200 N-m-sec (54,000 ft-lb-sec)
- Maximum station slewing rates
  - Magnetic bearings (normal and failure operations): $\leqslant 0.3°$/sec
  - Touchdown bearings (emergency survival operations): $\leqslant 5.0°$/sec
- Torque noise levels: < TBD
- Design life: 20 years and 10^5 charge/discharge cycles
- Support overall attitude control system bandwidth: $\geqslant 0.05$ Hz
- Redundancy criterion: fail-operational/fail-safe (FO/FS)
  - Single failure—energy storage and control capability at rated capacity
  - Fail safe—adequate energy storage and control capacity for crew survival and system recovery
- Automatic fault detection/annunciation/correction for flight-critical functions
- Thermal control: interface compatible with station system
- Capable of one-g testing

To develop momentum storage requirements that would represent an industry "concensus," the approach adopted was to take a broad based survey of these requirements, as well as by making "bottoms-up" estimates. The survey results are presented in Table 3. The broad variation in these momentum storage sizing values is due to the wide variation in the parameters discussed above, particularly those associated with the aerodynamic and gravity-gradient disturbance torque. The momentum storage sizing requirements taken for this study are given in figure 6. The requirements have been estimated on a relatively conservative basis, and include the effects of tolerance buildup and a 50% margin. They are based on the NASA "power tower" configuration. It is expected that future technology advances in adaptive momentum management policies will reduce these values rather than increase them.

TABLE 3.-SPACE STATION MOMENTUM STORAGE REQUIREMENTS SURVEY

Configuration/ Organization	Orientation		Momentum Storage Requirement N-m-s (ft-lb-sec)			
			Station Only		Orbiter Attached	
	Inertial	LVLH	IOC	Growth	IOC	Growth
Planar, 8/1983 (MSFC)	X		19,600 (14,500)		58,500 (43,100)	
		X	20,600* (15,200		29,900* (22,100)	
Building Block, 12/1983 (JSC)		X	12,200† (9,000)	16,900† (12,500)		
Delta, 12/1983 (JSC)	X		12,200† (9,000)	48,800† (36,000)		108,000‡ (80,000)
		X	17,600† (13,000)	33,900† (25,000)		
Tee, 12/1983 (JSC)		X	6,100† (4,500)	8,100† (6,000)		
Power Tower, 6/1984 (JSC)		X	9,400† (6,900) 3 Skylab CMG's		12,500† (9,200) 4 Skylab CMG's	
Power Tower, 7/1984 (Rockwell)		X	35,940 (26,500) 6 Sperry M4500		48,810 (36,000) 8 Sperry M4500	
Rockwell, 1/1983		X			18,300 (13,500)	30,500 (22,500)
Rockwell, 1/1984	X		11,400 (8,400)		29,000 (21,400)	
			13,200 (9,800)		39,200 (28,900)	

*16,000 N-m-s allotted to unwind solar arrays at night.
†Design margins not included
‡Gross extrapolation by study authors

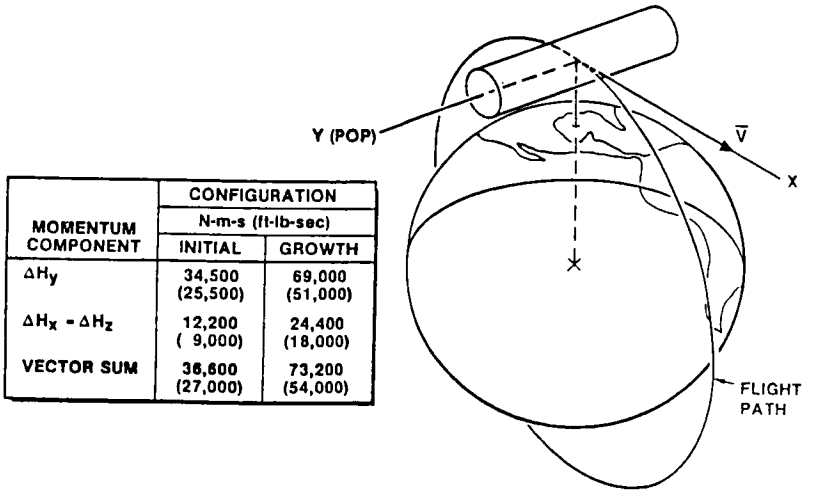

MOMENTUM COMPONENT	CONFIGURATION N-m-s (ft-lb-sec)	
	INITIAL	GROWTH
ΔH_y	34,500 (25,500)	69,000 (51,000)
$\Delta H_x - \Delta H_z$	12,200 (9,000)	24,400 (18,000)
VECTOR SUM	36,600 (27,000)	73,200 (54,000)

Figure 6.- Typical momentum storage envelope

The three-dimensional distribution of the momentum storage envelope can have appreciable influence on the MSS wheel array configuration selection. An example momentum storage envelope is illustrated in figure 6. It may be seen that the dominant component is along the y-axis (perpendicular to the orbit plane). Again, this distribution can be altered depending on the selection of momentum dumping/management approach employed.

Maximum Station Rotational Rates.-In an advanced IPACS that employs magnetic bearings, it is pertinent to establish the maximum precession rates that will be required of the rotor, since these rates will ultimately lead to some significant weight/power penalty. To accomplish this the rates for normal attitude hold, attitude maneuvering, and worst case emergency operations were established (see fig. 7). The maximum attitude maneuver rate of 0.3 degree/second can be the constraining requirement on the magnetic bearing precession rates, and the worst case rate for emergency operations of 5.0 degree/second becomes the touchdown bearing requirement. These values were selected as reasonable design requirements for the purpose of the current study, and encompass all currently known dynamic disturbance and attitude maneuver conditions.

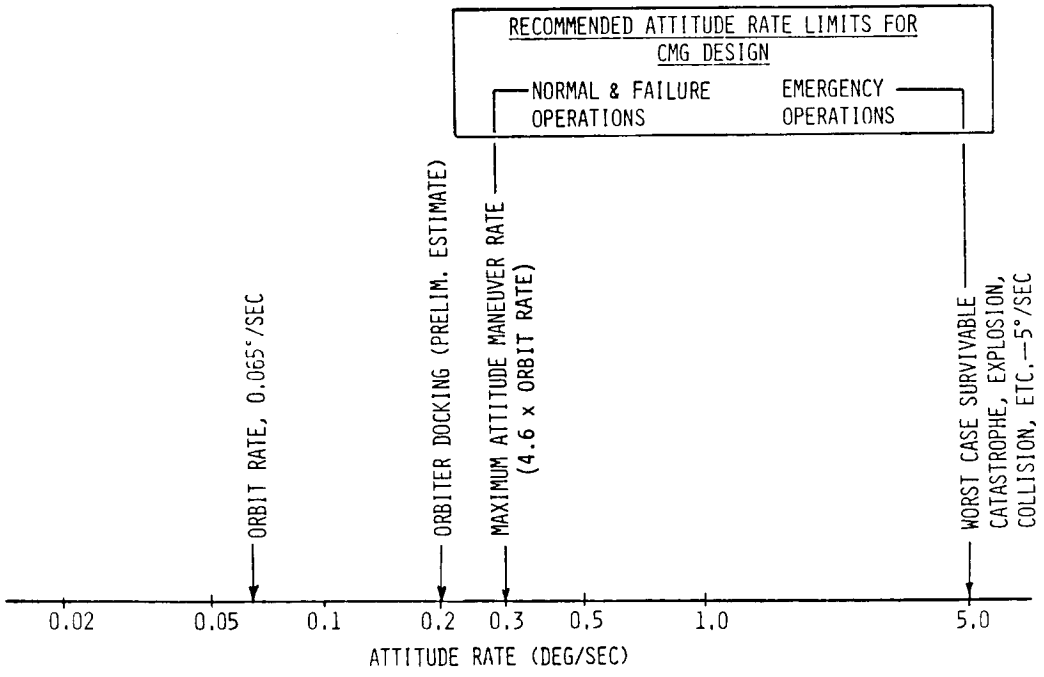

Figure 7.- Space Station body attitude rates

IPACS Bandwidth Requirements.-To insure that the IPACS can provide adequate attitude control stability and performance it is appropriate to establish a bandwidth requirement. Figure 8 presents study estimates for a variety of example frequencies from various dynamic phenomena. The overall rigid body attitude control bandwidth requirement is less than 0.01 Hz and is not particularly severe. If classical mechanical gimbaling is assumed it is estimated

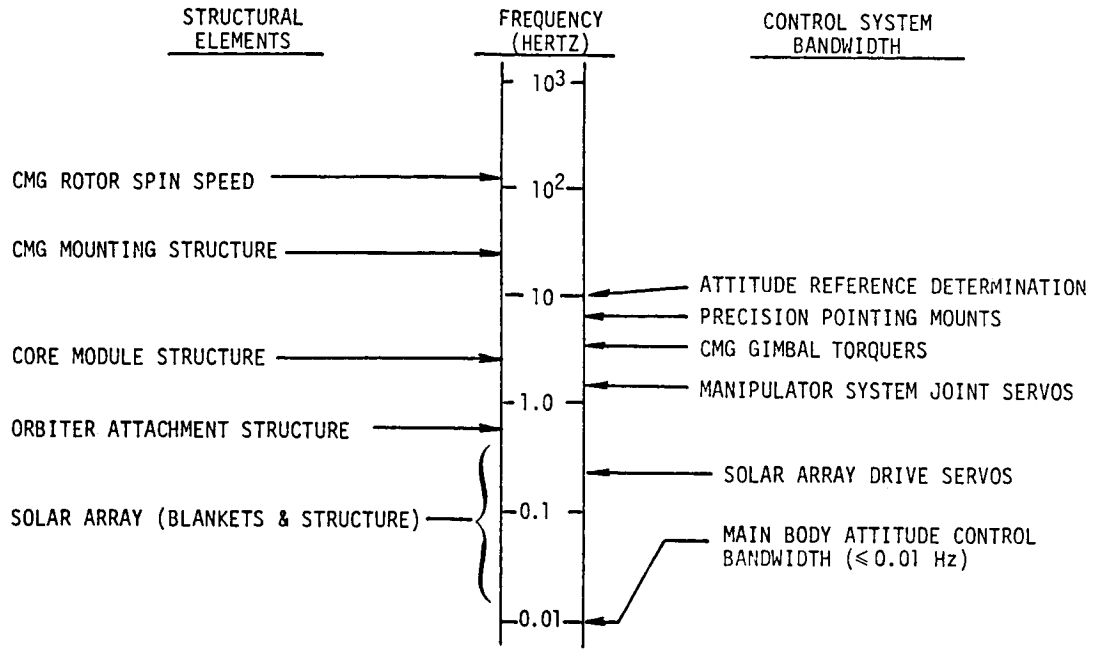

Figure 8.- Example structural and control frequencies

that torque command bandwidth greater than 1.0 Hz is easily achievable for wheels of the size under consideration. For the large-angle spherical magnetic bearing considered herein, much higher bandwidths are achievable. As may be seen (fig. 8), these bandwidths not only provide a great deal of frequency separation relative to the rigid body control modes, but also provide fast enough response for active damping of the structural bending modes should this requirement arise. For these reasons the bandwidth requirement that was adopted is that the IPACS be capable of supporting an overall attitude control bandwidth of 0.05 Hz.

Unlimited Gimbal Travel.-Studies of advanced CMG requirements for Space Station have suggested that unlimited gimbal travel was a desirable requirement. In anticipation that large-angle spherical magnetic bearings with limited tilt/gimbal travel will be considered, it is pertinent to establish the need for such a requirement. Limited gimbal travel will affect the deliverable momentum but, as will be subsequently shown, is not a problem. Several other considerations are given in Table 4. An examination of these considerations indicates that there are no firm requirements for unlimited gimbal travel, and that the merits of the large-angle bearing may well outweigh them. For these reasons, no requirement is established for unlimited gimbal travel.

Other Miscellaneous Requirements.-The other requirements listed in Table 2 have been extracted from Space Station general system design guidelines or have been included as a matter of good design practice. For instance, previous studies, as well as the current one, have indicated that an energy storage wheel depth-of-discharge of 75% (wheel speed reduction of 50%) specified in the contract statement-of-work is very near the optimum value.

TABLE 4.-GIMBAL TRAVEL ISSUES

Issues	Limited Travel	Unlimited Travel
• Software?	More sophisticated momentum distribution control policy (small penalty)	Simpler momentum distribution policy
• Slip/roll ring need?	No, avoid with momentum distribution policy (no failures) or physical stops/touchdown bearings (small penalty)	Yes, small cost and complexity penalty
• Failure Accommodation?	Physical stops/touchdown bearings can accommodate control failures (even tumbling)	Better failure accommodation
CONCLUSION: No hard requirement for unlimited gimbal travel— decision involves tradeoff of small penalties.		

Wheel Array Configuration Selection Trades

The purpose of this section is to present the system-level trades that lead to a definition of the preferred energy storage wheel (ESW) array configuration. This configuration will subsequently be employed in the system-level trades and in the development of the component-level requirements necessary for the IPACS component design. In this section it will be assumed that the attitude control function will be performed with ESW's. The trade study that investigates the advisibility of integrating the energy storage and the attitude control functions is presented in a subsequent section.

In order to synthesize an IPACS wheel array, it is pertinent to understand the mechanics of momentum transfer, how such systems are controlled, and what typical wheel arrays might potentially meet the current requirements. References 35 through 43 present a great deal of information that is helpful in this regard. References 35 through 37 describe the mechanics of momentum transfer and rationale for selecting different wheel arrays, with emphasis on CMG's. References 38 through 41 develop control policies for CMG's, and give insight into the use of these systems for attitude control. Reference 42 provides analytical sizing bases for the more massive elements within a CMG, and gives perspective into the design drivers and the relative mass of these elements. Relevant operational experience for the Skylab system is given in reference 43.

The IPACS application to the current Space Station is significantly different from the applications described in the above references and, thus, the preferred wheel configuration is not intuitively clear. Therefore, it was deemed appropriate to employ a more fundamental approach for synthesizing the wheel array. The approach employed utilizes the following sequence of steps:

- Identify a broad family of candidate arrays
- Screen the candidates and develop the trade data
- Develop an evaluation criterion and select the preferred system array
- Define the component-level performance requirements

Candidate Wheel Array Configurations.-The most fundamental requirement of admissible candidate wheel arrays is that they be capable of simultaneously satisfying the independent demands for energy extraction/addition and momentum transfer, and do so with negligible interaction resulting from the two demands. To facilitate subsequent discussion, this requirement will be referred to as the "basic requirement." They must also meet the overall system-level requirements identified above.

The number of configuration variables that must be specified is quite large and includes:

- Number of rotors
- Momentum bias vs. zero nominal momentum attitude control
- Nominal momentum (spin) vector orientation of each wheel
- Gimbal axis orientation and Euler angle rotation order
- Gimbal mechanical design options
- Energy storage with or without attitude control ("with" is assumed in this section).

The number of variables and their subsets are large (figs. 9 and 10). In order to deal with this myriad of variables, a number of prudent design assumptions and simplifications is possible. The simplifying assumptions employed herein are shown in Table 5.

The second simplification warrants explanation. The single-degree-of-freedom gimbal has the advantage of high "torque gain." When these torques must be transmitted through the magnetic spin bearings, the primary penalty for high torques is in the magnetic spin bearings and not the gimbal torquer. Scissored-pair systems have the advantage of providing output torque along a body fixed axis, thereby eliminating the need for a small amount of software. With the computational capacity available from current flight computers this mechanical complexity is unwarranted. The relatively large number of wheels required to satisfy the fail-operational/fail-safe (FO/FS) redundancy requirement, and the larger development cost of systems with a hybrid variety of wheel sizes and gimbal arrangements, make the hybrid approach less attractive. The advisability of these simplifications will be examined again when the trade study is complete and their validity can be judged in light of the trade study results.

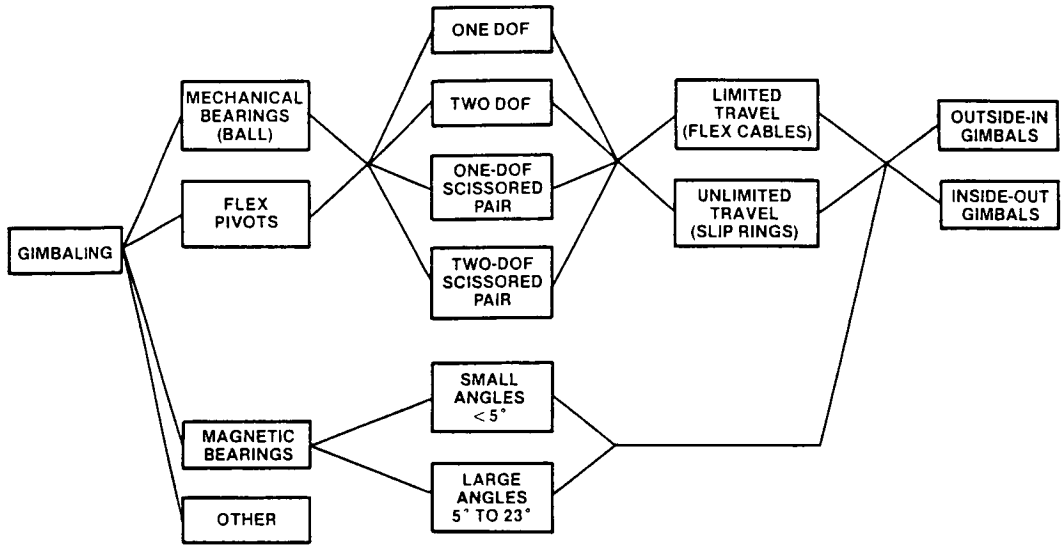

Figure 9.- Gimbal design options trade tree (example)

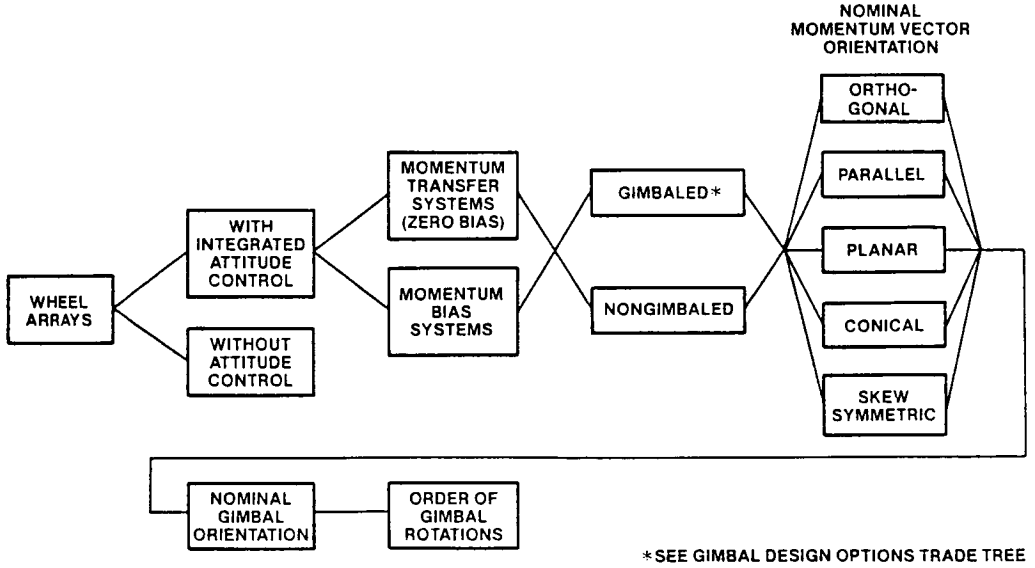

Figure 10.- Energy storage wheel array candidate systems trade tree

TABLE 5.-SIMPLIFICATIONS FOR FIRST-LEVEL TRADES

- Assume all energy storage wheel (ESW) units are identical, i.e., same size and gimbaling
- Delete single-degree-of-freedom gimbal, scissored pairs, and other hybrid multiple wheel/gimbaling arrangements
- Treat all gimbaling design options as second-level trades, and do after first-level trades
- Growth from 75 kW to 150 kW accomplished modularly with units of same capacity and functional capability
- Momentum bias system capable of momentum transfer in all three axes (i.e., active 3-axis control required)

Armed with these simplifications, a substantial reduction in the complexity of the trade study logic results. Figure 10 presents the ESW array trade study logic tree. The trade study options listed under "nominal momentum vector orientation" warrant further explanation. Figure 11 presents a pictorial description of these arrangements. They include a representative group of configurations and, although it is possible to conceive of others, it is felt that they closely represent many of the more practical ones. The number of wheels in the figure is not intended to imply a specific number of units. Thus, any number may be considered. For instance, the planar and conical arrangements can accommodate additional wheels, which would be symmetrically arranged in the plane or around the periphery of the cone. The nominal momentum vector arrangements given (fig. 11) are appropriate to gimbaled and nongimbaled wheel configurations with the exception of the parallel and planar arrangements. These two arrangements do not provide three-axis control for nongimbaled systems.

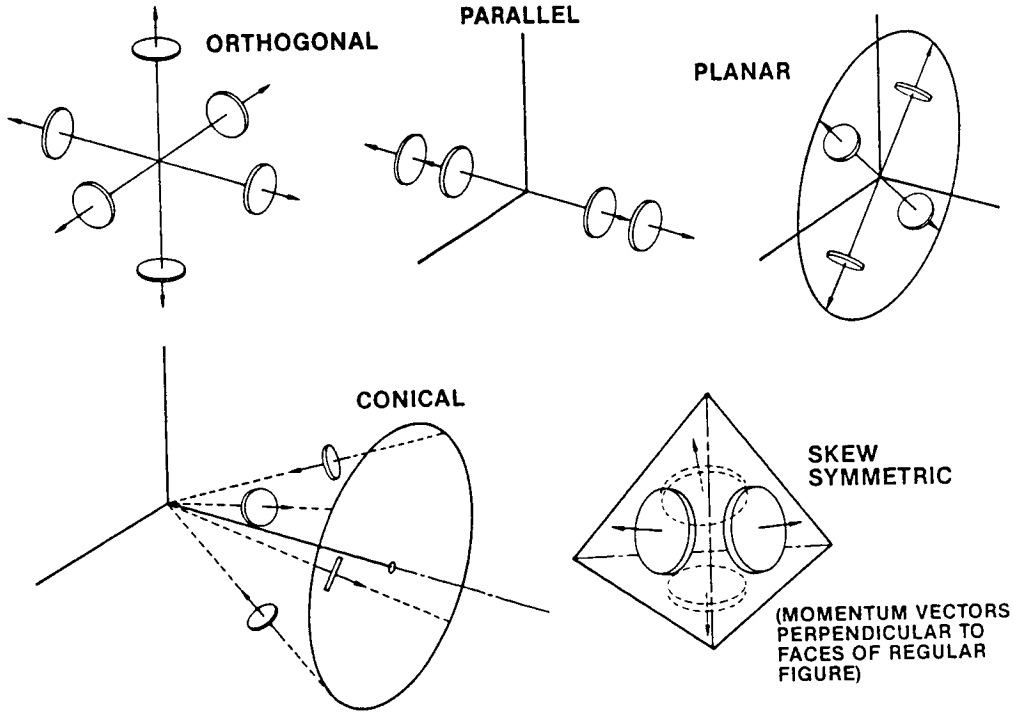

Figure 11.- Candidate momentum vector orientations

Redundancy and Selection of Number of Wheels.-For each of the arrays identified above, there is a minimum number of wheels that will permit the array to satisfy the "basic requirement" for simultaneous and independent energy and momentum transfer. In addition, more units must be added to meet the FO/FS requirement. A more explicit definition of the minimum FO/FS requirement is given at the top of Table 6. This table also illustrates the impact of the FO/FS requirement on the number of wheels required for the initial and final Space Station configurations.

TABLE 6.-THE FAIL-OPERATIONAL/FAIL-SAFE STORY

- One failure → fail operational (FO), must meet rated energy storage and attitude control requirements.
- Two failures → fail safe (FS), must provide sufficient energy storage for emergency operations. Attitude control functions not required (use RCS). Capable of recovery via maintenance.

Initial Station			Final Station
Number of Wheels Prior to Failure(s)	FO (One Failure) Case	FS (Two Failures) Case	Number of Wheels Prior to Failure(s)
3	2	1	5
4	3	2	7
5	4	3	9
6	5	4	11
7	6	5	13
8	7	6	15
9	8	7	17
10	9	8	19
11	10	9	21
12	11	10	23
N	(N-1)	(N-2)	2N-1

To explore the impact of these requirements on the number of wheels and the oversizing (additional mass) resulting from the redundancy requirement, the data in Table 7 were prepared. The table contains data for a variety of configurations, including those with and without an attitude control capability, gimbaled and nongimbaled, momentum bias and zero nominal momentum configurations, etc.

Table 8 presents a summary of the properties of some of the more attractive arrangements from the tables above. These were selected on the basis that they minimize the number of wheels as well as the oversizing needed to satisfy the redundancy requirement. It may be seen that some of the configurations require considerably more units than others.

TABLE 7.-OVERSIZING PENALTY TO MEET REDUNDANCY REQUIREMENT

Nominal Number of Wheels	Oversizing for Single Failure (%)	Energy Storage Available with Two Failures (% of Rated)	Comment
ENERGY STORAGE WITHOUT ATTITUDE CONTROL—CONFIGURATION: NONGIMBALED, PARALLEL ORIENTATION			
2	100	0	*
3	50	50	*
4	100	100	Minimum number of wheels satisfying requirements
5	25	50	Attractive configuration
6	50	100	
7	17	67	
INTEGRATED ENERGY STORAGE AND ATTITUDE CONTROL—CONFIGURATION: MOMENTUM BIAS, 2 DOF GIMBALED, CONICAL ARRAY			
3	50	-	*
4	33	67	Selected for example
5	25	75	
6	20	80	
7	17	83	
INTEGRATED ENERGY STORAGE AND ATTITUDE CONTROL—CONFIGURATION: NONGIMBALED ORTHOGONAL ARRAY			
3	*	*	*
6	50	50	*
9	50	67	Minimum number of wheels
12	20	80	Selected for example
INTEGRATED ENERGY STORAGE AND ATTITUDE CONTROL—CONFIGURATION: NONGIMBALED, SKEW ARRAY			
3	-	-	*
7	-	-	*
8	~33	~67	Selected for example
9	-	-	
10	~25	~75	
11	-	-	
12	~20	~80	
INTEGRATED ENERGY STORAGE AND ATTITUDE CONTROL—CONFIGURATION: 2 DOF GIMBALING, ORTHOGONAL ORIENTATION			
3	-	-	*
6	20	80	Selected for example
9	12.5	88	
12	8.3	91	
INTEGRATED ENERGY STORAGE AND ATTITUDE CONTROL—CONFIGURATION: 2 DOF, GIMBALED, SKEW ORIENTATION (ALSO REPRESENTATIVE OF PARALLEL, PLANAR AND CONICAL CONFIGURATIONS)			
3	50	0	*
4	33	67	Minimum number of wheels meeting "basic" requirement; selected for example
5	25	75	
6	20	80	
7	17	83	

*Does not meet "basic" requirement after two failures.

TABLE 8.-SUMMARY OF REPRESENTATIVE ENERGY STORAGE WHEEL CONFIGURATIONS

Configuration	Number of Wheels		Oversizing of Initial System for Single Failure (%)	Storage after Two Failures (% of Rated)
	Initial Station	Final Station		
Energy Storage without Attitude Control				
• Parallel wheels	5	9	25	50
Attitude Control, Integrated				
• Momentum bias				
- Double-gimbaled conical	4	7	33	67
• No momentum bias				
- Nongimbaled orthogonal	12	24	20	80
- Nongimbaled skew	8	15	33	75
- Double-gimbaled orthogonal	6	12	20	80
- Double-gimbaled skew, planar, conical, or parallel	4, 5, 6	7, 9, 11	33, 25, 20	67, 75, 80

Wheel Array Configuration Evaluation.-To evaluate the wheel configurations presented in Table 8, the evaluation criteria presented in Table 9 were developed. A close scrutiny of them yielded the following observations, and provided the basis for rejecting a number of the candidates. For the nongimbaled cases, control torques must be derived in the same manner as with reaction wheels. This requires that the control torques be derived through the asymetric charging (or discharging) of wheels. In the IPACS component design trades it is shown that for the smaller rotor diameters, the control torque derived in this manner was insufficient to meet the specified control torque requirements. On this basis, the nongimbaled configurations were abandoned.

TABLE 9.-WHEEL ARRAY TRADES EVALUATION CRITERIA

- Does it meet basic performance requirements?
  - Satisfy rated energy and momentum demands with one failed wheel?
  - Satisfy emergency power requirements with two failed wheels?
- Delivered momentum
  - Along axis perpendicular to orbit plane (POP)?
  - Along other axes?
  - With failed wheels?
- Ease of reconfiguring with failed wheels?
- Makes full use of redundant wheels for energy reserve?
- Adaptable to small gimbal angles?
- Number of wheels required?
- Mass penalty to meet redundancy requirements?
- Control law/software complexity?

For the momentum bias configurations, the gimbaling required to maintain the constant bias was found to reduce the amount of momentum that could be transferred for control. No intrinsic advantages relative to the other configurations could be identified for the momentum bias approach, and it was abandoned on this basis.

The parallel configurations were abandoned for the same reason as the nongimbaled configuration (insufficient control torque along the spin axis).

The gimbaled conical configurations are abandoned because, for small cone angles, they have insufficient control torques along the axis of symmetry. In addition, they possess no distinguishable merits relative to other systems, such as the planar array.

The remaining array configurations are the orthogonal, planar, and skew arrays. Table 10 presents a summary of the evaluation criteria presented above, as applied to these three configurations. For the planar and skew arrays, data are presented for 4, 5, and 6 wheels. This was done because no strong discriminators between them could be found. The 4-wheel arrays provide the minimum number of wheels, but require the use of reaction jet attitude control after the two wheel failures. The 5-wheel array is selected since it is the minimum number of wheels that still provides attitude control after two failures. Although the IPACS is only required to provide attitude control after one failure, the ability to accommodate two failures was deemed to be a desirable attribute. It may be seen that the planar configuration is superior to all the others on virtually all counts, and is selected on that basis.

TABLE 10.-EVALUATION OF REMAINING WHEEL ARRAY CONFIGURATIONS

Criteria	Wheel Array Configuration		
	Orthogonal	Planar	Skew
• Number of wheels required	6	4, 5, 6	4, 5, 6
• Mass penalty to meet redundancy requirements (%)	20	33, 25, 20	33, 25, 20
• Delivered momentum normalized to planar config. (% of H_{max})			
- POP axis	~67	~100	~75
- Other axes	~67	~ 67	~75
• Ease of reconfiguring after wheel failure	Good	Best	Good
• Utilization of redundant wheels for energy reserve	Good	Good	Good
• Adaptable for small gimbal angles	Poorest	Best	Good
• Control law/software complexity	Good	Best	Poorest
SELECTION: Planar array is preferred on basis of virtually all criteria.			

Gimbaling Technique Trades.-Having selected the nominal momentum vector orientation for the gimbaled array, the gimbaling techniques will now be considered. The various gimbaling options were identified in figure 9. Two-degree-of-freedom gimbaling was previously selected. The spherical large-angle magnetic bearing (LAMB) has a number of advantages relative to the more traditional mechanical gimbaling approaches. These include:

- More Compact Packaging.-The spherical bearing is an integral part of the supporting spin bearing in the hub region of the rotor. This is more compact than the use of separate "inside-out" torquers that are incorporated in the hub region with the magnetic spin bearings. It is considerably more compact and less massive than the classical "outside-in" mechanical gimbals located around the outer periphery of the rotor.

- Reliability/Maintainability Advantages.-With the large-angle spherical magnetic bearing, the complexity of the separate gimbal bearings, torquers, and gimbal ring structure is replaced with a small increase in the size of the magnetic spin bearing. The only mechanical moving part is the rotor which has a very high reliability. All the electronics are located external to the rotor and are maintainable as line replaceable units (LRU's).

- Long Life.-With the magnetic suspension there is no mechanical wear. Long structural life is assured through conservative use of fatigue life derating. The long-duration testing required to validate ball-bearing design lifetime is not required.

- Low Vibration/Noise/Jitter.-Orders-of-magnitude lower levels are achievable with the magnetic suspension.

- Very Wide Control Bandwidth.-Torque/force control bandwidths that are orders of magnitude larger than conventional gimbaling are possible with this type of suspension. This is a marked improvement relative to the inherent bandwidth limitations of the classical Eulerian gimbal suspension in the region of 3.0 Hz.

- Adaptability to Active Structural Vibration Control.-Although no specific requirement for active structural vibration control has been established for Space Station, the wide bandwidth potential is attractive for this purpose. In addition to control torques, active translational control forces are possible. In this regard the magnetic suspension is uniquely qualified as an active structural control actuator (5-degree-of-freedom controller).

The principal disadvantages of the spherical LAMB are:

- Gimbal Angle (Tilt) Limitations.-The IPACS magnetic bearing design studies (discussed in a later section) indicate that tilt angles of 10 to 23 degrees are achievable with relatively little penalty. The momentum transfer capability is 17 to 40% of that achievable from a large-angle gimbal. IPACS configurations generally tend to have an abundance of momentum and, as will be shown subsequently, the momentum

transfer requirement can still be satisfied with the LAMB for the current application. Another factor is the orbit rate torquing power needed to precess the wheel array around with the Station body. A system with unlimited gimbal travel does not have this requirement. This added power is almost negligible with a properly designed bearing. Also, the design penalties to achieve unlimited travel (slip rings and outside-in gimbal rings) are substantial.

- Spherical LAMB Technology Status.-Although the fundamental magnetic bearing technology is well established, the detailed LAMB design has not been developed and qualified, and this remains to be accomplished.

Based on the above considerations, the merits of the spherical LAMB appear to outweigh its disadvantages. It further appears to complement synergistically the advanced technology composite rotor IPACS approach which is the primary focus of this study. On this basis, the spherical LAMB is selected as the baseline gimbaling technique.

Separate Energy Storage and Attitude Control Wheels Versus Integrated Systems

The trade studies above have assumed that the energy storage and attitude control functions should be integrated and employ the same set of wheels. The rationale for this assumption is based on the logic presented in Table 11.

TABLE 11.-SEPARATE VS. INTEGRATED SYSTEMS

Approach: Evaluate on basis of weight and complexity

Simplified View:

	Separate ESW's + CMG's	IPACS
• Energy storage wheels	X	X
• CMG rotors	X	0
• Gimbals & torquers	X	X

Parametric View:

G = Gimbal and torquer mass
R = CMG rotor
CMG = R + G
IPACS = ESW + G

$$\frac{\text{IPACS}}{\text{ESW + CMG}} = \frac{\text{IPACS}}{\text{ESW + R + G}} = \frac{\text{IPACS}}{\text{IPACS + R}} < 1$$

CONCLUSION: IPACS approach saves CMG rotor mass and substantial complexity

The "simplified view" presented there illustrates that the Integrated Power and Attitude Control (IPACS) approach results in a savings approximately equal to the control moment gyro (CMG) rotors. The "parametric view" presents the same argument in an algebraic form, and concludes there is a weight and complexity saving for the integrated approach relative to separate systems. To explore this issue further the point design case data presented in Table 12 were prepared. It is assumed that the classical outside-in gimbal suspensions and torquers are employed for both the energy storage wheels and CMG's. The weight and complexity savings for the integrated approach are evident despite the conservatism of the assumptions employed. The use of the spherical LAMB approach for gimbal suspension (developed in this study) will result in further savings.

TABLE 12.-SEPARATE VS. INTEGRATED SYSTEM SIZING DATA

Items	Unit Mass (kg)	Number of Units	Mass (kg)	
			ESW's + CMG's	IPACS
• Energy storage wheels and bearings (electronics included)	521	6	3,126	3,126
• ESW gimbal structure	50	6	0	300
• ESW torquers	63.5	12	0	762
• ESW gimbal torquer electronics	6	6	0	36
• CMG rotors	113	6	678	0
• CMG gimbals	43	6	258	0
• CMG torquers	63.5	12	762	0
• CMG electronics	11	6	66	0
Total			4,890	4,224

Note: CMG estimates based on Sperry Model 4500

Other factors of concern in comparing the separate versus the integrated approach are given in Table 13. It may be seen that none of the arguments favor the separate approach, and the complexity issue favors the integrated approach.

Based on the above considerations, the IPACS approach is preferable to the separate systems concept, primarily on the basis of significant savings in weight, complexity, and probable cost.

TABLE 13.-OTHER FACTORS—SEPARATE VS. INTEGRATED SYSTEMS

- Complexity: Integrated energy storage and attitude control are significantly less complex and less costly than separate systems.
- Software: Integrated saves CMG wheel speed control; otherwise is very similar.
- Reliability: No major discriminators
- Testing: Combined power and attitude control system testing is significantly more complex, but will probably be less expensive than independent system testing.
- Design compromises imposed by power and attitude control on each other: No serious compromises noted in this study.
- Robust performance: Excess momentum frequently available with integrated approach.

IPACS Component-Level Requirements

The above trade studies have yielded an overall IPACS configuration for the Space Station application. To support the component level design trades and analyses, the component level performance requirements have been developed and are summarized in Table 14. A bus voltage level of 300 volts was selected as representative of the high-voltage levels being considered in the Space Station program.

TABLE 14.-COMPONENT-LEVEL REQUIREMENTS

Requirements/Configurations	System		
	4-Wheel	5-Wheel	6-Wheel
• Usable energy storage at electronics output—kWh	17.6	13.2	10.5
• Depth of discharge	75%	75%	75%
• Charge/discharge cycle efficiency:	⩾0.85	⩾0.85	⩾0.85
• Rated maximum power output (out of electronics)—kW	29.2	21.9	17.5
• Deliverable momentum (N-m-s)	13,500	10,100	8,100
• Control torque output (N-m)	⩾300	⩾300	⩾300
• Rotor precession rates - Normal operations (°/sec) - Emergency operations (°/sec)	 ⩾0.3 ⩾5.0	 ⩾0.3 ⩾5.0	 ⩾0.3 ⩾5.0
• Capable of one-g testing			
• Support overall attitude control Bandwidth (Hz)	⩾0.05	⩾0.05	⩾0.05
• Rated voltage at bus (V)	300	300	300

IPACS System Configuration Trade Study Conclusions

A methodical systems engineering trade study approach has been developed and applied to the synthesis of an IPACS configuration for the Space Station. It bridges the gap between top-level systems requirements and component-level functional and performance requirements. Some of the more noteworthy conclusions include:

- Integrated energy storage and attitude control wheel systems (IPACS) are preferable to systems that separate these two functions.
- The preferred wheel array configuration for the initial Station is the "planar" arrangement employing five double-gimbaled wheels. The gimbaled planar wheel arrangement was selected over orthogonal, parallel, conical, and skew symmetric wheel arrangements.
- Nongimbaled and single-gimbaled wheels, scissored wheels, and momentum bias configurations were considered and abandoned.
- The spherical large angle magnetic bearing is selected as the baseline gimbaling approach, and offers numerous advantages relative to the more conventional gimbaling techniques. Although it will require significant development work, it synergistically complements the advanced composite material energy storage wheel, and can be nested within the annulus of the selected hoop-type rotor.
- The wheel configuration trade study results are focused toward Space Station requirements, and are not necessarily valid for other applications (such as unmanned spacecraft). The general synthesis methodology can be adapted to other applications. For instance, it can easily be applied to large unmanned space platforms.

SPACE STATION SYSTEM-LEVEL TRADES

The purpose of this section is to present overall Space Station system-level trade study results that compare the merits of the IPACS approach with other competing energy storage systems. For the current study, photovoltaic power generation is assumed. The competing energy storage systems have been narrowed to those under serious consideration for Space Station at the inception of the study and were given in the contract statement-of-work. These are the regenerative fuel cell (RFC) and nickel-hydrogen battery (NHB) systems. To explore the impact of the various performance variables of these energy storage devices on the complete system, it is necessary to consider their interaction with:

- Solar array and circuit sizing
- Attitude control system (control moment gyro) sizing
- Thermal control system sizing to reject the heat associated with the different energy storage system efficiencies
- Operational servicing requirements associated with different components and their lifetimes.

The approach employed herein is to size the complete electrical power system (EPS) and the portion of the other systems that interact with the energy storage system (ESS) variables. The resulting systems data may then be compared on conventional engineering bases and on the basis of life-cycle costs.

Trade Data Development

This section presents the sizing bases and rationale for the various interacting systems.

Electrical Power Systems (EPS).-The assumptions and rationale employed in sizing the EPS to the study ground rules are presented in Table 15. These are based on the best estimates of Space Station requirements as they existed at the time of the study. Performance parameters are based on best estimates of existing or near-term technology. IPACS performance is based on the results of the current study.

Planar Silicon Solar Array Description.-Since the objective of this study was to compare the energy storage wheel with other energy storage systems, a planar silicon, deployable, flexible substrate solar array was selected. The baseline solar array is the product of an evolutionary

TABLE 15.-ELECTRICAL POWER SYSTEM SIZING ASSUMPTIONS AND GROUND RULES

Power Requirement

- 75 kW (initial) and 150 kW (growth)

Station Growth

- Growth configuration is achieved ~5 years after initial configuration through modular addition of functionally identical components

Orbit

- Altitude: 476 km (257 nmi)
- Inclination: 28.5 degrees
- Eclipse time: 36 minutes
- Time in sun: 57 minutes
- Orbital period: 93 minutes

Redundancy

- Energy storage system: 1/3 (4 units provided; 3 provide rated capacity)
- Solar arrays: None, numerous circuits lessen failure impact

Solar Array

- Planar silicon based on SEPS/PEP/PM deployable blanket designs
- End of life (at array interface): 8.92 m^2/kW
- End of life (including solar array structure): 22.7 grams/watt

Regenerative Fuel Cells

- Sizing based on data from United Technology Corp. (Power Systems Division), General Electric, and Life Systems, Inc.
- Electrical storage efficiency (electric to electric): 58%
- Life expectancy: 5 years, with more frequent servicing of accessory section (pumps and separators)

Nickel-Hydrogen Batteries

- Depth of discharge: 34%
- Electrical storage efficiency: 74%
- Life expectancy: 5 years
- Mass estimates based on COMSAT/INTELSAT technology

Energy Storage Wheel System

- Depth of discharge: 75%
- Electrical storage efficiency: 85%
- Energy storage density: 22 Wh/kg (including processing circuitry and attitude control capability)
- Life expectancy: 20 years, random failures are assumed to require 5% changeout per year

Thermal Control

- Radiator sizing based on maximum temperatures in energy storage element of:
  - Regenerative fuel cells—68.3°C
  - Nickel-hydrogen batteries—4.4°C
  - Energy storage wheels—65.6°C

Control Moment Gyros: Sperry Model 4500 assumed

technology growth spanning the solar electric propulsion system (SEPS), power module (PM), and power extension package (PEP) design and development programs. Under these programs, a lightweight full-scale wing (32.0 m x 4.06 m) was fabricated and tested to demonstrate technology readiness. Additionally, the solar array flight experiment (SAFE) flown as a Space Shuttle flight experiment in September 1984, demonstrated the technology readiness of this lightweight deployable blanket concept. The data base established by these programs, particularly that for the PEP program (ref. 44), provides a basis for sizing and weight estimation for the solar array system.

The initial Space Station array is composed of eight wings as configured in figure 12. The sizing shown is for the regenerative fuel cell energy storage option. For the growth Space Station configuration, the number of blankets will be doubled. The array wing components are the extendible/ retractable extension mast, a dual blanket, two ascent support containment boxes for the blankets, preloadable box covers, and a blanket tension/guide wire system. The two array blankets, after the containment boxes are pivoted into place, are deployed by a single continuous longeron coilable lattice structure mast that can be extended or retracted from its storage canister to full length or an intermediate length.

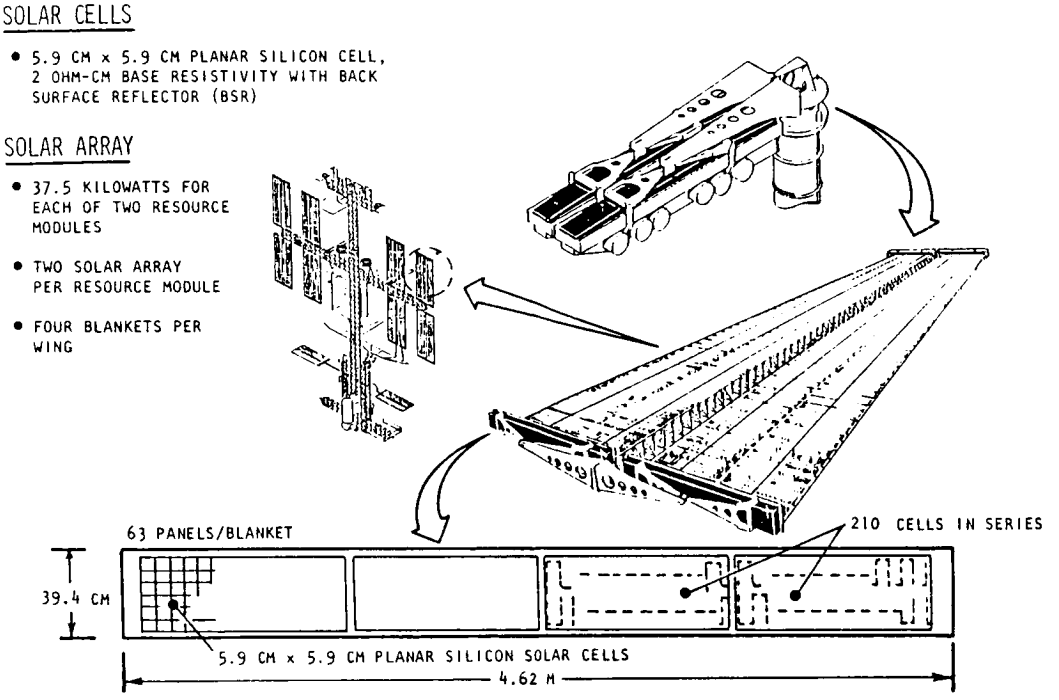

Figure 12.- Solar array panel and cell layout

The array blanket construction consists of 63 hinged panels that are flat folded for ascent and entry. The panel hinges provide panel stiffness and tear resistance in addition to flat stiffness provided on the blanket panel substrate. The printed circuit flexible substrate is a lamination of two sheets of 1 mil Kapton with 1/2 mil of high temperature adhesive. The etched copper interconnect is imbedded between the Kapton laminates. Prepunched holes in the Kapton are precisely aligned to permit parallel gap welding of the large area (5.9 cm x 5.9 cm) wraparound solar cells which forms the only attachment for the solar cells.

The harness assembly folds up in the same manner as the array panels for retraction and storage. Since the harnesses are placed at the edge of the array, the solar cells are not subjected to stresses as would occur with the harnesses placed behind the blanket.

The selected generic cell design is the 2 ohm-cm back-surface-reflector (BSR), 5.9 x 5.9 cm, 0.02 cm-thick, multilayer anti-reflective coating, redundant contact wraparound silicon photovoltaic solar cell. This cell was developed by the Applied Solar Energy Corporation in the "Large Area, Low-Cost Solar Cell Development and Verification Program" funded by the NASA/JSC.

The selected design consists of a single series circuit of 612 solar cells, 5.9 cm x 5.9 cm in size. This circuitry, with a nominal 254 volts, creates the worst case hot spot for a single shadowed cell. The maximum cell temperature was calculated to be 246°C (steady-state temperature) in the absence of any shunt diodes. Since welded contacts are expected to survive 260°C temperatures, the design would be satisfactory, especially since shadowing of only one cell is highly unlikely except as a transitory event. When more than one cell is shadowed in a given string, the reverse bias current heating is shared over a larger cell area with consequent reduction in maximum temperature.

The magnitude of the hot spot problems is greatly reduced by provision of shunt diodes. Transient shadowing of portions of the solar array by Space Station components will occur when the solar array is tilted for high beta angles. Provision for shunt diodes every 18 to 24 cells will reduce the transient power losses significantly as well as eliminate hot spots as a serious problem.

Regenerative Fuel Cell (RFC) System.-There are two options for the regenerative fuel cell: (1) the alkaline electrolyte system, and (2) the solid polymer electrolyte (SPE) system. The alkaline system has higher fuel cell efficiency, has been flight-verified by Space Shuttle, and will have lower development costs. However, there are stringent reactant purity requirements and performance is sensitive to load cycle. The SPE has a higher energy density, less voltage variability, higher tolerance to reactants impurity, higher electrolyzer efficiency, and an electrolyzer which has been verified in U.S. Navy programs. Disadvantages are that the SPE fuel cell powerplant accessory components are not developed and development costs will be greater. On the basis of technology readiness, the alkaline electrolyte system was selected for this study. A five-year cycle life capability is expected.

The extensive experience derived from the Space Shuttle orbiter program with the alkaline electrolyte fuel cell provides a technological basis for a selection of the alkaline fuel cell unit. NASA/Lewis design studies indicate that an RFC system with a life greater than eight years can be expected (ref. 45) with present state-of-the-art technology. The system will require more frequent servicing and changeout of components that fail randomly. For the purpose of this study, the RFC servicing and maintenance are assumed to be equivalent to a complete system changeout every five years.

Accessory section components are identified as requiring additional development. The SPE electrolysis cell (EC) unit is selected based on the U.S. Navy operational units developed by General Electric. Life-cycle capabilities of the electrolysis unit are expected to be the same as for the fuel cell.

The RFC module design and configuration are based on providing one RFC module for each of the four buses. Two RFC modules are located in each of the two resource modules (RM). Each RFC consists of an alkaline fuel cell (FC) unit, an SPE EC unit, a water storage tank, a hydrogen storage tank, and an oxygen storage tank. Figure 13 displays the RFC concept.

Reasonable weight estimates for the fuel cell were obtained using the fuel cell data from the Space Shuttle orbiter fuel cells. Estimates for the electrolysis unit were based on General Electric's experience in producing SPE electrolysis units for the U.S. Navy program.

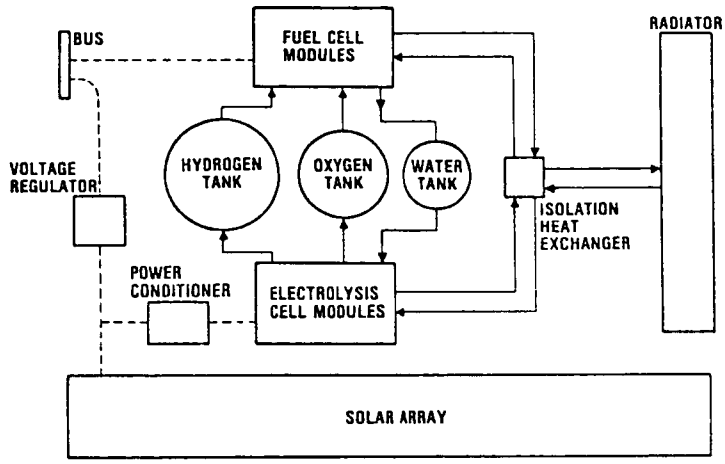

Figure 13.-Regenerative fuel cell schematic

The RFC system is sized such that any three RFC's can provide the 75-kW power requirement at the buses. A power flow diagram for the solar array/RFC electrical power system is presented (figure 14). To provide this power, each RFC must be capable of producing 29-kW at its interface. This takes into account the power conversion and distribution inefficiencies. Also, each RFC must be capable of producing enough O_2 and H_2 during the 57-minute period of sunlight during each orbit to power the Space Station during the 36-minute dark period. The RFC includes water, hydrogen, and oxygen storage tanks to store these fluids for closed-loop operation.

The baseline FC, rated at 29 kW continuous power output, consists of 170 individual cells electrically connected in series. This number is chosen due to a requirement that the maximum open-circuit voltage of the FC must not exceed the minimum dc bus voltage of 223 Vdc. With each cell producing a nominal 1.22 Vdc at open-circuit, the FC voltage at its interface is 208 Vdc. The FC unit operates at a nominal 414×10^3 Newton/meter^2 pressure and 82°C temperature. Figure 15 shows a schematic of an alkaline FC.

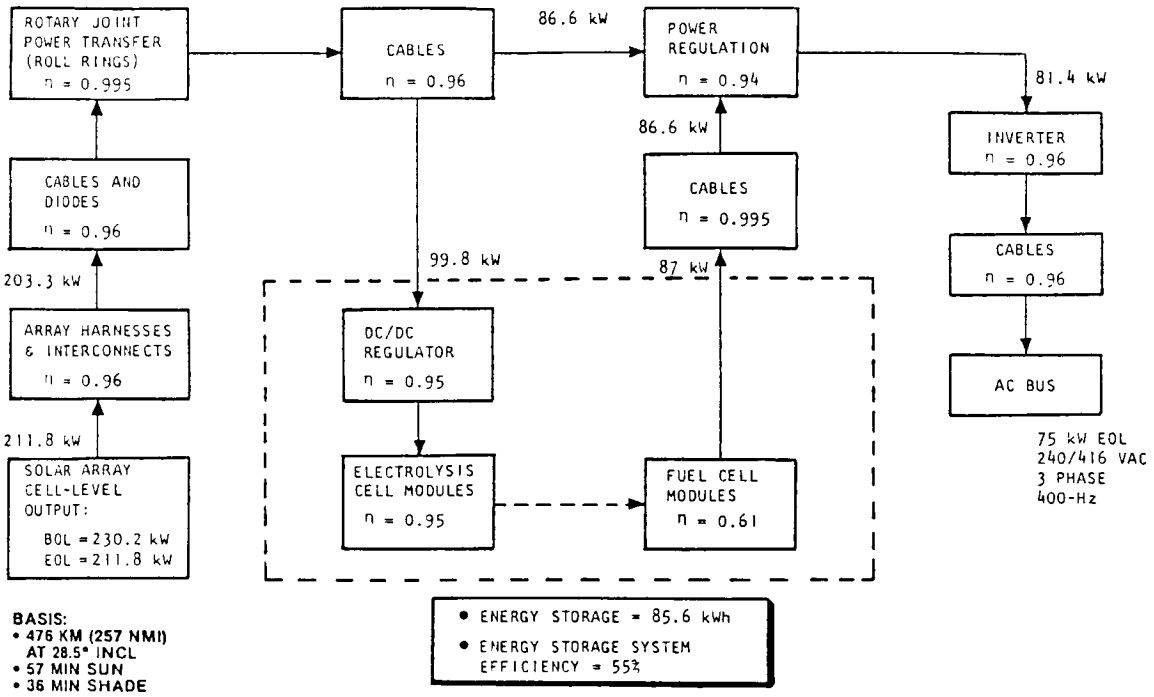

Figure 14.- Electrical power system—RFC option

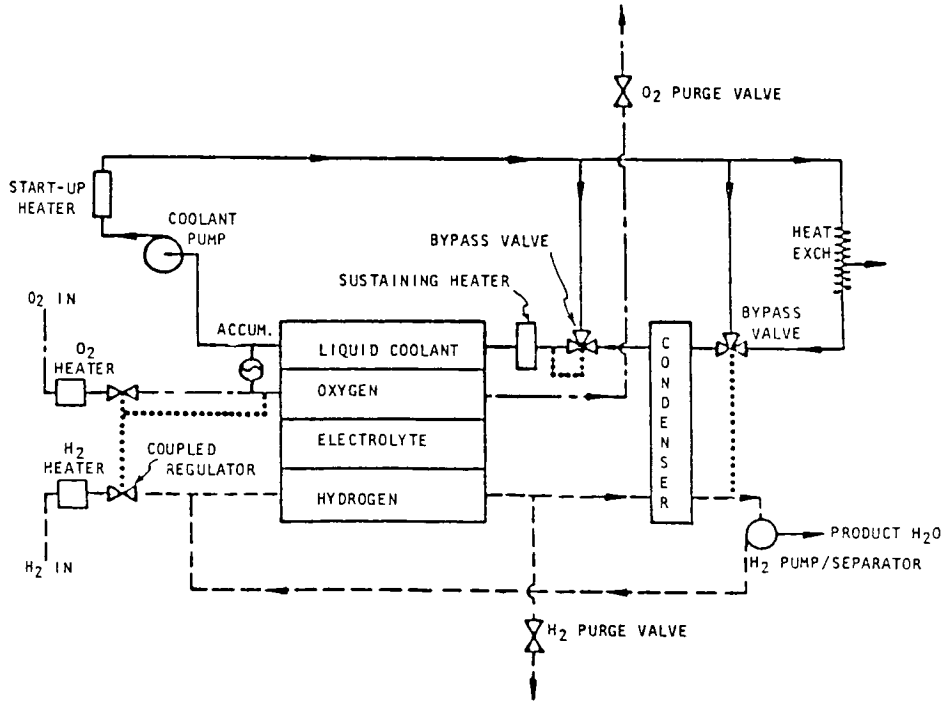

Figure 15.- Alkaline matrix fuel cell subsystem schematic

The reactant control subsystem has several specific functions. These are delivering reactants to the cell stack on demand, providing purge capability of the reactant passages, and circulating the moist hydrogen flow. The major components of this subsystem include the reactant preheaters, coupled reactant regulator, reactant purge valves, H_2 pump/separator, and the condenser.

The baseline EC is rated at 25 kW continuous power input. The EC unit consists of 155 individual cells electrically connected in series. At the design current density of 1614 A/m^2, the individual cell voltage for an SPE cell is 1.445 Vdc.

The operating pressure of the EC unit is 345 N/cm^2 which deletes the need for a compressor to raise the pressure of the reactants for storage. The average operating temperature of the EC is 82°C. Figure 16 shows a schematic of the SPE EC unit.

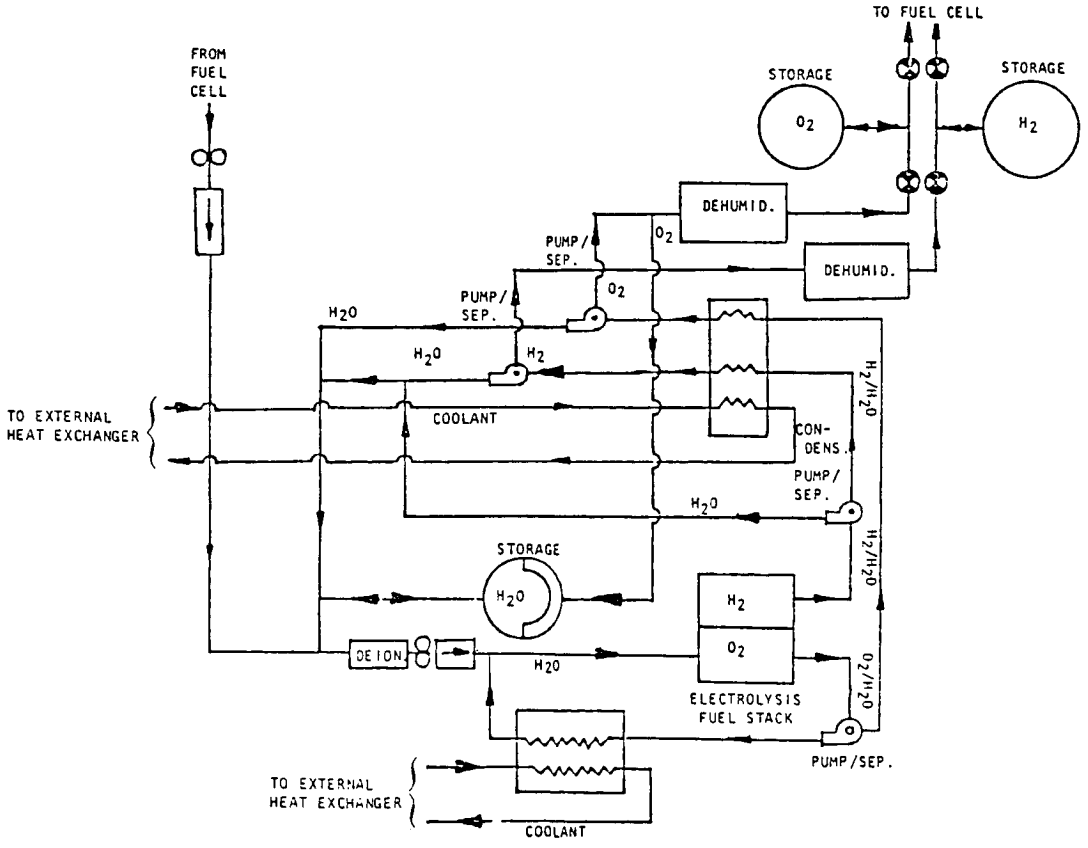

Figure 16.- SPE electrolysis unit schematic

The EC unit consists of four subsystems: the water feed, reactant conditioning, thermal control, and electrical subsystems. The water feed subsystem is a circulating feed system operated with the O_2 side of each cell supplied with process water in excess of that required for electrolysis to facilitate waste heat removal. The major components of the water feed system are the water storage tank, deionizer, O_2 pump/separator, and the water heat exchanger.

The reactant conditioning subsystem essentially takes the generated reactants from the EC stack, removes the water and stores the reactants in their respective tanks. The major components in this subsystem are the pump/separators, the condenser, and the dehumidifiers.

The thermal control subsystem maintains proper temperature and humidity control for the EC stack and removes any waste heat generated. The thermal control subsystem circulates water through the O_2 side of the EC stack to remove the waste heat and transfer it to an external coolant loop. The major components of this subsystem are the O_2 pump/separator, water heat exchanger, and a flow control valve.

The electrical control subsystem provides electrical power to the EC stack, controls startup and shutdown, and monitors and transmits EC instrumentation readouts. The major components include power cables, wiring harness, start/sustaining heaters, pump motors, solenoid valves, relays, and an electrical control unit (ECU) which controls the startup and shutdown of the EC by the actuation and deactivation of the pumps, heaters, and solenoid valves.

The reactant and water storage system must store water and reactants for closed-loop operation of the RFC. During the dark portion of the orbit, the FC's are generating water which is stored in the water tanks. During the sunlit portion, water from the storage tanks is electrolyzed into hydrogen and oxygen which is stored in reactant tanks for use during the dark period. Each RFC will have its own set of reactant and water storage tanks (four sets). The maximum storage pressure of the system is 345 N/cm^2. The minimum pressure is 69 N/cm^2. The tank sizing is based on a two-hour full power operating time. Thus the reactant tanks are able to supply reactants to the RFC's for two-hours at full power.

Nickel-Hydrogen Battery System.-Electrochemical batteries have been identified as an energy storage option for use in the Space Station. A nickel-hydrogen battery with 50 ampere-hour individual pressure vessel (IPV) cells has been selected, and has been developed to the point of operational verification status. It has a higher energy density than the nickel-cadmium battery currently in use in unmanned satellites. The potential exists for additional weight savings by use of common pressure vessels (CPV) or bipolar cells. However, these advanced cells are not yet state of the art.

Extensive prototype cell life-cycle data (15,000 plus LEO cycles) have been demonstrated (refs. 46, 47). However, continuing life-cycle testing of IPV nickel-hydrogen batteries at 80% DOD shows significant performance degradation on some cells at only 5,000 cycles (ref. 48). Also, the nickel-hydrogen batteries have not been actually employed in a low Earth environment. For Space Station application, the cells preferably should be series-connected in numbers required for a 120 to 200 V system, which has never been demonstrated. Charge/discharge control and thermal control design for a nickel-hydrogen battery system of this magnitude must also be proven. For these reasons, nickel-hydrogen battery technology is not fully developed for the Space Station application. In summary, the primary issues are system operational voltage, charge control, and thermal conditioning. Cycle life capability continues to be questionable, but a five-year capability probably can be met at the 34% depth of discharge established for this study.

The nickel-hydrogen battery system is sized for a 34% depth of discharge with no failures, and a 45% with one battery system failed. Without random failures, this sizing might optimistically be expected to provide a 10-year life. However, considerable uncertainty exists in the life-cycle capability of these batteries. Applying the same level of design conservatism employed throughout this study, and assuming a factor for maintenance of random failures, a system sized in this manner is expected to result in the equivalent battery system lifetime of five-years. On this basis, the life-cycle-cost trades assume the equivalent of a complete battery system changeout every five years.

Using a 74% battery electrical efficiency, the 75 kW initial Space Station requires 93 kW battery output with 65 kWh energy storage for eclipse operations during one orbit (see power flow diagram, figure 17). The usage of a nickel-hydrogen battery system for excess storage capability beyond that for eclipse period (0.6 hour) will be limited to a depth of discharge of 80%. Consequently, requirements definition for some minimum energy storage capability beyond that for one orbital eclipse period could impact the nickel-hydrogen size and weight.

The nickel-hydrogen battery system for the IOC Space Station consists of four batteries, one for each of the four electrical buses. Each battery consists of seven hundred fifty, 50 ampere-hour nickel-hydrogen battery cells. The 750 cells are wired in five parallel circuits, 150 wired in series for each circuit, which provides a total discharge battery voltage of 180 V. The basic battery building block is a module consisting of 30 cells, arranged as shown on figure 18. Hence, each battery contains 25 battery modules. The nickel-hydrogen battery cell weight used in determining the battery system weight was derived from the Comsat/Intelsat battery technology (ref. 49).

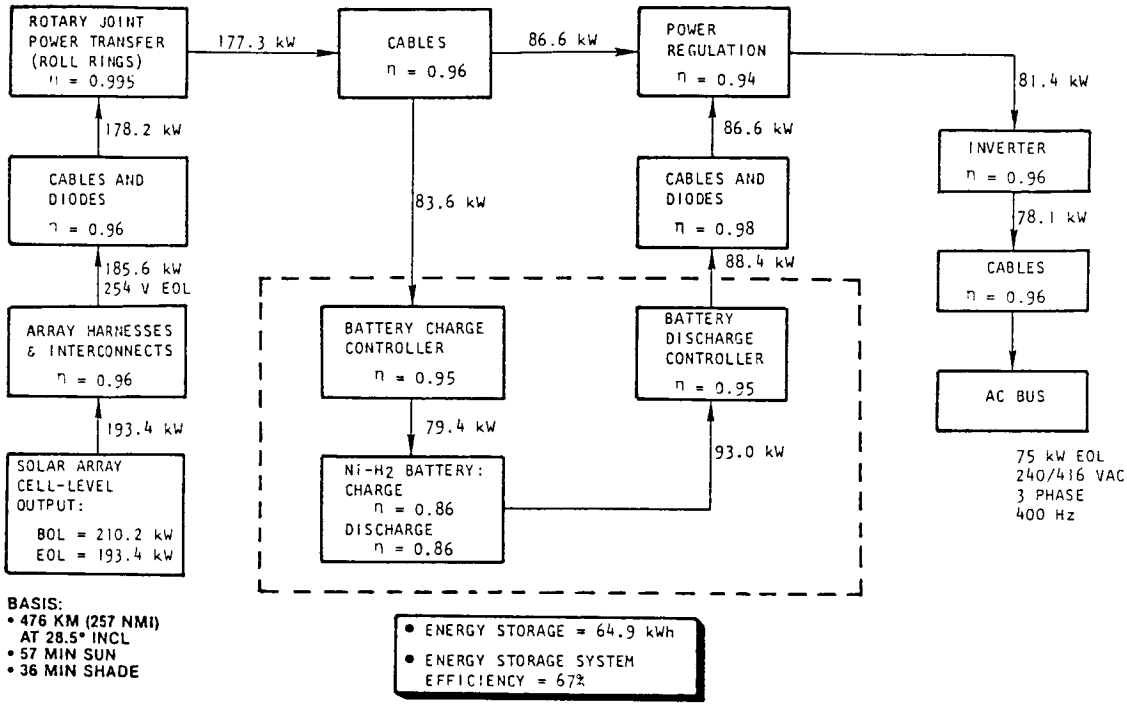

Figure 17.- Electrical power system—NHB option

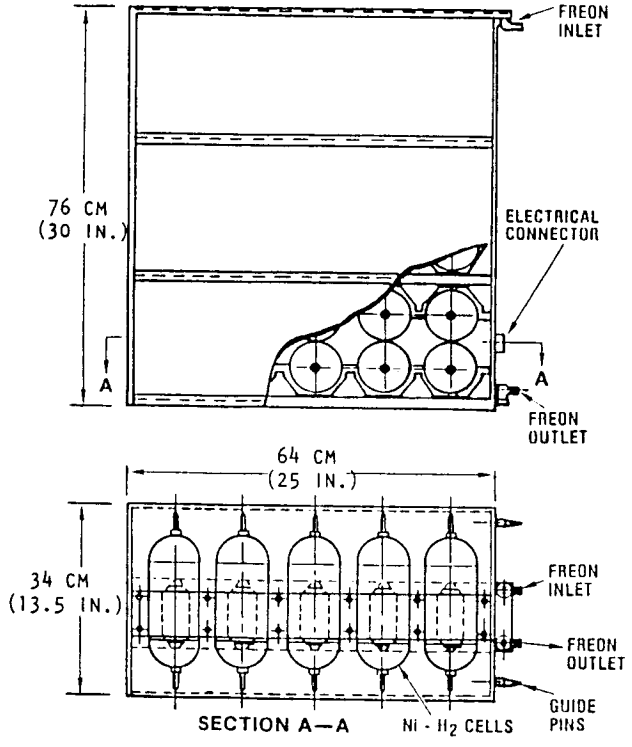

CELL CHARACTERISTICS

CAPACITY (NOM)	50 A-H
VOLTAGE (SUGG LOAD)	1.2 V
LENGTH (P.V.)	21 cm (8.4 in.)
DIAMETER	9 cm (3.5 in.)
PRESSURE VESSEL	Inconel 718
H_2 PRESSURE	690-5520 x 10^3 N/m^2 (100-800 psig)
ELECTROLYTE	31% KOH
WEIGHT	1.45 kg (3.2 lb)

BATTERY MODULE CHARACTERISTICS

NUMBER OF CELLS	30
CAPACITY (NOM)	50 A-H
VOLTAGE	36 V
WEIGHT	63 kg (139 lb)
THERMAL CONTROL	Active integral Freon loop

BATTERY—5 50 A-H modules connected in series

Figure 18.- Ni-H_2 battery module

The effective life of the battery is extended by providing series redundancy; i.e., including more cells than required in each series string. Thereby, the loss of spare cells due to shorting will reduce performance but not below rated performance. Each cell will be provided with diode bypass in the forward direction so that the full discharge current can bypass any defective cell. The diode bypass connection is illustrated below.

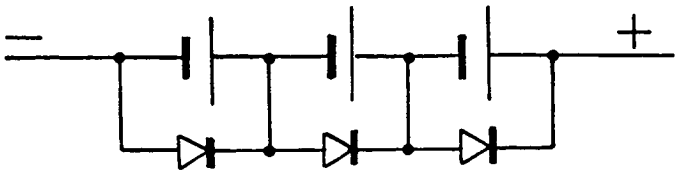

By this arrangement, the open-circuit cell cannot be recharged, only discharged. Individual cell voltages need to be recorded at critical times, such as at end of discharge, to identify shorted or open-circuited cells. The battery should be so constructed that each cell can be bypassed by astronauts through the use of a simple cell shorting plug. Once the defective cell is bypassed, then normal charge/discharge can be resumed. Series redundancy provides significantly reduced weight, volume, and cost relative to redundant parallel batteries.

Charging of the batteries can be accomplished by either a constant-current or voltage-limited charge technique. A constant-current power regulation unit will impact the peak power capability of the solar array system. The solar array is cold at sunrise and can deliver substantially more power than when the solar array has come to thermal equilibrium. If the power regulation unit is not current-limiting, the peak power tracker can permit utilization of the highest power capabilities of the solar array.

Normally, charging of a battery is accomplished in a temperature-compensated, voltage-limited charge mode to provide a fully charged system with minimum possibility of overcharge. The power regulation unit sets the charging voltage so that operation at the array peak power point occurs. When the battery voltages rises to the selected voltage-to-temperature ratio level during charge, it is held constant by the power regulation unit.

In the current-limited charge mode, the power regulation unit maintains charge current at a predetermined current level. Individual batteries are removed from charge if their temperature exceeds 35°C.

Energy Storage Wheel System.-The energy storage wheel (ESW) system assumed for this trade study is an IPACS concept that integrates the energy storage and attitude control functions. A planar array employing four gimbaled wheels is employed for the initial Station. Four more functionally identical units are added to achieve the growth configuration. The performance of the IPACS units is conservatively taken to provide an energy density of 22.05 Wh/kg (10 Wh/lb), and a round-trip energy conversion efficiency of 85%. These values are corroborated by the work in subsequent sections of this report. Further discussion of the design conservatism is given there. For the initial Station configuration, the rated energy storage

capacity is provided by three wheels with one wheel providing the necessary "fail-safe" redundancy. Although a five-wheel configuration was ultimately selected in the study, these trades were performed prior to that selection. The use of a five- or six-wheel configuration will reduce the mass penalty for redundancy and the trade study results may be interpreted in this light.

The overall electrical power system (EPS) sizing is based on the energy balance diagram presented in figure 19. The required energy storage capacity of 57.5 kWh is provided by three wheels. The fourth wheel provides 33 percent additional energy storage capacity. This will permit the four-wheel system to be operated at a reduced depth-of-discharge (DOD) which, in turn, will improve the energy conversion efficiency by several percent. Conversely, the fourth wheel may be employed to simply provide an energy storage reserve. The energy conversion efficiency of 85% is based on the rated DOD of 75% and includes the power processing electronics.

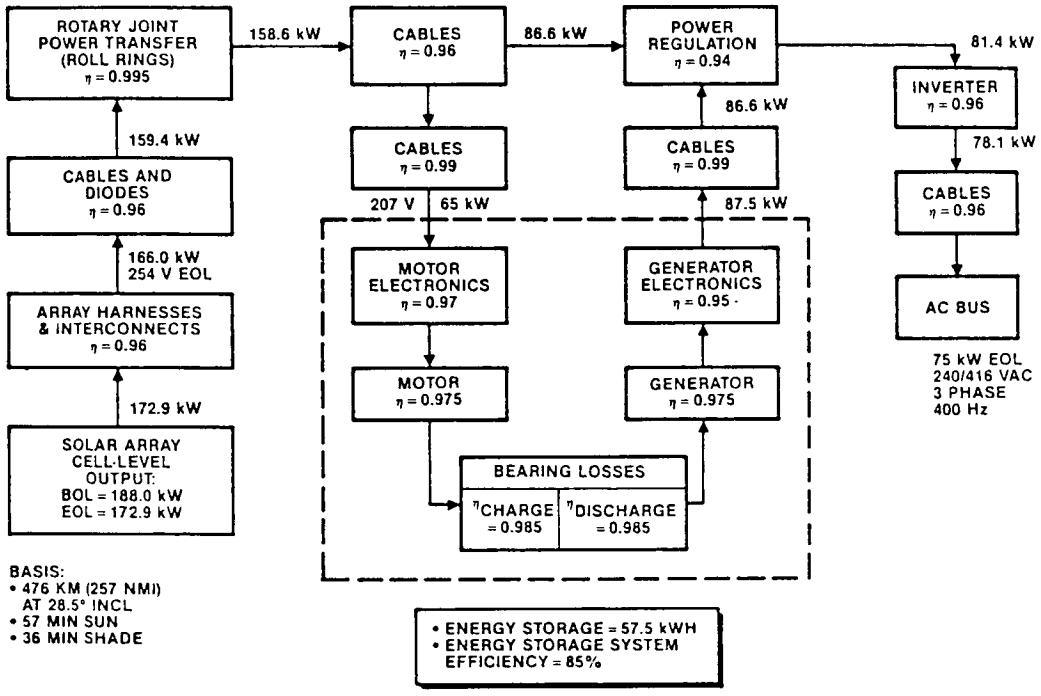

Figure 19.- Electrical power system—ESW option

The IPACS concept developed herein has only one moving part; namely, the rotor. Since the rotor is a single structural element, its reliability is quite high and it is, therefore, questionable that redundancy needs to be applied to this element. The more failure-prone electronics can be made redundant and serviced as line replaceable units (LRU). However, similar arguments may be made for the RFC and battery systems, and the redundant IPACS unit is included to provide a conservative but fair basis for comparison with these systems.

Attitude Control System (ACS).-The RFC and battery systems require the use of separate control moment gyros (CMG's) for attitude control; whereas, the IPACS system provides this function and does not require the CMG's. The Sperry Model 4500 CMG is selected for this trade study and has appreciably greater momentum density than the Skylab CMG's. It represents a reasonable conservative design that is consistent with the technology level used in this study. It is a double-gimbaled unit that provides 6100 N-m-sec (4500 ft-lb-sec) of momentum transfer and has a mass of 250 kg (550 lb) per unit (including electronics). Based on the momentum transfer requirements developed in an earlier section, six of these units are required for the IOC Station, and twelve are required for the growth Station. The other elements of an ACS are common to all three systems and are not included in subsequent trade data.

Thermal Control System (TCS).-The three energy storage systems being considered have varying heat dissipation requirements due to the different energy conversion losses. To dissipate this heat, an active fluid pumped system with external radiators is assumed. The IPACS is a candidate for a passive TCS with its modest heat rejection needs, high heat rejection temperature, and fairly large areas. However, the active TCS is assumed to insure a fair basis for the trade study, and is illustrated in figure 20. For the trade study, only the fraction of the TCS mass required to dissipate the energy storage system heat is computed. The results and basis for the sizing are given in Table 16. It may be seen that the TCS mass required by IPACS is much less than for other systems. This is due to the combined effects of less heat to be dissipated, and higher heat rejection temperatures. The IPACS electronics are the most temperature-sensitive item requiring thermal control.

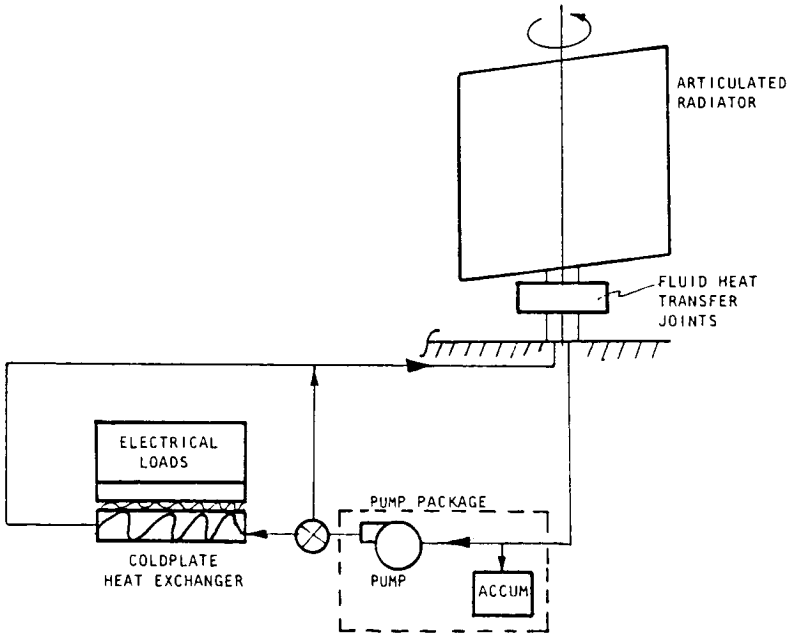

Figure 20.- Typical coolant loop system (Primary only)

Additional assumptions include: an articulated radiator (pointed edge-on to the sun) with surface absorptivity of 0.2 and emissivity of 0.78, single-phase system, and ammonia coolant. The system mass includes the radiators,

heat pipes for conduction out of the element, heat exchangers, ammonia, and circulation pumps.

TABLE 16.-THERMAL CONTROL SYSTEM SIZING SUMMARY

ITEM	SYSTEM PROPERTIES		
	RFC	NiH_2 BATTERIES	IPACS
• RADIATOR TEMPERATURE, °C (°F)	68 (155)	4.4 (40)	66 (150)
• ENERGY STORAGE SYSTEM MAXIMUM TEMPERATURES, °C (°F)	74 (165)	10 (50)	71 (160)
• MAXIMUM HEAT REJECTION, kW	61	25	13
• RADIATOR AREA, m^2	71	84	16
• FRACTION OF TCS MASS FOR THERMAL CONTROL OF ENERGY STORAGE SYSTEM, kg*	560	750	140

*MASSES FOR IOC STATION, DOUBLE FOR GROWTH VERSION

Reaction Control Propellant.-The propellant required for drag makeup will vary for the three systems due to the differences in the size of the solar array. The propellant quantity of concern here is the amount associated with the solar array drag only, since the other drag areas will remain essentially constant. The solar array areas required for the RFC, battery, and IPACS concepts are 1810, 1650, and 1480 meters squared, respectively. These are for the initial Station and are doubled for the growth Station. The average annual propellant requirement for the RFC, battery, and IPACS designs is 2010, 1840, and 1650 kg. These are doubled for the growth Station. The propellant is assumed to be hydrazine, and the average orbital altitude is 500 km. It should be noted that for lower altitudes and atmospheric density extremes, these propellant consumption rates can be increased very substantially. However, these average consumption rates are most representative for the purpose of computing long-term propellant consumption.

System Servicing and Maintenance Schedule.-To support the life-cycle costing trades which follow, it is necessary to estimate the system maintenance and servicing requirements. The schedule developed for the study is presented in Table 17. To simplify the analysis, the schedule is broken into five-year intervals. The treatment of the repair of random failures or unscheduled maintenance is also simplified by lumping it in as a fraction of the scheduled maintenance. This effectively results in a pessimistic assessment of the scheduled maintenance. The percentages given in the table indicate the amount of equipment that will be changed out in each time interval. The change from the IOC Station configuration to the growth version is assumed to occur by the five-year point. For example, 100% of the initial solar array elements are added at t = 0. At the five-year point, 25% of that equipment is changed out and 100% of the growth equipment is installed. At the 10-year point, the complete initial system is changed out and 25% of the delta growth equipment is changed, etc. The simplifications and assumptions employed here reduce a very complex life-cycle cost analysis to a relatively

simple spreadsheet analysis that can be accomplished in a few hours on a personal computer.

TABLE 17.-SYSTEM SERVICING SCHEDULE

ITEM	TIME FROM IOC (YEARS)			
	0	5	10	15
ELECTRICAL POWER SYSTEM				
• SOLAR ARRAY BLANKETS • SOLAR ARRAY STRUCTURE • CABLES	100% (a)	25% (a) 100% (b)	100% (a) 25% (b)	25% (a) 100% (b)
• GIMBAL DRIVES AND ROLL RINGS	100% (a)	100% (b)	100% (a)	100% (b)
• ENERGY STORAGE (ES)				
- REGENERATIVE FUEL CELLS	100% (a)	100% (a) (b)	100% (a) (b)	100% (a) (b)
- Ni H_2 BATTERIES	100% (a)	100% (a) (b)	100% (a) (b)	100% (a) (b)
- ENERGY STORAGE WHEELS	100% (a)	25% (a), 100% (b)	25% (a) (b)	25% (a) (b)
• ES CHARGE/DISCHARGE ELECTRONICS	100% (a)	100% (b)	100% (a)	100% (b)
• CONDITIONING/REGULATION/INVERTERS	100% (a)	25% (a), 100% (b)	25% (a) (b)	25% (a) (b)
ATTITUDE CONTROL SYSTEM				
• CONTROL MOMENT GYROS (CMGs)	100% (a)	25% (a), 100% (b)	25% (a) (b)	25% (a) (b)
• CMG ELECTRONICS	100% (a)	25% (a), 100% (b)	25% (a) (b)	25% (a) (b)
THERMAL CONTROL SYSTEM				
• RADIATOR AND GIMBAL DRIVES	100% (a)	10% (a), 100% (b)	10% (a) (b)	10% (a) (b)
• HEAT EXCHANGERS, LINES, AND AMMONIA	100% (a)	5% (a), 100% (b)	5% (a) (b)	5% (a) (b)
• PUMPS AND VALVES	100% (a)	100% (a) (b)	100% (a) (b)	100% (a) (b)
REACTION CONTROL SYSTEM	NEGLIGIBLE VARIATION WITH ENERGY STORAGE TYPE			

(a) = IOC HARDWARE
(b) = ADDED HARDWARE TO ACHIEVE GROWTH CONFIGURATION

Trade Data Summary

The quantitative bases, requirements, assumptions, and ground rules for establishing the trade data have been established above. A summary tabulation of the mass of the interacting systems involved in the trade is presented in Table 18. A more detailed breakdown is presented in Table 19.

TABLE 18.-MASS SUMMARIES FOR CANDIDATE ELECTRICAL POWER AND INTERACTING SYSTEMS

ITEM	SYSTEM MASS — KG (LB)		
	REGENERATIVE FUEL CELL	Ni-H_2 BATTERIES	ENERGY STORAGE WHEELS
ELECTRICAL POWER SYSTEM (EPS)			
• POWER GENERATION	5,390 (11,890)	4,940 (10,880)	4,400 (9,700)
• PROCESSING AND CABLES	544 (1,200)	535 (1,180)	494 (1,090)
• ENERGY STORAGE	4,930 (10,960)	4,640 (10,220)	4,055 (8,940)
SUBTOTAL — KG (LB)	10,910 (24,050)	10,110 (22,280)	8,950 (19,730)
ATTITUDE CONTROL SYSTEM (ACS)	1,950 (4,290)	1,950 (4,290)	0 (0)
THERMAL CONTROL SYSTEM (TCS)	564 (1,244)	753 (1,660)	141 (311)
HARDWARE TOTAL — KG (LB)	13,420 (29,580)	12,810 (28,230)	9,090 (20,040)
ANNUAL REACTION CONTROL SYSTEM (RCS) PROPELLANT REQUIREMENT (SOLAR ARRAY DRAG ONLY)	2,010 (4,440)	1,840 (4,060)	1,650 (3,630)

TABLE 19.-IMPACT OF ENERGY STORAGE CONCEPT ON SPACE STATION SUBSYSTEMS WEIGHTS

ITEM	SUBSYSTEM MASS (kg)					
	REGENERATIVE FUEL CELL		Ni-H_2 BATTERIES		ENERGY STORAGE WHEELS	
	IOC	GROWTH	IOC	GROWTH	IOC	GROWTH
ELECTRICAL POWER SYSTEM (EPS)						
• SOLAR ARRAY (SA) BLANKETS	3,310	6,620	3,020	6,040	2,700	5,400
• SA STRUCTURE (BOOMS, SUPPORTS, AND DEPLOYMENT MECHANISMS)	1,320	2,640	1,210	2,420	1,080	2,160
• BETA GIMBAL DRIVES	218	436	209	418	177	354
• ALPHA GIMBAL DRIVES	363	726	331	662	295	590
• ROLL RINGS	181	362	166	332	148	296
• ENERGY STORAGE (ES)	4,971	9,942	3,710	7,420	3,480*	6,960*
• ES SUPPORT STRUCTURE	Included in ES		558	1,116	349	698
• ES CHARGE/DISCHARGE CONTROLLERS	Included in ES		363	726	227**	454**
• CABLES	272	544	261	522	222	444
• CONDITIONING/REGULATION	127	254	127	254	127	254
• INVERTERS	147	294	147	294	147	294
SUBTOTAL (EPS)	10,909	21,818	10,102	20,204	8,952	17,904
ATTITUDE CONTROL SYSTEM (ACS)						
• CONTROL MOMENT GYROS (CMG's)	1,700	3,400	1,700	3,400	0	0
• CMG ELECTRONICS	68	136	68	136	0	0
• SUPPORT STRUCTURE	177	354	177	354	0	0
SUBTOTAL (ACS)	1,950	3,900	1,950	3,900	0	0
THERMAL CONTROL SYSTEM (TCS)						
• RADIATORS AND GIMBAL DRIVES	496	992	617	1,234	112	224
• HEAT EXCHANGERS, LINES, AND AMMONIA	45	90	91	182	20	40
• PUMPS AND VALVES	23	46	45	90	10	20
SUBTOTAL (TCS)	564	1,128	753	1,506	142	284
REACTION CONTROL SYSTEM (RCS)						
• ANNUAL PROPELLANT REQUIRED (kg/year), SOLAR ARRAY DRAG ONLY	2,010	4,020	1,840	3,680	1,650	3,390

*Includes gimbaling for attitude control
**Includes electronics for magnetic bearings and attitude control gimbaling

These same data are presented more graphically in the bar chart of figure 21. The bar chart data are for the IOC configuration. The data for the growth configuration are double these values. Some observations may be made at this point. The IPACS approach results in savings in virtually all the systems, and has a pyramiding (compounding) influence on the savings in the other systems.

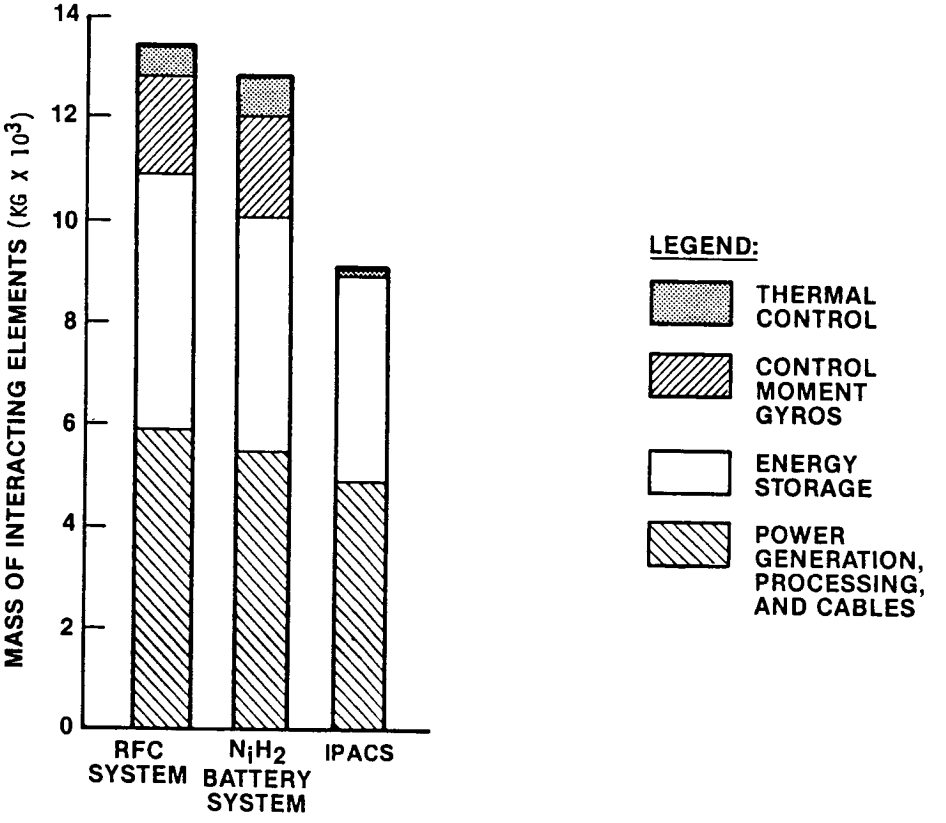

Figure 21.- Comparison of system mass (IOC)

In fact, the mass savings in some of the other systems are appreciably larger than the savings in the energy storage element itself. This is due to the powerful influence of the relatively high energy conversion efficiency of the IPACS concept (85%).

The life-cycle mass delivered to orbit is also of interest since the life-cycle costing data will be based on these data. Figure 22 presents the average annual hardware mass delivered to orbit during the post-IOC time period. The data are based on the system servicing schedule developed above. It may clearly be seen that the servicing and maintenance requirements of the RFC and battery systems require more than twice the mass of the IPACS, to be procured and delivered to orbit. This will clearly have a substantial impact on the life-cycle costs.

The cumulative mass delivered to orbit including the IOC configuration, growth configuration, and servicing is presented in figure 23. Again, the IPACS mass delivered to orbit is appreciably less than for the other two

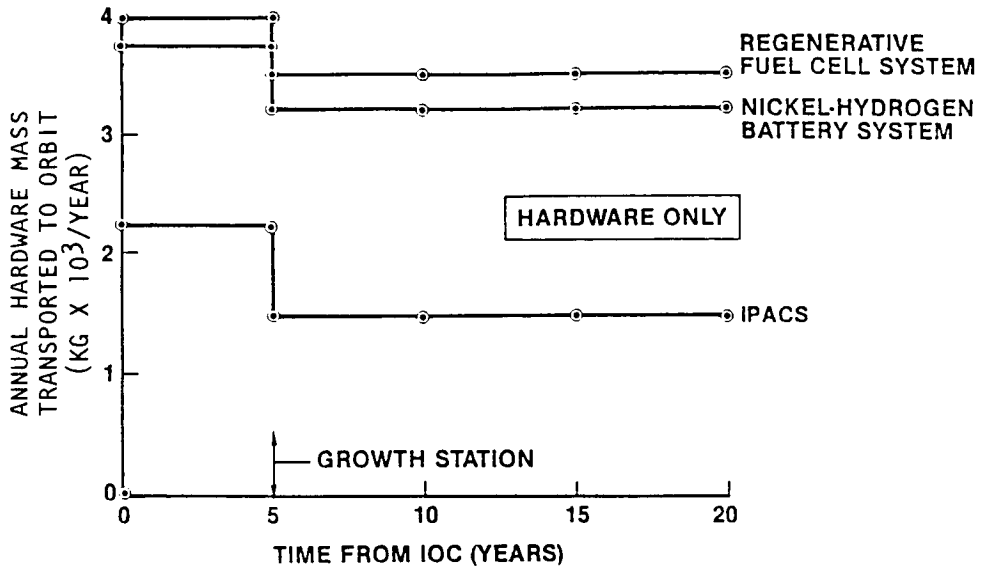

Figure 22.- Annual mass transported to orbit—
post-IOC servicing and maintenance

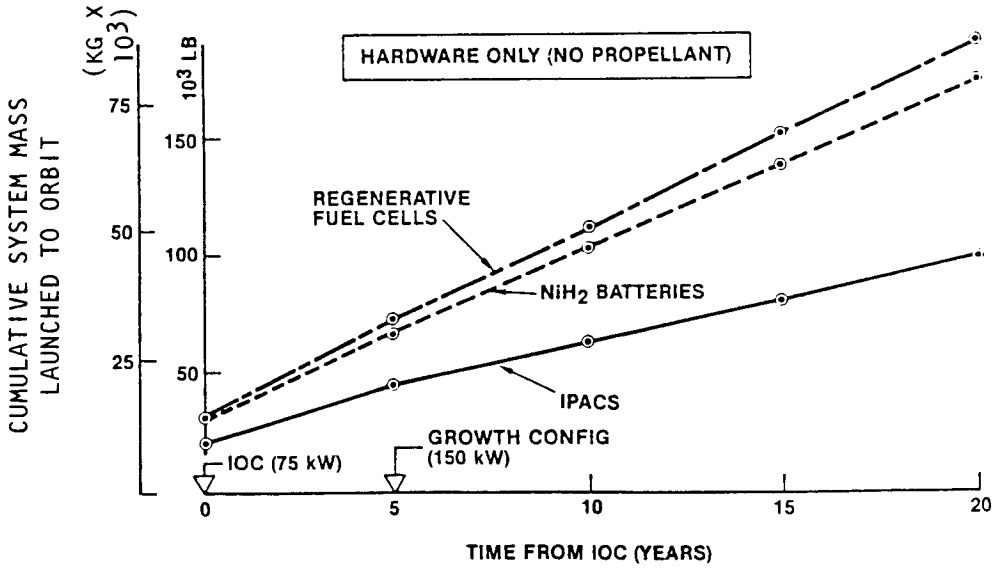

Figure 23.- Electrical power and interacting systems
cumulative launch weight versus time for
three energy storage systems

systems. The solar array drag makeup propellant is in the same order of magnitude as the hardware, but is not a major concern, since the propellant and delivery costs are small compared to the hardware items. It is concluded that the long life of the IPACS results in life-cycle mass savings that are even greater than for the IOC configuration.

Life-Cycle Cost Trades

Having developed the system definition and engineering trade data in the sections above, this section will develop cost estimates for the same systems. The items to be costed include all the subsystem items that vary as a function of the energy storage system variables, as discussed above. These include the complete electrical power system, the control moment gyros, the portion of the thermal control system needed to reject the excess heat from these elements, the drag makeup propellant required for different solar array sizes, the operational servicing and maintenance, and the transportation cost for bringing these elements to the Space Station. The cost data are developed for the initial Station (IOC) systems, the growth systems, and the maintenance and servicing through the assumed life-cycle of twenty years. A list of some of the more pertinent assumptions and ground rules employed in the study are presented in Table 20.

TABLE 20.-COSTING ANALYSIS ASSUMPTIONS AND GROUND RULES

- All costing data presented in normalized form for relative interpretation only (orginal calculations in 1984 dollars)
- Parametric pricing approach using primarily Shuttle orbiter data base
- NASA CER's used for CMG's and launch costs
- Solar array and battery CER's from extended-duration orbiter studies
- Life cycle assumed to be 20 years
- 90% Crawford learning curve used on changeout items
- Cost growth removed from orbiter CER's (design-to-cost environment assumed)
- Complexity factors furnished by subsystem design specialists

Due to the sensitive nature of cost data and the wide variations in the different costing bases employed in the industry, only normalized cost data will be presented herein. Considerable effort has been made to develop the data on common bases so that high accuracy is preserved for comparison on a relative basis. The Shuttle orbiter cost data base is the primary one employed and is based on actual program cost data. The solar array and battery cost estimates were derived from Extended-Duration Orbiter study

estimates. The CMG cost-estimating-relationships (CER's) employed are from the NASA cost data base, and were corroborated with study estimates. The IPACS CER was derived in the study. A list of some of the more dominant CER's used in the study are presented in Table 21. The complexity factors estimated by the various subsystem technical specialists are included. Again, every effort was made to develop the costing data on a common basis so as to obtain a fair comparison.

TABLE 21.-CER's FOR SELECTED COMPONENTS

Component	Normalized* CER
Solar array blankets	1.15
Regenerative fuel cells	1.46
Nickel-hydrogen batteries	0.73
Energy storage wheels	1.00
Control moment gyros	0.88

*Normalized to energy storage wheel

Cost of Initial Operational Configuration.-The system costs for the Station initial operational configuration (IOC) are given in bar chart form in figure 24. The relative magnitudes of the contributing cost items can readily be noted. It may be seen that the total IPACS cost is appreciably less than the other two candidates. The costs appear to follow the same trends that were evident in the mass breakdowns for these systems; i.e., the lower mass system costs less.

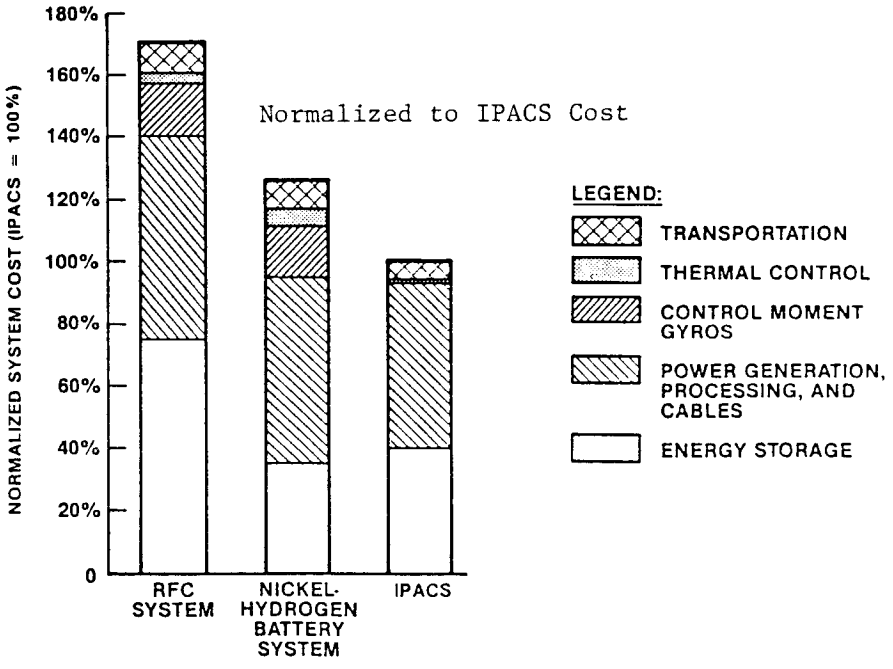

Figure 24.- Comparison of system cost at IOC

An interesting perspective regarding the IOC costs may be obtained by examining the overall CER's for the three systems (or the $/kg) that resulted from the analysis. These data are presented in Table 22. It may be seen that the $/kg for each of the three systems is somewhat comparable, and that the lower cost of the IPACS results primarily from its lower mass. This was the result of its higher round-trip energy recovery efficiency, and higher energy density.

TABLE 22.-SYSTEM COST ESTIMATING RELATIONSHIPS

System	Normalized* CER
Regenerative fuel cell system	1.152
Nickel-Hydrogen battery system	0.895
IPACS	1.00*
*CER's ($/kg) normalized to IPACS value	

Growth, Maintenance, and Servicing Costs.-The average annual cost of the three systems for growth, maintenance, and servicing over the assumed twenty-year life-cycle are illustrated in figure 25. These cost data are normalized to the IPACS average annual cost. The same trends that were apparent in the IOC costs are also apparent here. To avoid complication in the figure, the breakdown of the contributing subsystems is not given since it is very similiar to the breakdown given in the IOC bar chart. The one exception to this is in the maintenance and servicing of the IPACS units which is much less than the other energy storage systems.

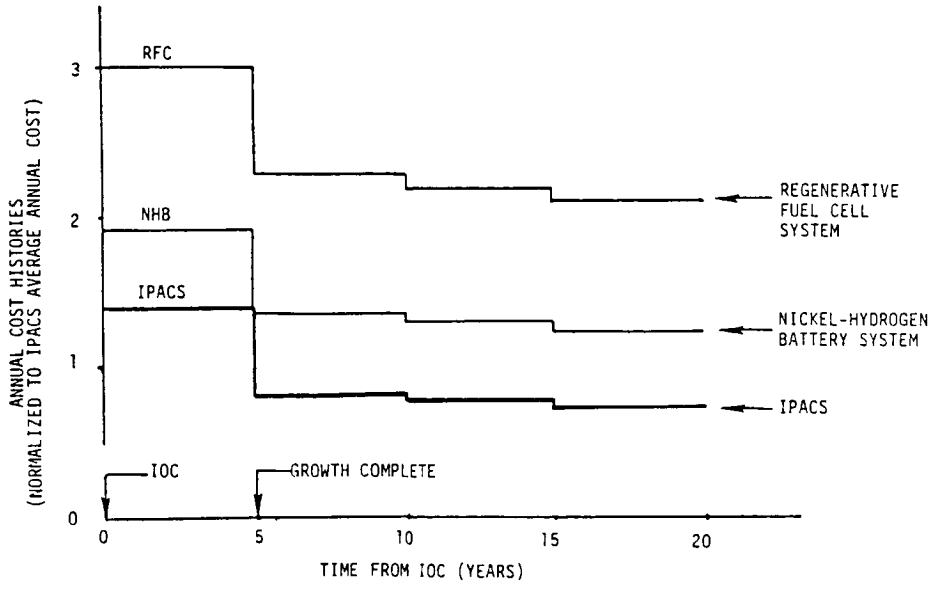

Figure 25.- Post-IOC average annual cost histories (growth, servicing, and maintenance)

Life-Cycle Costs (LCC).-The normalized LCC and IOC costs are given in Table 23. Several different normalizations are used to give perspective into the various cost aspects of these systems and for the growth/maintenance scenarios that contribute to the LCC. A time-phased cumulative cost history of these same data is presented in figure 26. Several observations may be made from these data:

- The life-cycle costs are much greater than the IOC costs, which illustrates the need for LCC analysis to get a true cost perspective for this type of problem.
- The life-cycle costs of the IPACS are much less than either of the two other systems, due primarily to the lower cost at IOC and a much lower servicing cost.

TABLE 23.-NORMALIZED COST DATA

CANDIDATE SYSTEM	INITIAL SYSTEM COST (IOC)	TOTAL LIFE-CYCLE COST (LCC)		LCC/IOC
REGENERATIVE FUEL CELL	1.70	8.51	2.34	5.01
NICKEL-HYDROGEN BATTERY	1.26	5.43	1.49	4.31
IPACS	[1.00]	3.64	[1.00]	3.64
	NORMALIZED TO IPACS COST AT IOC	RELATIVE TO NORMALIZED IPACS COSTS AT IOC	NORMALIZED TO IPACS LCC	

Cost/Risk Considerations.-In a trade study of this type it is prudent to consider the risks, both technical and programmatic, associated with each of the candidate systems being considered in the trade. These risks may then be weighed along with the cost data to reach a practical conclusion. Considerable technology development remains for each of the three candidate systems, and each is at a different level of engineering development. The risks will be discussed on a qualitative basis since a quantitative cost/risk analysis is beyond the scope of the current study. In all cases, a fall-back position is available in the form of nickel-cadmium batteries. These batteries are technically mature, and could be substituted in the event of development problems in the other candidates.

For the RFC system, the fuel cell technology is relatively mature, having been used in the Apollo and Shuttle programs. The regenerative portion of the system has seen some development for terrestrial applications (submarines). It remains to develop and qualify the higher performance techniques needed for the space application. The technical and schedule risks may be regarded as significant considering the 1987 technology readiness need date.

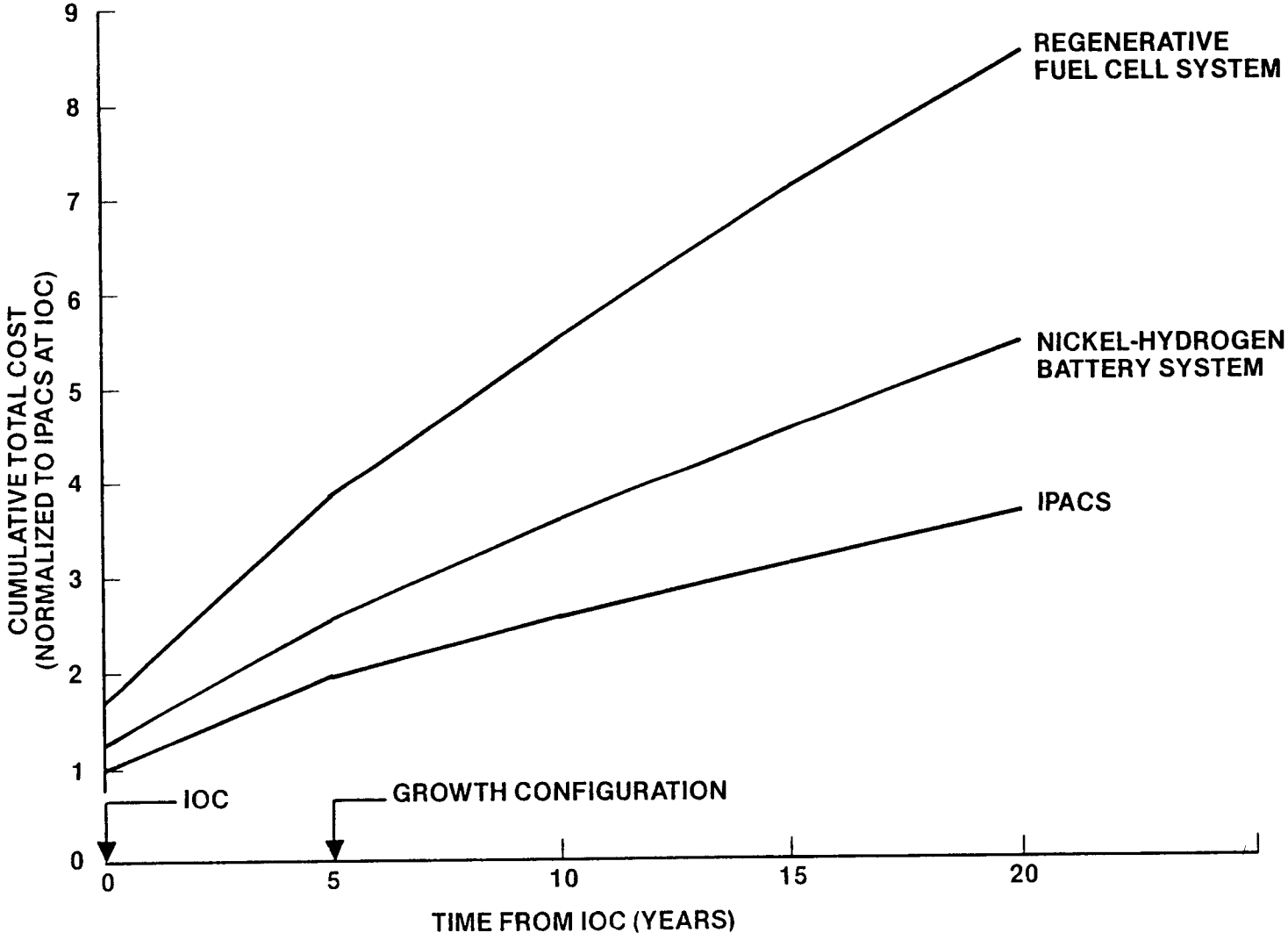

Figure 26.- Cumulative total cost histories

The NHB technology has been developed and flown for relatively low-energy density and low cycle-life applications. It remains to validate the techniques needed to achieve higher energy density, cycle efficiency, and cycle life. The Power Systems Panel of the 1983 Space Station Technology Workshop concluded that the NHB technology was not ready for Space Station. The technical and schedule risks are moderate, but could be reduced to low by accepting lower performance.

The IPACS technology has seen limited laboratory testing in the earlier IPACS program (pp. 5-21 of ref. 15), and numerous other developments primarily for terrestrial application. The development of this technology for space application during the last decade has been quite modest, and the developmental funding has been insignificant relative to the other two candidates. The fundamental technology advances that now make an IPACS concept much more attractive have occurred in three areas: composite rotors, magnetic bearings, and motor/generator/electronics. These advances are discussed in greater detail in the introductory section of this report. The technology in each of these three areas has been independently tested and validated in numerous situations. The remaining technology development is to integrate the technology from these three areas into a single unit and validate the combined system in the laboratory. The technical risk in integrating these three technologies is no higher than the risk in developing an advanced CMG. An IPACS technology development program of sufficient magnitude to provide laboratory proof-of-concept in the near future does not currently exist. For this reason, the schedule risk must be regarded as high, in light of the current IPACS development status and the assumed 1987 technology readiness need date.

A summary of the risk assessment is presented in Table 24. It may be seen that the IPACS offers the highest schedule risk and the NHB system the lowest. The principal problem with the IPACS schedule risk is due to its immature design and the lack of any significant development program. This schedule risk is deemed to be unacceptably high. However, IPACS cost advantages are substantial, and it would be a preferred approach were it not for the development schedule risk. Therefore, it is recommended that the IPACS technology development be pursued so that it can support the needs of future spacecraft.

TABLE 24.-RISK ASSESSMENT SUMMARY

System	Risk*	
	Technical	Schedule
RFC	Moderate	Moderate
NHB	Moderate	Low
IPACS	Moderate	High

*Risk scaling ranges from low, to moderate, and high.

CONCLUSIONS AND RECOMMENDATIONS

The system-level trade study has shown the IPACS to result in appreciable mass and cost savings relative to competing systems (regenerative fuel cells and nickel-hydrogen battery systems). This is true for the initial system, the growth system, and the operational life of 20 years. The mass and cost savings are greatest over the life cycle due to the lower maintenance cost of the IPACS. The mass and cost savings occur in the energy storage, solar arrays, thermal control, attitude control, drag makeup propellant, maintenance, and transportation items. These savings are due primarily to the higher energy conversion efficiency of the IPACS and attitude control system savings, and only secondarily due to higher energy density. The study conclusions are summarized in Table 25 below.

TABLE 25.-STUDY CONCLUSIONS

SYSTEM CONFIGURATION DEFINITION • System- and component-level requirements developed for Space Station application. • System trade studies indicate that a planar arrangement of five double-gimbaled IPACS wheels is the preferred configuration for initial Station. • Integration of energy storage wheels and attitude control functions (IPACS) is preferred over independent systems, and offers appreciable cost and weight savings. • Spherical, large-angle magnetic bearing design concept developed in this study is attractive alternative to more traditional mechanical gimbaling—offers savings in weight and power. Concept is very attractive for other applications, such as momentum storage/transfer equipment, and its development should not be tied solely to IPACS applications.
SYSTEM-LEVEL TRADES • IPACS offers appreciable cost and mass savings relative to competing energy storage systems. This is primarily due to higher energy conversion efficiency (85% vs. 67% for NiH_2 batteries and 55% for regenerative fuel cells)—includes savings in solar arrays, energy storage system, thermal control, drag makeup propellant, servicing, and transportation. • Life-cycle costing data indicate that the virtually unlimited life of the IPACS (>20 years) makes a major reduction in the operational servicing costs relative to the NiH_2 batteries and regenerative fuel cells (typical lifetime of five years). • Savings include smaller solar array size, energy storage mass, reduced thermal control sizing, less drag makeup propellant, and less operational servicing (equipment changeout and crew time). • Technical risks in IPACS development are small. • IPACS technology development program that will meet Space Station technology need date (1987) does not presently exist.
ROTOR DESIGN ANALYSIS • Thin-wall annular rotor is preferred shape. • Boron epoxy is preferred existing material. • Filament-wound layup. • Conservative stress derating procedure employed (10^6 fatigue cycles and 1.56 safety factors).
MAGNETIC SUSPENSION • Spherical, large-angle magnetic bearing employing Lorentz force is feasible—provides tilt angles up to approximately 20 degrees. • Bearing losses (including torquing and orbit rate precession) less than one percent of delivered power.
ENERGY CONVERSION • MOSFET power semiconductors preferred circuit approach. • Permanent magnet ironless (PM rotating back-iron) motor/generator selected. • Roundtrip energy conversion efficiency of 85% is feasible.
INTEGRATED COMPONENT ANALYSIS • 22 Wh/kg energy density is achievable with conservative design, current materials, and circuitry (includes attitude control capability). • Projected near-term materials advances and less conservative safety factor (with lab test experience) can double available energy density.

An advanced Integrated Power and Attitude Control System (IPACS) design concept employing a thin-wall annular composite rotor, a new spherical large-angle magnetic bearing, and highly efficient motor/generator/circuitry has been developed. Conservative system energy densities of 22 Wh/kg (10 Wh/lb) and round-trip energy recovery efficiencies of 85% are feasible using current materials, circuitry, and conservative design practices. New composite materials now emerging can potentially double the energy density.

A system-level trade study indicates that the IPACS approach can result in substantial life-cycle cost and mass savings relative to regenerative fuel cell (RFC) or nickel-hydrogen battery (NHB) systems. This is primarily due to higher energy recovery efficiency and much longer operational life.

A spherical large-angle magnetic bearing design concept has been developed that is an attractive alternative to the more traditional mechanical gimbal and single-axis torquer systems. The bearing permits appreciable weight and power savings in the IPACS application, as well as in other spacecraft momentum transfer attitude control system and pointing system applications.

The three basic technology areas required for an advanced IPACS (composite rotors, magnetic bearings, and highly efficient motor/generator/electronics) are now mature and ready for this application. It remains to perform a laboratory validation of an IPACS that integrates these three proven technologies into a single system.

An IPACS technology development program of sufficient magnitude to meet the Space Station technology readiness need date of 1987 does not presently exist. The lack of an IPACS detailed design concept and laboratory test data for an engineering model unit precludes its serious consideration by the Electrical Power System community. It is the major recommendation of this study that an appropriate technology development program be established that will make this technology available, both for future manned and unmanned spacecraft applications. Table 26 presents a more detailed summary of recommendations for the development of this technology.

TABLE 26.-RECOMMENDATIONS FOR FUTURE WORK

• Perform further design optimization and laboratory demonstration of the advanced IPACS concept developed in this study.
• Perform early laboratory demonstration of subscale magnetically suspended composite rotor to demonstrate high-energy storage density and conversion efficiency.
• Perform further design trades and optimization of the large-angle spherical bearing approach. Its potential utility in other momentum storage equipment dictates that its development proceed independent of the IPACS technology development.
• Power conversion electronics efficiency advances highly desirable (dominant loss item).
• Investigate thermal control techniques for motor/generator (conventional conduction paths non-existent).
• Develop safe touchdown bearing design approaches and validate through testing.
• Rotor-to-hub attachment structure poses design challenge.
• Perform rotor dynamics investigations and develop necessary design guidelines to assure robust stability.
• Define preferred design approaches for reconfiguring system after one and two wheel failures.

APPENDIX A

ROTOR DESIGN ANALYSIS

by
Patricia A. Burdick

Introduction

The flywheel rotor is a key component of the proposed IPACS design because the system's overall performance is strongly dependent upon its storage capacity and interfacing compatibility with other hardware. It is desirable to specify a rotor configuration most suitable for the application of interest, which first necessitates understanding how various design factors influence the performance level. The end goals of this study are, therefore:

- To investigate the factors of rotor design
- Ultimately to reach conclusions about "best" designs for the IPACS application

It is noted that "best" design here is defined as that which allows high integrated system performance with acceptable developmental risk. As commonly encountered, tradeoffs are likely among the various measures of performance; thus, more than one design may meet IPACS needs.

Approach.-The work effort is divided into two areas, reflecting the two primary factors of rotor design. First, potential rotor materials are evaluated to determine relative merits and the state of associated technology. The scope of this study emphasizes modern high-performance fibrous composites, including those with metal matrices. Degradation of mechanical properties due to fatigue is also considered. The concluding remarks identify areas of necessary development.

Secondly, attention is given to rotor profile to determine the effect on storage capacity of various parameters used to describe the flywheel's geometry. Emphasis is placed on those profiles, both solid and annular with variable thicknesses, suitable for fibrous composites. Computations include only those stresses induced by rotation; other dynamic and environmental effects are addressed in the concluding section as important future concerns.

In general, conclusions and recommendations are based largely on results from the materials and profile studies. However, findings from other flywheel research programs are also reflected, as much useful information has been generated by government and private agencies in recent years. In addition, the final section discusses component scaling to meet the IPACS requirements introduced in the next paragraphs. Parametric rotor scaling data are developed in a form that is suitable for use in Appendix E (Integrated Component Design Trades) for final component sizing.

Design Criteria.-Three different sources were used when establishing IPACS design criteria:

Source	Type of Criteria
• NASA/Rockwell	Basic performance: energy, momentum, service life, and volume constraints
• Composite materials industry	Fabrication: limitations in part geometry and process reliability
• Draper Laboratory	System integration: operating speeds, dimensional stability, and geometry preferences.

Basic performance requirements are considered the primary measures, with other criteria serving as necessary guidelines.

Materials

Although development of modern composites dates from the 1930's when glass fiber production began, so-called "advanced" (structural) composite technology is considered by many to coincide with the introduction of boron filaments (around 1960, refs. 50, 51). Carbon fibers, available since 1959, were first used when phenolic resins in rocket nozzles; however, their first structural uses came after improved pyrolysis methods resulted in "high-modulus" products (1965). At this same time, the DuPont Corporation marketed aramid fibers under the Kevlar trademark. Thus, moving into the 1970's, the primary reinforcing fibers fell into one of three basic categories (ref. 51): boron-based, carbon/graphite, and organic (aramid). That decade saw extensive development of these fibers (such as coatings to improve matrix capability), reinvestigation of experimental fibers (such as alumina), and the intorduction of new reinforcements (e.g., silicon-carbide filaments). Table 27 contains a list of primary reinforcements, enabling a comparison of their respective material properties.

TABLE 27.- COMPARISON OF FIBER PROPERTIES

Fiber	Diameter (μm)	Specific Gravity	Tensile Strength (MPa)	Tensile Modulus (GPa)	Source of Data*
1. Boron	100-200	2.46-2.57	3516	400	AVCO
2. HS-Graphite	100-280	1.80	3103	234	Hercules, Inc. (AS fiber)
3. Aramid	15	1.44	3792	128	Dupont & Co., Inc. (Kevlar® 49)
4. S-Glass	10	2.49	4137	87	Owens-Corning Fiberglas, Inc. (S-2 Glass®)
5. Silicon Carbide	140	3.04	3447	427	AVCO
6. Alumina	20	3.90	1379	379	Dupont & Co., Inc. (Fiber FP®)

*Also used: ref. 63 and 64

When combined with a suitable matrix, fibrous reinforcements have distinct advantages over common isotropic materials (refs. 52, 53), including:

- High specific strength and stiffness resulting in sizeable weight and/or performance improvements
- Synergistic ability which combines the assets of constituents while suppressing flaws (thus frequently surpassing predicted properties based on simple mixture rules.
- Performance "tailorability," allowing optimal structure design heretofore not possible.
- Versatility due to the essentially infinite combinations of materials available to the intelligent designer.

A major consideration in achieving these benefits is selection of the matrix, which falls into one of three categories: polymeric (e.g., epoxies), metallic, and ceramic (refractory). The first two classes are appropriate for structural use, with polymeric-matrix composites (PMC's) receiving much attention in the past two decades (refs. 52, 54). In contrast, metallic-matrix composites (MMC's), such as reinforced aluminum, were investigated under aerospace auspices in the 1960's but not fully developed due to severe fabrication difficulties (refs. 51, 53). However, at present, there is a resurgence of interest backed by government funding and much improvement in these latter materials is occurring (refs. 55, 56, 57).

Composites in Flywheel Design.-When used in flywheel components, fibrous composites are attractive for several reasons. In addition to high specific properties and fiber-placing ability, these materials fail in a benign mode when excessively stressed (refs. 20, 58, 59); this non-fragmentable disintegration compares favorably with the dangerous manner observed in metallic components and is discussed more extensively later. These perceived advantages resulted in various technical investigations, many in the U.S. under government auspices (refs. 58, 60). One such program was organized by the Department of Energy. It commenced in the mid-1970's and emphasized fiber-reinforced resins (ref. 61). Although limited in focus, the program (through 1981) resulted in much useful information concerning material and rotor designs. A summary of these designs is presented in Table 28. Results of the DOE program aided in establishing a list of viable flywheel materials (Table 29) for this study. In addition to PMC's, metal-matrix types are included; these materials have become attractive due to recent technical advances in MMC fabrication processes (refs. 51, 55) not developed at the time of the DOE study. The properties in Table 29 may not represent very new improvements in the materials listed, but do reflect accepted nominal values. Also, use of moderate properties lends conservatism to the study's results, as discussed later in this report.

Titanium, beryllium, and particulate MMC's were also initially considered. However, in discussions with M. Mittnick of AVCO's Specialty Materials Division in Lowell, Massachusetts, and from reference 62, it has been confirmed that titanium still presents severe compatibility problems to designers,

TABLE 28.-SUMMARY OF DOE ROTOR PROGRAMS

Developer	Design Description	Materials			Maximum Energy Density (Wh/kg)
		G-Glass/ Epoxy	Aramid/ Epoxy	Graphite/ Epoxy	
Brobeck	Multi-material/rim with tension-balanced spokes	X	X		63.7
Garrett	Multi-material/rim with graphite/ epoxy hub	X	X		79.6
Hercules	Wound, contoured rim	(graphite/polysulfone)			37.5
Rocketdyne	Wound rim with overwrap and Al twin-disk hub			X	36.2
LLNL	Tapered, laminated disk			X	62.6
LLNL	Quasi-isotropic disk	X			67.3
General Electric	Alpha-ply, laminated disk with graphite epoxy rim	X			56.4
OCF/Lord	Laminated SMC disk with graphite/ epoxy rim	(S-Glass/polyester)			27.8
AVCO	Radially/circumferentially reinforced disk	X			70.6
API	Sub-circular rim on four-spoked Al hub		(Metglas®)		24.5

Note: Based on informations from Reference 10

TABLE 29.-AVERAGE PROPERTIES OF FIBER-REINFORCED COMPOSITES

Fiber/Matrix	Specific Gravity	Static Tensile Strength (MPa)	10^6-Cycle Tensile Strength (MPa)	Tensile Modulus (GPa)	Poisson's Ratio
PMC					
1. Boron/Epoxy	2.02	1324 (69)	1062 (55)	207 (21)	.21 (.02*)
2. HS-Graphite/ Epoxy	1.52	1448 (62)	869 (37)	131 (9)	.25 (.02)
3. Aramid/Epoxy	1.38	1379 (28)	965 (19)	76 (6)	.34 (.02*)
4. S-Glass/Epoxy	1.99	1558 (41)	310 (8)	55 (21)	.30 (.02*)
MMC					
5. Boron/Aluminum	2.63	1413 (139)	690 (68)	207 (131)	.23 (.12)
6. HS-Graphite/ Aluminum	2.35	621 (21)	310 (10)	200 (24)	.24* (.12*)
7. HS-Graphite/ Magnesium	1.94	690 (21)	586 (18)	276 (28)	.27 (.13*)
8. Silicon Carbide/ Aluminum	2.91	1517 (110)	896 (66)	207 (117)	.26 (.15)
9. Alumina/Aluminum	3.32	552 (190)	414 (145)	214 (145)	.24*(.12*)

Note: Values in parentheses indicate direction normal to fiber axis.
* Indicates estimated values

due to fiber degradation at the high fabrication temperature involved. Beryllium is attractive for its high specific properties, but its toxicity is a serious deterrent (ref. 51). Aluminum-matrix composites offer similar and reliable properties. The latter (particulate) class (e.g., silicon carbide-aluminum and beryllium-titanium) is still highly experimental, and preliminary property data do not indicate suitability for rotor usage (ref. 57). Thus, these materials were eliminated at an early stage. Propery data in Table 29 are based on published values as well as those from contacts made within the composites industry. A summary of these sources is contained in Appendix B. Both static and derated (fatigue) properties are given for comparison, with the latter estimated in many instances due to insufficient data.

Materials Comparison.-Different rotor materials can be compared by assuming a common geometry and loading, and calculating measures of performance. A simple annular flywheel of uniform axial thickness (equal to the outer radius) is chosen for several reasons.

- It is a convenient profile allowing straightforward calculation of maximum speed, given a material's mechanical properties. Also, displacement at the inner radius can be determined as an indication of dimensional stability. Refer to Appendix B for details.
- The results can serve as baseline checks for later computations involving more complicated profiles.
- It is a suitable geometry for fibrous composites, which can be wound to place maximum strength in the circumferential direction. (Many of the DOE prototypes used this principle.)

Derated material properties are used in calculations to reflect a 10^6-cycle lifetime. Once determined, the maximum rotational speed possible for each material can be used to calculate energy and momentum-storage quantities as defined below:

- Energy per mass, e_m = KE/M
- Energy per volume, e_v = KE/V
- Momentum per mass, h_m = H/M
- Momentum per volume, h_v = H/V

Where: KE = total energy stored, M = rotor mass, V = rotor volume, and H = total momentum stored. These and other measures (to be discussed) are ultimately used to rank the materials.

Results.-Table 30 contains calculated performance quantities for each material. The data are for an annular rotor with an inner to outer radius ratio of 0.7. These values form the basis for a relative comparison of material attributes. To rank the materials (relative to each other), a set of four pertinent categories was established.

- Energy storage (e_m and e_v used)
- Momentum storage (h_m and h_v used)
- Dimensional stability (displacement values used)
- Technology readiness (subjective measure of materials state of development).

TABLE 30.-MATERIALS STUDY—RESULTS OF CALCULATIONS

Material	Max Tip Speed (m/sec)	Maximum Speed, R = .305 m(12.0 in) (rad/sec)	e_m (Wh/kg)	e_v (kWh/m^3)	h_m (Nms/kg)	h_v (KNms/m^3)	Displacement at r = R_i (m x 10^{-2})
1. Boron/Epoxy	765	2510	60.6	122.0	173.5	353.9	1.09
2. HS-Graphite/ Epoxy	795	2608	65.3	97.6	180.1	274.6	2.03
3. Aramid/Epoxy	641	2103	42.6	61.0	145.5	201.4	1.96
4. S-Glass/Epoxy	350	1147	12.6	24.4	79.4	158.7	0.23
5. Boron/Aluminum	539	1770	30.2	79.3	122.6	323.4	0.10
6. HS-Graphite/ Aluminum	347	1140	12.6	30.5	78.9	183.1	0.23
7. HS-Graphite/ Magnesium	513	1682	27.1	54.9	116.4	225.8	0.36
8. Silicon Carbide/ Aluminum	584	1916	35.3	103.7	132.5	384.4	0.15
9. Alumina/Aluminum	372	1219	14.3	48.8	84.5	280.7	0.05

Note: Details of calculations are contained in Appendix B

It is not clear at this time which attributes should govern a selection for the IPACS design; therefore, all categories were weighted equally. Table 31 lists the ratings, with low numbers assigned to attributes of high storage capacity, low displacement, and high state of development. A total rating was obtained by simple summation. To view these final values, consider a moderate-performance material receiving average ratings in each category; the total in this case would equal:

$$5 + 5 + 5 + 5 + 5 + 2 = 27$$

TABLE 31.-MATERIALS STUDY—FINAL RATINGS

Material	(1) Energy Storage (e_m)	(e_v)	(2) Momentum Storage (h_m)	(h_v)	(3) Dimensional Stability	(4) State of Technology	(5) Total Rating
1. Boron/Epoxy	2	1	2	2	7	1	15
2. HS-Graphite/ Epoxy	1	3	1	5	9	1	20
3. Aramid/Epoxy	3	5	3	6	8	1	26
4. S-Glass/Epoxy	8	9	8	9	5	1	40
5. Boron/Aluminum	5	4	5	3	2	1	20
6. HS-Graphite/ Aluminum	9	8	9	8	4	3	41
7. HS-Graphite/ Magnesium	6	6	6	7	6	3	34
8. Silicon Carbide/ Aluminum	4	2	4	1	3	2	16
9. Alumina/Aluminum	7	7	7	4	1	2	28

Rating System

(1), (2): 1 through 9, with 1 = highest storage value
(3): 1 through 9, with 1 = lowest displacement value

(4): Subjective rating with 1 = available materials
2 = materials in developmental stage
3 = new materials in experimental stage

(5): Total = sum of ratings (1) through (4)

Thus, materials with ratings below this average are considered the most attractive rotor candidates. Aramid/epoxy and alumina/aluminum fall into the "moderate" class; however, four materials have noticeably lower final ratings: boron/epoxy, HS-graphite/epoxy, boron/aluminum, and silicon carbide/aluminum. Later computations will emphasize materials of this latter class.

Rotor Profile

Energy or momentum storage devices have been in use for centuries, resulting in extensive study of optimal profiles (refs. 58, 59). These analyses assumed use of metallic materials, with well-established and isotropic mechanical properties. In contrast, the study of composite-material rotors is relatively new, despite the perceived potential for great performance improvement over isotropic counterparts (refs. 20, 60). The newness of advanced composites is one reason for past research inactivity: these materials in many cases still lack a satisfactory level of reliability and property data (refs. 50, 51). However, their very nature is also a drawback, for inherent anisotropy requires more complex analytical models and techniques. Although much progress has been made in developing mathematical tools (refs. 53, 63), the fiber-matrix interactions which so strongly influence material behavior are still not fully understood.

Focus of Study.-One goal of the previously mentioned DOE program was to establish analytical tools appropriate for composite rotor design. These methods were employed by the various participants, resulting in a number of different prototypes (refer to summary in Table 28). The program helped to identify potential advantages and drawbacks of these different types, which can be generally categorized as solid ($R_i = 0$) or annular ($R_i > 0$). Candidates from both categories should be considered when beginning an investigation of rotor shapes. Those suitable for composites include: (solid) laminated disks, with uniform or variable (axial) thickness; and (annular) filament-wound rims, with uniform variable thickness. Figure 27 illustrates these two basic types. As demonstrated in the DOE program, "hybrid" geometries are also possible by combining the two types; however, these many combinations are considered outside the scope of this work. Indeed, given time and budgetary constraints, it is desirable to narrow (rather than widen) the focus of this study. This is accomplished by comparing solid and annular classes in a qualitative manner.

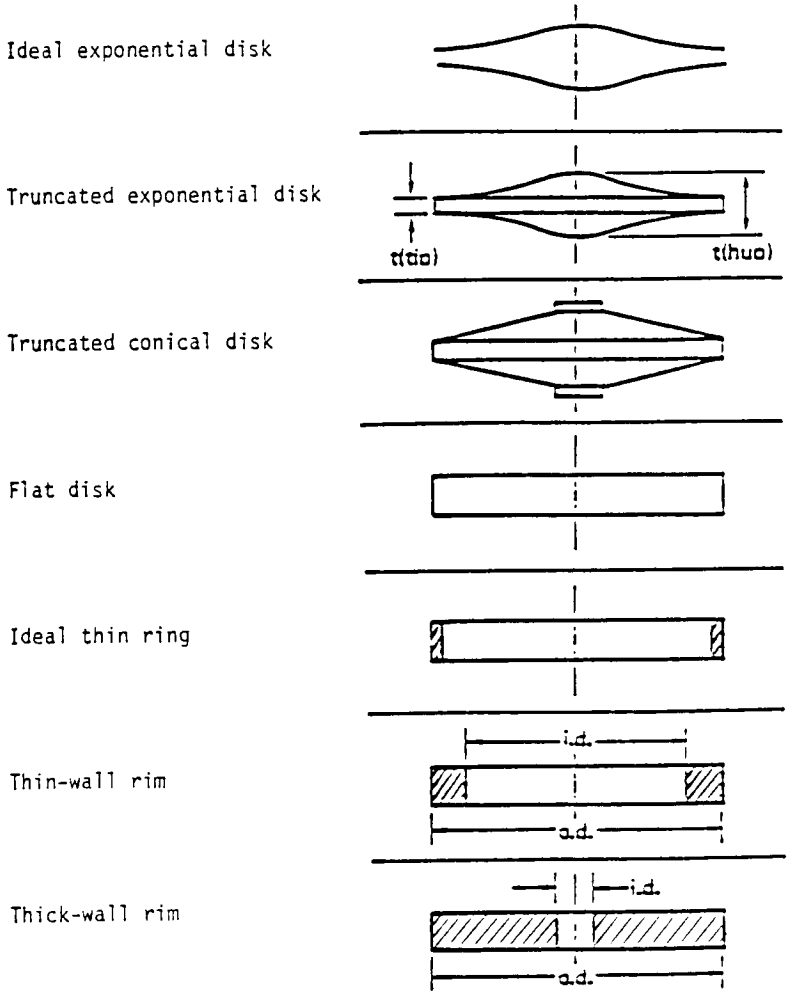

Figure 27.-Solid and annular rotor shapes

Solid composite rotors are commonly fabricated using ply lamination or (MMC) casting methods. Brush-type designs are radially reinforced with continuous fibers, while "quasi-isotropic" disks use continuous or chopped fibers to approximate uniform properties in the plane of the rotor. The literature indicates that these rotors do not fully utilize fiber strengths (refs. 59, 65). The first fail prematurely due (mostly) to uneven stress along the fiber, while the second sacrifice the high directional properties that make fibrous composites attractive. Axial thickness is a salient concern, as thick sections may suffer from incomplete cures, internal flaws, and high void content (ref. 10). Non-destructive testing techniques, continually sought to aid in quality verification, are complicated by the multiphase nature of the material (ref. 10). Variable profiles are obtained by shaped molds and/or subsequent machining; the first is a convenient and time-saving feature if possible, while the second may result in damaged surface fibers. Shaft attachment is achieved with hubs either elastomerically or mechanically adhered to the rotor surface (ref. 20). Problems have arisen when using these methods, resulting in premature rotor failures during testing, and this area is identified as needing much development (ref. 66).

Construction of the second (annular) class of composite rotors may employ filament winding, a technique developed for both polymeric and metallic matrices. From Table 28, it is seen that one-half of the DOE designs fall into this category. Variable profiles can be precisely formed during the winding process, making subsequent griding operations unnecessary. Also, any desired pre-tensioning can be included during fabrication, and is considered an effective way to improve stress distribution and radial stability (ref. 10). Radially thick parts are feasible using "stepped" cure procedures or nested rim concepts (refs. 66, 67), while large axial dimensions are possible by drawing on demonstrated composite-pipe technology. Wound cylinders constructed using these techniques are reported to utilize their weight very efficiently for storage (ref. 65). Shaft attachment for annular designs is commonly achieved via a spoke-hub system which may or may not be part of the original winding mandrel (refs. 20, 65, 67).

Two other factors are relevant to this comparison of solid and annular designs. First, the Draper Laboratory has investigated the suitability of an annular shape in an energy-storage/attitude-control system (ref. 18); the available interior region makes possible convenient and efficient integration of rotor and adjacent hardware. A second relevant factor involves the IPACS system of interest. Large-scale energy requirements, possibly resulting in large rotor dimensions, make less attractive any fabrication methods limited at this time to small-scale components. These considerations, along with previous comments, influenced the decision to emphasize annular geometries in this study; this class of rotors appears best to utilize both the advantageous attributes of composites, through circumferential fiber placement, and the highly developed techniques of filament winding.

Parametric Investigation.-An annular geometry is described by specifying the inner radius (R_i), outer radius (R), and the variation of axial thickness (t) with radial position [i.e., profile t(r)]. The following parameters are useful:

- Radius ratio, $\alpha = R_i/R$
- Slope of profile, m = m(r)

The rotor profile can be dependent on radial position in either a linear or nonlinear manner. As a first step, linear functions are considered (i.e., m(r) = constant). More complex profiles are possible as extensions of this preliminary work. Figure 28 shows schematically the various shapes of interest. In the following text, descriptive terms "flared," "annular," and "conical" correspond to positive, zero, and negative slope values, respectively. These values of m are varied between practical negative and positive limits, while those of α range between 0.1 and 0.9.

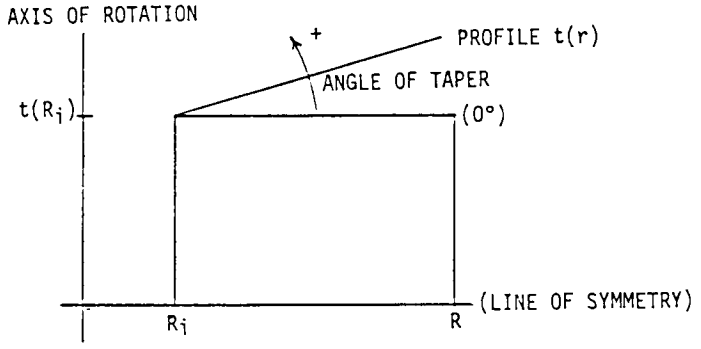

Definition of Parameters:

R = outer radius

R_i = inner radius

α = radius ratio, R_i/R

m = slope of profile = $\tan^{-1}$ (angle of taper)

t(r) = rotor profile (i.e., variation of axial thickness with radial position)

Note: For a linear profile, $t(r) = m\,r + r_o$ (m = constant)

Figure 28.- Definition of parameters describing rotor geometry

The first goal in the profile study is to determine the effects made on performance by the m and α parameters; trends thus observed will aid later when possible IPACS designs are investigated. A parametric study was completed using the following procedure:

- As previously described, energy and momentum quantities were expressed in terms of rotor geometry and rotational speed.

- For various m and α values, energy (and momentum) terms were calculated as explained in Appendix B.

- Results were plotted as functions of m and α to indicate the effect of each parameter on storage capability.

Graphical results can use a variety of forms. Figure 29 is one example, illustrating the relationship between energy density and rotor geometry for different rotational speeds. It allows several observations concerning the significance of geometry parameters.

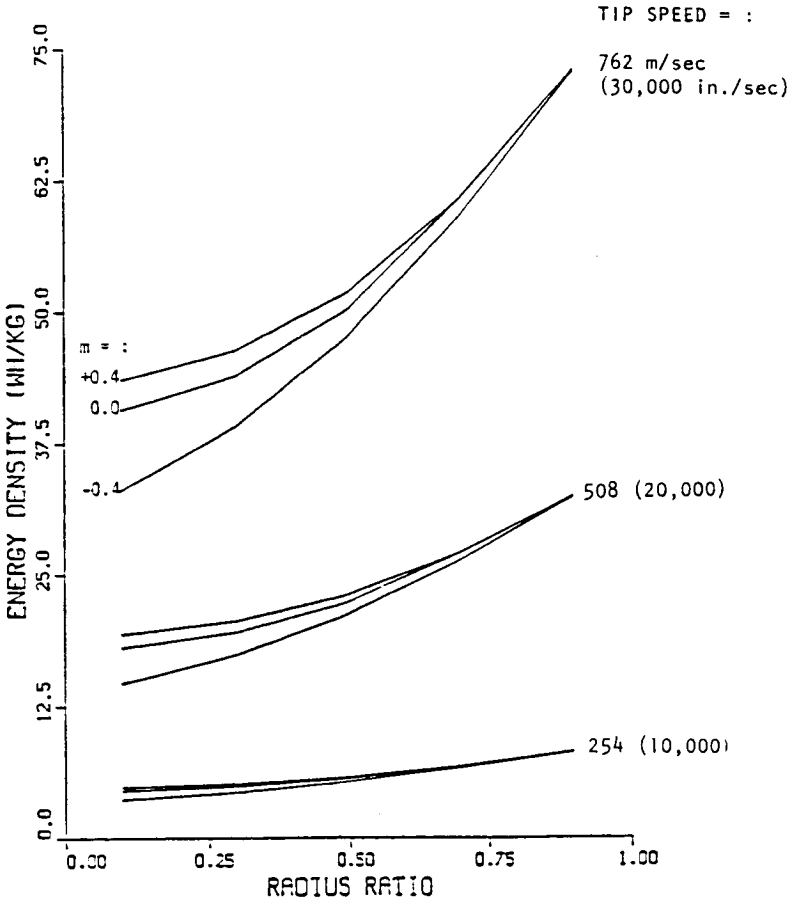

Figure 29.- Energy density as a function of radius ratio and profile slope at several rotational speeds

Effect of Radius Ratio.-The upward-sloping curves in figure 29 indicate that energy density increases with radius ratio. Thus it appears that high values of α will result in the most storage capability. From a materials viewpoint, "thin-wall" geometries are well-suited for filament-wound

composites, as they have reduced stresses in the weakest (radial) direction compared with "thick-wall" counterparts. Fabrication problems are also minimized.

Effect of Profile Slope.-Figure 29 also shows that (for each rotational speed) curves corresponding to negative, zero, and positive m values converge at high radius ratios. Thus, when using the attractive "thin-wall" geometry, the effect of rotor shape on performance is greatly diminished and selection of profile brings other factors (e.g., cost and ease of fabrication) into more prominence.

If relatively thick-walled rotors are considered, the most advantageous profile slope is not unique. It depends on the type of operating situation which exists for a given application. For example, if the condition is speed-limited (such as when bearing capabilities constrain system operating speed), then "flared" geometries yield highest storage density. Figure 29 corresponds to this case, and illustrates the observation: at each rotational speed, the positive m curve lies above the other two. Intuitively, "flared" shapes have the greatest moments of inertia and thus yield highest storage values if speed is specified.

In stress-limited situations, the most appropriate shape is that which allows highest rotational speed for a given stress level. To examine this case, a method was developed to relate speed and stresses induced by rotation. Appendix B contains a description of these speed-stress computations. Results therein show that negative-slope (conical) profiles have the greatest speed capability, given a stress-level constraint. Once again, this observation is intuitive: conical shapes concentrate mass at the interior region where maximum stresses occur.

It is important to note that while storage densities increase with some m and α values, the total energy and momentum stored may decrease due to differences in mass and volume. Each design must be examined to ensure that all performance requirements are satisfied.

IPACS Rotor Sizing

The following conclusions, established in the preceding text, are employed in the rotor sizing.

- Four composite materials appear particularly attractive for IPACS usage, considering performance potential and state of development. These are boron/epoxy, graphite/epoxy, boron/aluminum, and silicon carbide/aluminum.

- Annular geometries appear best suited to utilize the attractive attributes of composite materials, and are emphasized here. In this

category, thin-wall (high-alpha) designs offer performance and fabrication advantages.

- Using available theoretical and finite-element techniques, maximum speeds can be related to geometry and material properties, and form the basis for sizing computations.

- A number of tradeoffs exists as parameters are varied, making necessary the examination of individual designs to ensure that performance levels are met. Designs can be evaluated using the sizing procedure described below.

Rotor Sizing Procedure.—One of the ultimate objectives of this entire rotor design study is to evaluate potential material/profile combinations meeting specified requirements. The IPACS rotor design requirements are approximately:

- Energy storage per wheel, KE = $\approx$20 kWh (5-wheel system)
  = $\approx$15 kWh (6-wheel system)

- Momentum storage per wheel, H = $\approx$140 kNms (5-wheel)
  = $\approx$120 kNms (6-wheel)

- A (system) design lifetime of 10^5 cycles

- A (system) volume appropriate for Shuttle transport

The penultimate requirement is reflected by using derated strength properties to determine maximum allowable speeds. As indicated earlier (Table 29), 10^6-cycle fatigue values were determined for use in earlier calculations; available fatigue data commonly correspond to this length of run-out. Also, 10^6-cycle properties give conservatism to the reported results, as will be discussed.

The first two requirements incorporate anticipated circuit losses in the IPACS design, but do not include derating factors for safety purposes. In accordance with common aerospace practice (ref. 7), maximum speeds are thus reduced an additional amount; that is, maximum operating speed = 0.80 (maximum stress-limited allowable speed). The implications of speed-derating will be discussed subsequently.

Two materials are chosen to illustrate the sizing procedure: (1) boron/epoxy, due to its high performance rating relative to other material candidates; and (2) boron/aluminum, to allow a comparison between PMC and MMC performance using a common reinforcement. The following steps are used:

1. Maximum allowable speeds are determined for each material, as explained in Appendix B. These are derated to yield maximum operating values. Each material is thus characterized by a final tip speed operating limit which is a strong function of radius ratio.

2. A maximum operating speed of 8,000 to 12,000 rpm is chosen to reflect energy conversion system design preferences. A minimum operating speed of 4,000 to 6,000 rpm (50 percent speed variation) is selected as the desired minimum based on motor/generator performance considerations).

3. Maximum speeds from step 1 allow calculation of maximum radius values as a function of α. Once again, an assumption of inner-radius height equal to R is made as a convenient starting point. Axial height need not be constrained for filament-wound parts (as wound-pipe technology has demonstrated), and gives leverage advantages in bearing operation.

4. Corresponding volume, mass, energy, and momentum quantities are calculated as functions of α, based on expressions developed earlier; refer to Appendix B for computational details. Energy and momentum can be plotted as functions of geometry parameters to indicate rotor designs meeting the specified requirements. If necessary, the initial operating speed is modified and the procedure repeated.

Sizing Results.-Maximum allowable speeds for annular boron/epoxy and boron/aluminum rotors are reflected in the tip speed operating quantities, plotted as a function of α, in figure 30. It is seen that the tip speed term decreases after $\alpha = \approx 0.5\text{-}0.6$. This trend is generally observed for composite rotors, and indicates the point at which radial stresses become dominated by those in the tangential direction (refs. 58, 45). Use of

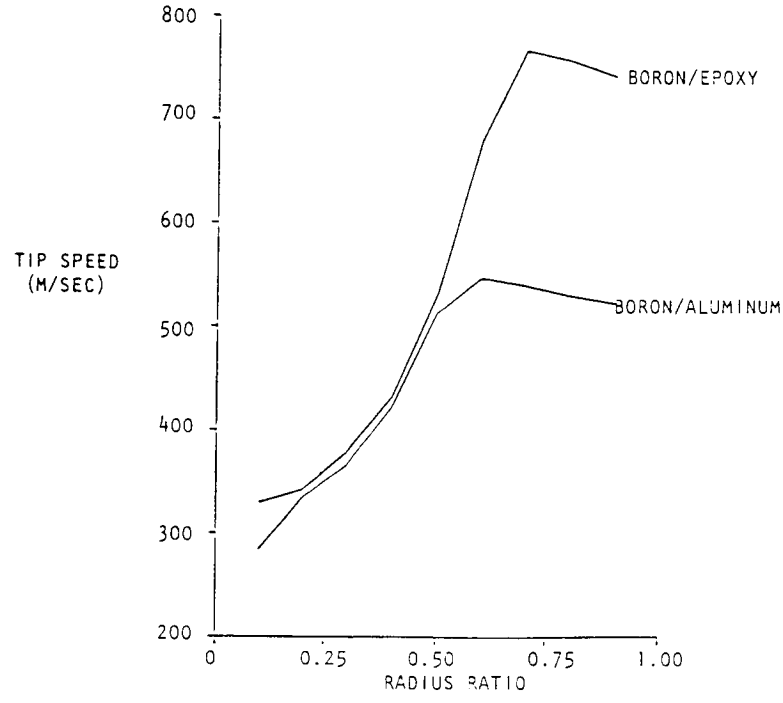

Figure 30.- Tip speed versus radius ratio for boron-reinforced annular rotors

α values in this high range emphasizes the great tangential strength of filament-wound composites. In contrast, isotropic materials show a uniform decrease in tip speed values as α increases; their high radial strengths are neither required nor well used in thin-wall rims where radial stresses are minimized.

Radius, volume, mass, energy, and momentum quantities are calculated for boron/epoxy and boron/aluminum rotors for various operating speeds; partial results are tabulated in Appendix B and are based on the expressions and assumptions discussed there. For illustrative purposes, stored energy and momentum for a 10,000-rpm operating speed are graphed as functions of α in figures 31 and 32, respectively; values correspond to an annular profile, with the five-wheel performance requirements also shown. Figures of this type are particularly convenient in scaling computations, as obtainable rotor performance can be easily compared with required levels. For example:

- Figure 31 indicates that annular boron/epoxy rotors with $0.6 < \alpha < 0.8$ will meet 5-wheel IPACS criteria using a 10,000 rpm operating speed, while corresponding boron/aluminum rotors do not show sufficient storage capability.

- Figure 32 indicates that the momentum requirement is generally satisfied if sufficient energy storage is achieved.

By lowering the operating speed (thus increasing the allowable radial dimension), higher energy and momentum storage is obtained. This increase in performance is achieved at the expense of compactness (as volume and mass increase) and fabrication ease (as wall thickness increases). Tradeoffs of this type, as previously mentioned, are common in engineering practice and all factors must be considered when determining the most suitable IPACS rotor design(s). The parametric sizing results given here are utilized in the Integrated Component Design Analysis section for final rotor sizing.

Based on the work completed in this study, the following observations are made. First, several composite-material rotors have high performance potential, particularly thin-rim designs requiring high circumferential strength. Filament winding is one fabrication technique which has reached a high state of development and is very suitable for rim-type rotors with any chosen profile. Wall thicknesses must be limited or accommodated by stepped consolidation, but axial length is not as crucial a concern. Thus, this particular configuration appears suitable for applications with large storage requirements (leading to large rotor dimensions).

Stress Derating Procedure and Impact on Energy Storage.-The second observation concerns the large degree of conservatism included in this study. Performance estimates should be viewed while noting the following:

- Properties of materials candidates used in calculations do not reflect recent technical developments in composite technology. Projections of future fiber and composite strengths (such as included in reference 20) indicate tremendous improvements in performance which would translate to higher rotor storage capabilities.

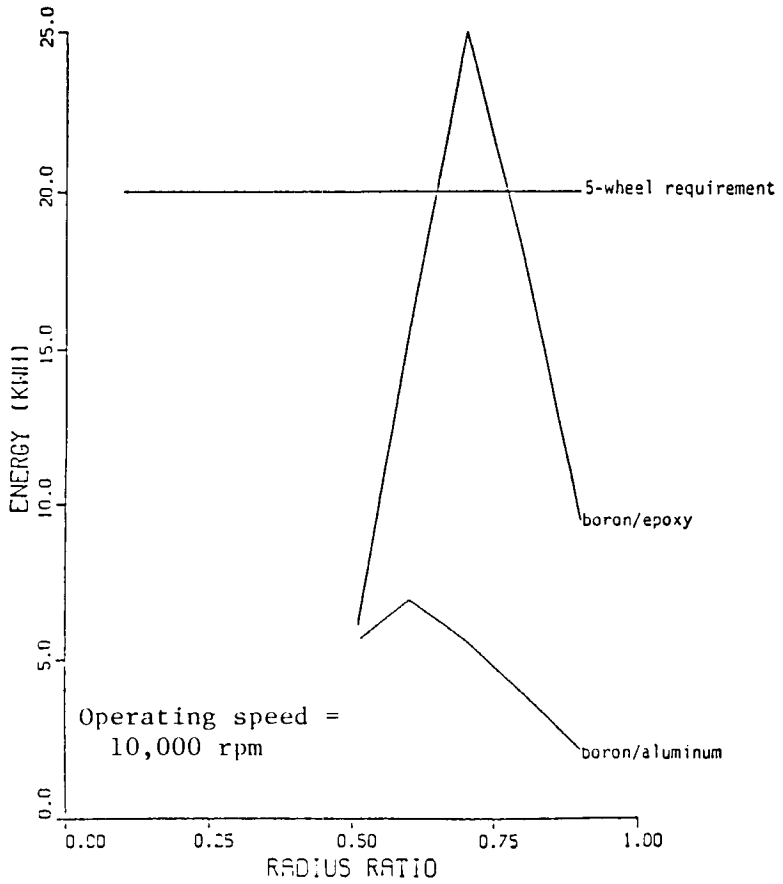

Figure 31.- Energy versus radius ratio

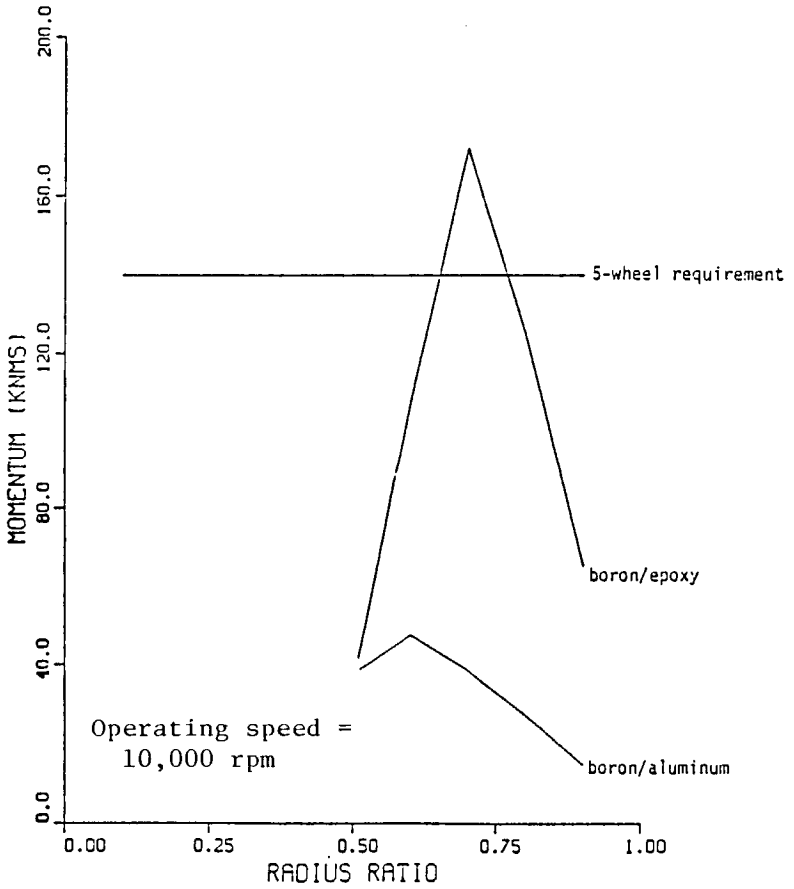

Figure 32.- Momentum versus radius ratio

- As previously mentioned, these moderate properties were derated to a level lower than the 10^5-cycle lifetime specified. More data were available for 10^6-cycle tests and these values were used in calculations.

- A 0.80 derating factor was applied to the calculated maximum speed, rather than strength, of each material when determining storage quantities.

This last point in particular deserves clarification, as the method of applying derating factors strongly affects performance estimates and its importance is easily overlooked. To begin, use of derating factors is a common practice in engineering design; indeed, it is a necessary one for developing technologies such as the flywheel storage and composite materials of interest here. However, the manner in which these factors are applied can vary, as does the degree of conservatism which results. For example, in this study, the maximum operating speed for a given rotor design was determined by: maximum operating speed = 0.80 (maximum allowable speed). Noting that $KE = 1/2\ I\omega^2$, this practice, in effect, derates the total energy to 0.64 of the maximum amount. Similarly, the maximum rotor stresses are reduced to 0.64 of the maximum allowable value. A less conservative approach is to apply the derating factor to material strength instead of rotor speed. Noting that σ is proportional to ω^2, this method results in: (maximum operating ω^2) = 0.80 (maximum allowable ω^2). Thus, total energy stored is derated by the same (0.80) amount.

To illustrate the derating procedure, consider the constant-thickness annulus used in the materials study. Boron/aluminum is chosen as the example material and the same computational procedure is employed. The various derating steps and corresponding energy storage are summarized in Table 32.

TABLE 32.- STRESS DERATING

Derating Step	Basis of ω_{max}	ω_{max} (rad/sec)	KE at ω_{max} (kWh)	Stress Derating (% of Yield)
1. No derating	Yield strength (1413 MPa)	2531	7.46	100
2. Fatigue considered	Fatigue strength—10^6 cycles (690 MPa)	1770	3.65	49
3. Derating factor applied:				
(a) Strength x 0.80	Fatigue strength x 0.80	1582	2.91	39
*(b) Speed x 0.80	Fatigue strength x 0.64	1416 (1770 x 0.80)	2.33	31

The asterisk indicates the method employed in this study. Comparison of 3(b) with 3(a) shows that the manner by which derating factors are applied does affect performance estimates. Note that energy storage 3(b) is the lowest in the table, well below the value corresponding to underrated yield strength. Thus, the technique amployed herein yields very conservative

results. The need to establish clearly the degree of conservatism appropriate for a given application is discussed further in the following Conclusions and Recommendations section.

Conclusions and Recommendations

The following conclusions are drawn regarding rotor material selection, rotor shape, and fabrication method:

1. Four composite materials appear to be particularly attractive for IPACS rotors. These are boron/epoxy, graphite/epoxy, boron/aluminum, and silicon carbide/aluminum.

2. An annular rotor shape is preferred and is best suited to utilize the anisotropic properties of composite materials. Thin-wall designs offer high performance, and can employ simple, proven filament-winding fabrication methods.

3. Conservative stress derating procedures have been employed. Rotor energy densities twice those indicated in this study are estimated to be possible using more advanced materials and less conservative stress derating (achievable with laboratory testing experience).

The following issues are recommended for future investigations:

1. It is important to maintain an awareness of the improvements in existing reinforcements (such as graphite), new composites (such as those using aluminum and magnesium matrices), and fabrication processes (such as composites casting) which are continually occurring. These developments will affect the performance levels which can be achieved using composite rotors. As previously mentioned, it is anticipated that improved properties of these new material systems will result in appreciably greater storage capabilities than those presented here. In fact, materials with approximately 80% greater strength than those used herein became available a few months after the study completion.

2. Simplifying assumptions deemed appropriate for this preliminary study (given in Appendix B) should be examined before more detailed analyses are commenced. Also, computation of composite-rotor storage capability is limited in accuracy by the lack of available data, especially that pertaining to high-cycle fatigue properties. Designs based on present data and a reasonable degree of conservatism can be used with confidence; however, this information must be viewed with the possible sources of inaccuracy kept in mind.

3. The degree of conservatism appropriate for rotor designs in space applications should be specifically determined. Much derating of maximum performance values was included in this preliminary study and

results should be viewed accordingly. Less conservative practices may be more appropriate, including: less fatigue derating (although this area is susceptible to inaccuracies due to the dearth of composites data); use of current properties which credit materials with recent technical improvements; and, application of derating factors to material strength rather than maximum rotor speed, since energy storage is proportional to specific strength in a linear manner.

4. Salient issues such as shaft attachment (i.e., hub design), dynamic instabilities (such as whirl and critical-speed locations) and temperature effects must be reviewed before any design reaches a final stage. While outside the scope of this present study, the information herein forms a basis for further evaluations incorporating these design concerns. Finite-element analytical techniques, such as those employed here, are particularly appropriate for this type of work.

APPENDIX B

ROTOR DESIGN CALCULATIONS AND MATERIALS DATA SOURCES

by

Patricia A. Burdick

Valuable information concerning the state of composites technology was obtained from members of the composites community, where much active development is taking place. Contacts of particular value are included in Table 33.

TABLE 33.- MATERIALS DATA SOURCES

Source	Type of Information Supplied			
	Materials	Fabrication	Literature	Meeting
1. ALLIED CHEMICAL Parsippany, NJ	X		X	X
2. AVCO, Lowell, MA	X		X	X
3. AMMRC, Watertown, MA	X			X
4. DUPONT & CO., INC. Wilmington, DE	X		X	X
5. DWA COMPOSITE SPECIALITIES, INC. Chatsworth, CA		X	X	
6. DYNAMET TECHNOLOGY Burlington, MA		X	X	X
7. EXXON ENTERPRISES Fountain Inn, SC		X	X	
8. FMI, Biddeford, ME		X	X	
9. HERCULES, INC. Southfield, MI	X	X	X	
10. IMT, INC., Handover, MA		X	X	
11. MCI, Columbus, OH		X	X	
12. MIT MATERIALS PROCESSING CENTER Cambridge, MA	X	X		X
13. OWENS-CORNING FIBERGLAS, INC. Granville, OH	X		X	
14. TECHNIWEAVE, INC. E. Rochester, NH		X	X	X
15. UNION CARBIDE CORP. Danbury, CT	X		X	

Calculation Details

Theoretical Maximum Speeds.-A relationship between geometry, speed, and material properties must be established before maximum rotor speed can be determined. In the case of a constant-thickness annulus ($0.0 < \alpha < 1.0$), a closed-form expression is available based on theoretical development (ref. 70)

$$(\omega_r)^2 = \frac{1}{R^2}\left(\frac{8}{3 + \nu_r}\right)\left(\frac{1}{\rho}\right)(\sigma_r)\left(\frac{1}{1 - \alpha}\right)^2 \tag{B1}$$

$$(\omega_\theta)^2 = \frac{1}{R^2}\left(\frac{4}{3 + \nu_\theta}\right)\left(\frac{1}{\rho}\right)(\sigma_\theta)\frac{1}{1 + \left(\frac{1 - \nu_\theta}{3 + \nu_\theta}\right)\alpha^2} \tag{B2}$$

where: ω = rotational speed

σ = tensile strength

ν = Poisson's ratio

ρ = material density

$\alpha = \frac{R_i}{R}$

R = outer radius of rotor

R_i = inner radius of annular rotor

and subscripts r and θ refer to the radial and tangential directions, respectively.

In the case of a simple annulus, calculation of radial displacement u(r) (due to rotational stresses) is also straightforward (ref. 70). At the inner radius:

$$u(R_i) = \frac{\rho\omega^2 R^3}{8E_r}\left[(3 + \nu_r)(1 - \nu_r)(\alpha^2 + 1)\alpha + (3 + \nu_r)(1 + \nu_r)\alpha - (1 - \nu_r^2)\alpha^3\right] \tag{B3}$$

where E = tensile modulus.

Development of Energy and Momentum Expressions.-It is useful to relate energy and momentum quantities to rotor geometry, speed, and material properties; that is,

energy (KE) = f[R, t(r), ω,ρ], and

momentum (h) = f[R, t(r),ω,ρ].

where: R = outer radius

t(r) = rotor profile

ω = rotational speed

ρ = material density

Note that:

$$M = \rho \cdot V$$
$$KE = \frac{1}{2} I\omega^2 \qquad \text{(B4)}$$
$$H = I\omega$$

where M = mass, V = volume, and I = moments of inertia. KE and H are total stored energy and momentum, respectively.

Thus:

$$e_m = \frac{KE}{M} = \frac{\omega^2}{2} \frac{I}{\rho V}$$
$$h_m = \frac{H}{M} = \omega \frac{I}{\rho V} \qquad \text{(B5)}$$
$$h_m = \frac{2}{\omega} e_m$$

where e_m = energy density, and h_m = momentum density.

With geometry parameters as defined in figure 28, and a linear profile $t(r) = m \cdot r + r_o$ (with m = constant), expressions for inertia I and volume V are derived (ref. 71):

$$\left.\begin{aligned} I &= 4\pi\rho \int_{R_i}^{R} r^3 \cdot t(r)\, dr \\ &= 4\pi\rho \left[\frac{m}{5} (R^5)(1 - \alpha^5) + \frac{r_o}{4} (R^4)(1 - \alpha^4)\right] \\ &\text{since} \quad R_i = \alpha R. \\ V &= 4\pi \int_{R_i}^{R} r \cdot t(r)\, dr \\ &= 4\pi \left[\frac{m}{3} (R^3)(1 - \alpha^3) + \frac{r_o}{2} (R^2)(1 - \alpha^2)\right] \end{aligned}\right\} \qquad \text{(B6)}$$

Using equations (B6) in e_m and h_m expressions yields:

$$\left.\begin{aligned} e_m &= (\omega R)^2 \left[\frac{Am + B}{Cm + D}\right] \\ h_m &= \left(\frac{2}{\omega}\right)(\omega R)^2 \left[\frac{Am + B}{Cm + D}\right] = \left(\frac{2}{\omega}\right) e_m \end{aligned}\right\} \quad \text{(B7)}$$

where: $A = \frac{1}{20}(\alpha^5 - 5\alpha + 4)$

$$B = \frac{1}{4}(1 - \alpha^4)\left[\frac{t(R_i)}{R}\right]$$

$$C = \frac{1}{3}(\alpha^3 - 3\alpha + 2)$$

$$D = (1 - \alpha^2)\left[\frac{t(R_i)}{R}\right]$$

Also:

$$\left.\begin{aligned} e_v &= \frac{KE}{V} = \frac{KE}{(M/\rho)} = \rho\left(\frac{KE}{M}\right) = \rho(e_m); \text{ and, similarly} \\ h_v &= \rho(h_m) \end{aligned}\right\} \quad \text{(B7 cont.)}$$

It is perhaps useful to relate these developed expressions into the commonly used concept of rotor shape factor. In the literature (such as refs. 20, 58, 59),

$$\frac{KE}{m} = e_m = K\left(\frac{\sigma}{\rho}\right)$$

where: K = flywheel shape factor, a measure of how efficiently a rotor geometry uses rotational stresses

$\frac{\sigma}{\rho}$ = material specific strength

The concept of shape factor is relatively straightforward for isotropic materials (refs. 20, 60). However, in the case of anisotropic composite rotors, it is convenient to separate K into two parts, say

$$K = K_1 \cdot K_2$$

where K_1 depends on geometry only, while K_2 depends on other effects including material properties, so:

$$e_m = K_1 \cdot K_2 \left(\frac{\sigma}{\rho}\right)$$

Now, from equations (B7),

$$e_m = (\omega R)^2 \cdot C_1$$

where C_1 is the developed expression which depends only on geometry parameters; and,

$$(\omega R)^2 = C_2 \left(\frac{\sigma}{\rho}\right)$$

from equations (B1) and (B2), where C_2 is a function of geometry and material properties. Together

$$e_m = C_2 \left(\frac{\sigma}{\rho}\right) \cdot C_1$$

or, in the above form,

$$e_m = C_1 \cdot C_2 \left(\frac{\sigma}{\rho}\right)$$

Thus, the developed expression in (B7) can be thought of as a portion of the total shape factor for annular-type composite rotors; that is, the portion depending only on rotor geometry.

Parametric Computations.-To evaluate the effects of geometry (m and α parameters) on rotor performance, expressions (B7) are incorporated into a simple computerized algorithm. Defining ERATIO = $e_m/(\omega R)^2$, the procedure and necessary input are shown in figure 33. Sample output values in Table 34 pertain to an inner-radius height equal to the outer radius; that is $t(R_i) = 0.5R$. The ERATIO values allow calculation of energy and momentum quantities given specified values of rotor speed (ω) and radius (R).

$$\begin{aligned} e_m &= \text{ERATIO} \cdot [\omega \times R]^2 \\ h_m &= \left(\frac{2}{\omega}\right) \text{ERATIO} \cdot [\omega \times R]^2 \end{aligned} \qquad \text{(B8)}$$

Volumetric (e_v, h_v) and total (KE, H) quantities require further specification of material density, ρ:

$$\left.\begin{aligned} e_v &= e_m \cdot [\rho] \\ h_v &= h_m \cdot [\rho] \\ KE &= e_m \cdot [\rho \cdot V] \\ H &= h_m \quad [\rho \cdot V] \end{aligned}\right\} \qquad \text{(B8 cont.)}$$

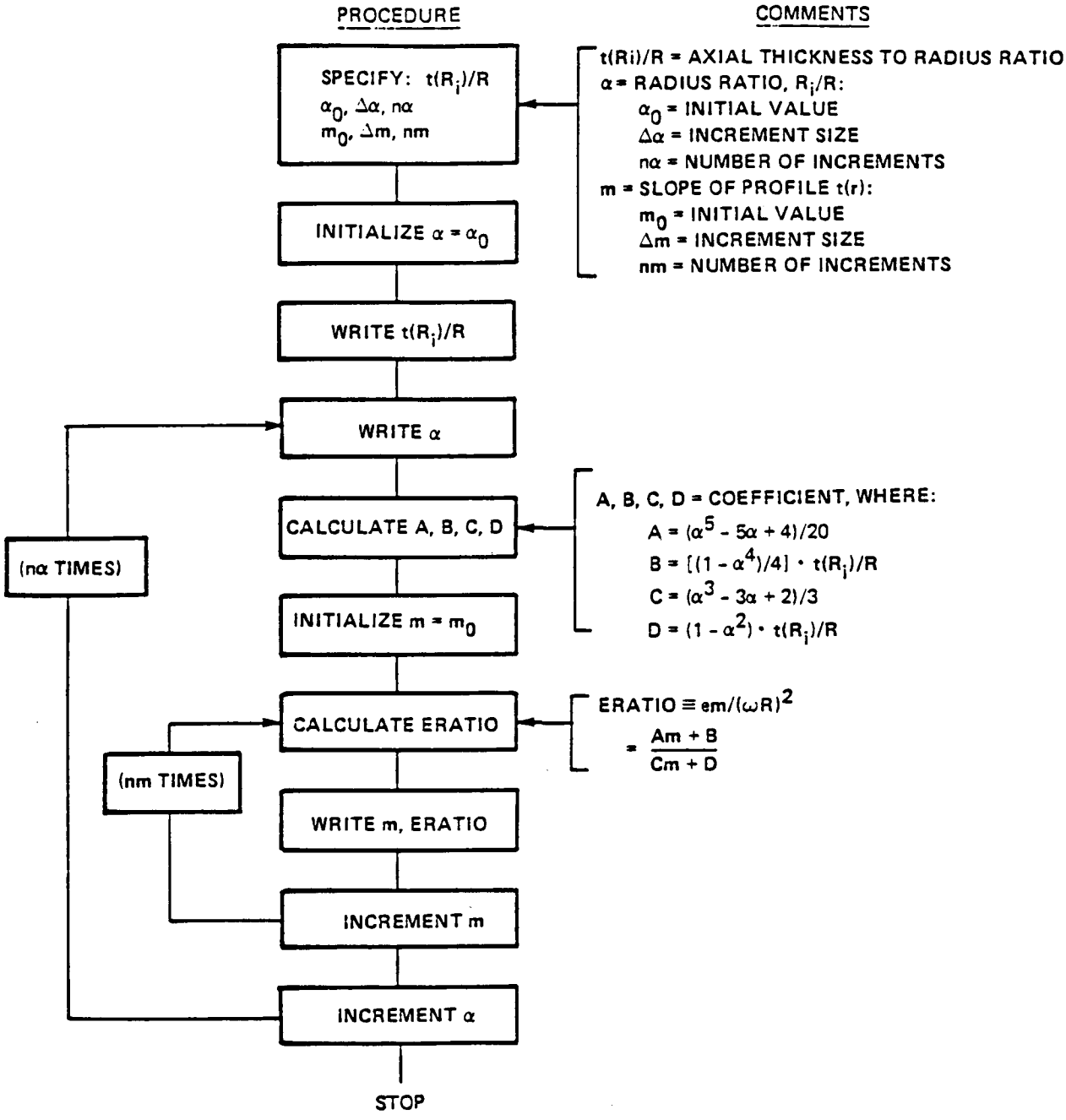

Figure 33.- Flow chart for parametric computations

TABLE 34.-SAMPLE OUTPUT: PARAMETRIC COMPUTATIONS

	ERATIO		
α	m = -0.4	m = 0.0	m = +0.4
0.1	5.694×10^{-5}	7.008×10^{-5}	7.502×10^{-5}
0.3	6.736	7.567	7.984
0.5	8.240	8.678	8.955
0.7	10.181	10.465	10.469
0.9	12.547	12.564	12.581

Note: Values based on assumption that total height = outer radius; i.e., $t(R_i) = 0.5R$

Slope (m) and radius ratio (α) defined in figure 28

Units of ERATIO are $\left(\frac{Wh \cdot sec^2}{kg \cdot m^2}\right)$

Maximum Speeds for Variable-Thickness Geometries.-A method is needed to determine maximum speed given a rotor's material properties and geometry. The basic problem is one of estimating stresses induced by rotation and comparing these values to the defined strength of the rotor material, However, rotor profiles which differ from a constant-thickness disk or annulus will lead to complicated theoretical expressions requiring numerical solutions. The process in these cases is time-consuming and requires much iteration (ref. 70). An attractive alternative is stress calculation using finite-element analysis (FEA) (references 65, 66); it can be easily adapted to any geometry and yields results with very satisfactory accuracy. The latter technique is employed here, with previous calculations (pertaining to the constant-thickness annulus) providing a means for checking the validity of this approach.

Six finite-element models were used to establish trends in relative stress levels. For each, the outer radius and total axial height at the inner radius equaled 0.229 m (9.0 in.). Using parameters as defined in figure 28, the models can be described as follows:

Geometry	m	α
Conical	-0.4	0.2 = 0.046/0.229 (= 1.8/9.0) 0.7 = 0.160/0.229 (= 6.3/9.0)
Annular	0.0	0.2 0.7
Flared	+0.4	0.2 0.7

An available finite-element program allows computation of stresses induced by rotation. In addition to geometry definition, material properties must be specified. Radial and tangential stresses plotted as a function of speed allow comparison with material (fatigue) strengths, thus determining approximate maximum speeds for each material geometry.

To illustrate, consider boron/aluminum with properties as given in Table 29. Using the annular (i.e., constant-thickness) geometries, stresses were computed for several different speeds; the corresponding graphs are shown in figure 34. Also indicated are maximum radial and tangential strengths for this material. Comparison allows maximum speeds to be estimated.

α	$\approx\omega_r$ at (σ_r) max	$\approx\omega_\theta$ at (σ_θ) max
0.2	13,000 rpm	24,000 rpm
0.7	37,000	23,000

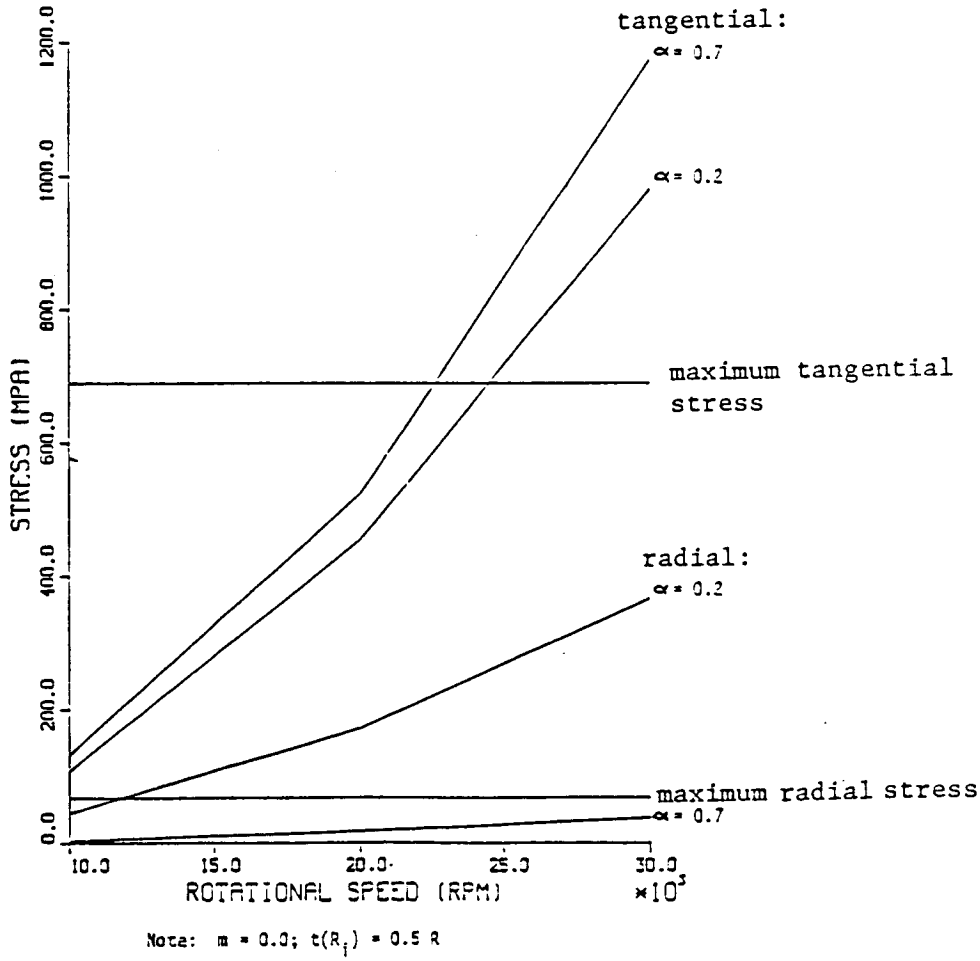

Figure 34.- Stress versus rotational speed for boron/aluminum

For each model, the lowest speed is used as the maximum value, and indicates which stresses (radial or tangential) are the limiting quantities. Thus,

α	limiting stress	ω_{max}
0.2	radial	$\approx$13,000 rpm
0.7	tangential	$\approx$23,000 rpm

Note that, for $\alpha = 0.7$,

$$(\omega R) = (23{,}000 \times \frac{\pi}{30}) \frac{\text{rad}}{\text{sec}} \cdot (0.229 \text{ m})$$

$$= 552 \text{ rad} \cdot \text{m/sec}$$

which is close to the theoretical value (539 rad • m/sec) shown in Table 30.

Repeating the procedure for conical and flared profiles gives the following results for the $-0.4 < m < +0.4$ range investigated:

- Thick-wall geometries are limited in their operating speed by radial stresses, while thin-wall rotors are limited by those in the tangential direction. The latter is a desirable condition for composite rotors with circumferential reinforcement.

- For $\alpha = 0.2$, different shapes yield different stresses (and corresponding maximum speeds). Conical shapes have the lowest stresses at each speed, thus giving higher maximum speeds than the annular and flared shapes. This result agrees with intuitive expectations: the conical profile has mass concentrated at the interior region where maximum tangential and radial stresses occur (ref. 70).

- For $\alpha = 0.7$, stresses and maximum speeds are approximately equal for all profiles.

The first and third observation above will be used to simplify the sizing calculations, as explained in the following section.

IPACS Sizing Calculations.-Energy and storage calculations based on relationships developed in the previous sections are incorporated into a simple sizing algorithm. The procedure and required input values are described in figure 35. Sample output is contained in Tables 35, 36, and 37 for boron/epoxy and boron/aluminum using:

$t(R_i) = R$

$m = -0.4$ (conical), 0.0 (annular), and +0.4 (flared)

System operating speeds = 8,000 (Table 35), 10,000 (Table 36), and 12,000 (Table 37) rpm.

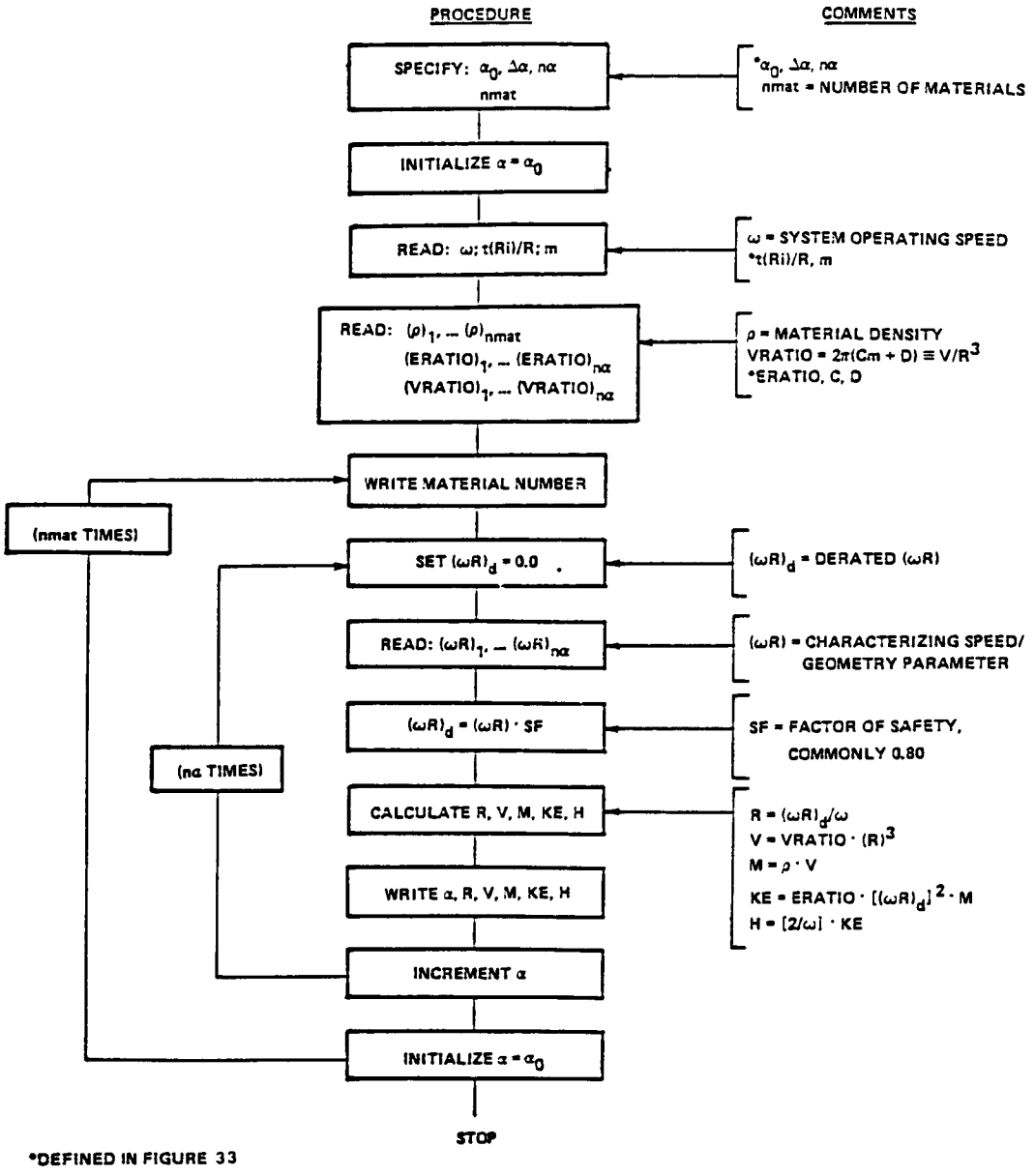

Figure 35.- Flow chart for scaling calculations

TABLE 35.-SCALING CALCULATIONS (OPERATING SPEED = 8,000 RPM)

		Boron/Epoxy					Boron/Aluminum				
α	m	R	V	M	KE	H	R	V	M	KE	H
0.5	-0.4	.508	.239	482.0	7.16	61.6	.490	.215	566.3	7.86	67.6
	0.0	.508	.307	619.5	9.70	83.3	.490	.277	727.9	10.6	91.4
	+0.4	.508	.375	757.3	12.2	105.	.490	.338	889.8	13.4	115.
0.7	-0.4	.729	.544	1098.9	41.9	360.	.513	.190	499.7	9.44	81.1
	0.0	.729	.623	1258.4	48.7	418.	.513	.218	572.2	11.0	94.4
	+0.4	.729	.702	1418.6	55.6	477.	.513	.245	645.0	12.5	108.
0.9	-0.4	.706	.201	406.4	17.8	153.	.498	.070	184.9	4.03	34.6
	0.0	.706	.208	419.4	18.4	158.	.498	.073	190.8	4.16	35.7
	+0.4	.706	.218	440.9	19.4	167.	.498	.076	200.6	4.38	37.6

Note: Units are: radius (R) = m; volume (V) = m^3; mass (M) = kg;
total energy (KE) = kWh; total momentum (H) = KNms.
Calculations assume total height equal to outer radius R.

TABLE 36.-SCALING CALCULATIONS (OPERATING SPEED = 10,000 RPM)

		Boron/Epoxy					Boron/Aluminum				
α	m	R	V	M	KE	H	R	V	M	KE	H
0.5	-0.4	.406	.122	247.1	3.67	25.3	.391	.110	290.4	4.03	27.7
	0.0	.406	.157	317.6	4.97	34.2	.391	.142	373.2	5.46	37.5
	+0.4	.406	.192	388.3	6.27	43.1	.391	.174	456.2	6.88	47.3
0.7	-0.4	.584	.279	563.4	21.5	148.	.411	.097	256.2	4.84	33.3
	0.0	.584	.319	645.2	25.0	172.	.411	.112	293.4	5.63	38.7
	+0.4	.584	.360	727.4	28.5	196.	.411	.126	330.7	6.43	44.2
0.9	-0.4	.564	.103	208.4	9.14	62.9	.399	.036	94.8	2.06	14.2
	0.0	.564	.106	215.0	9.45	65.0	.399	.037	97.8	2.13	14.7
	+0.4	.564	.112	226.1	9.94	68.4	.399	.039	102.9	2.25	15.4

Note: Units and assumptions as listed in Table 35

TABLE 37 .-SCALING CALCULATIONS (OPERATING SPEED = 12,000 RPM)

		Boron/Epoxy					Boron/Aluminum				
α	m	R	V	M	KE	H	R	V	M	KE	H
0.5	-0.4	.338	.071	142.8	2.12	12.2	.328	.064	167.8	2.33	13.3
	0.0	.338	.091	183.6	2.87	16.5	.328	.082	215.7	3.15	18.1
	+0.4	.338	.111	224.4	3.62	20.8	.328	.100	263.6	3.98	22.8
0.7	-0.4	.488	.161	325.6	12.4	71.0	.343	.056	148.0	2.80	16.0
	0.0	.488	.185	372.8	14.4	82.6	.343	.064	169.5	3.25	18.6
	+0.4	.488	.208	420.3	16.5	94.3	.343	.073	191.1	3.71	21.3
0.9	-0.4	.470	.060	120.4	5.28	30.3	.330	.021	54.8	1.19	6.83
	0.0	.470	.062	124.3	5.46	31.3	.330	.022	56.5	1.23	7.06
	+0.4	.470	.065	130.7	5.75	32.9	.330	.023	59.5	1.30	7.43

Note: Units and assumptions as listed in Table 35

Computations were simplified by considering two salient points presented in the previous section: (1) thin-wall geometries are particularly advantageous for composite rotors, and (2) rotor profile does not strongly affect maximum speed capability at these high α values. Thus, for illustrative purposes, only high α values (0.5 to 0.9, inclusive) were used; and, in this range, maximum speed was assumed to be a function of this sole parameter.

The parametric scaling data presented in Tables 36 and 37 are used in Appendix E (Integrated Component Design Trades) for final rotor sizing.

APPENDIX C

MAGNETIC BEARING DESIGN ANALYSIS

by

James R. Downer

This task was directed toward determining the most promising magnetic bearing system for a Space Station IPACS. The decision was based upon determination of the weight, volume, and power consumption characteristics of several magnetic bearing options under given assumptions. A viable five-degree-of-freedom (5-DOF) baseline magnetic bearing system could be made from either a homopolar attraction type, or a Lorentz force type, large-angle magnetic bearing. In terms of weight and power consumption, neither of the two candidates shows marked superiority, and it is felt that with continued development, either candidate could be successfully employed for a Space Station IPACS having an angular freedom requirement less than about 10°. When control issues are added to the decision-making process, the selection is pushed toward the Lorentz force type magnetic bearing due to its reduced destablilizing effects that are characteristic of magnetic bearings. In addition, for an IPACS that requires more angular freedom (10° to 20°), Lorentz force bearings show a distinct superiority in terms of weight and power consumption. During ground testing, the weight of the rotor will be supported by a flat-faced armature electromagnet whose attractive surfaces have spherical shapes. The remainder of this section discusses the assumptions that were made, the options that were examined, and the results that were obtained. Reference 78 contains more details regarding the design and fabrication of large-angle magnetic bearings.

Assumptions

In an IPACS, the magnetic bearing performs the functions of rotor support, center-of-mass positioning, vibration isolation, torquing and, possibly, torque measurement. Of all the components of a flywheel energy storage system, the magnetic suspension is the most heavily influenced by other components and system configuration. This is particularly true for an IPACS where the attitude control of a spacecraft is performed by having the flywheels act as double-gimbaled control moment gyros, which are gimbaled by the magnetic suspension. The magnetic suspension must allow the rotor sufficient angular freedom (precession and nutation) in order to transfer the required angular momentum between the flywheels and the Space Station. In some IPACS configurations, the magnetic suspension must also allow sufficient angular freedom to reconfigure the IPACS wheel array to a new nominal momentum vector orientation in the event of wheel failure. A configuration of the latter type has the benefit of not requiring the shutdown of a working counterrotating wheel following the failure of its counterpart. Additionally, a configuration such as the planar six-wheel orientation, discussed in the Integrated Components Design Trades section, does not acquire the penalty of mechanical gimbals.

It was assumed that the IPACS would be tested on Earth, but that a secondary suspension system could be used to support the weight of the flywheel rotor if a ground testing requirement tended to drive the primary suspension design. Even when ground testing was assumed to occur with the nominal spin axis of the IPACS rotor aligned with the local vertical, the weight and power consumption of the 5-DOF magnetic bearing options that were examined were driven by the ground test requirements. However, a lifting magnet designed only to support the weight of the rotor on Earth can be made quite light and power efficient (ref. 79, 86).

The magnetic suspension is required to exert control torque on the Space Station and to precess the flywheels at the Space Station orbit rate. The flywheels, however, are allowed to operate on touchdown bearings during some severe maneuvers (emergency operations).

Parameters for the magnetic bearing study were obtained from the results of preliminary sizing calculations. Projection from these values to the final design specifications is the focus of the Integrated Components Design Trades section. These parameters are given in Table 38. Two baseline systems were examined, corresponding to the five- and six-wheel planar configurations. The five-wheel planar configuration requires a crude single-degree-of-freedom mechanical gimbal for reconfiguration following a wheel failure, while the six-wheel planar configuration can be reconfigured by tilting the remaining wheels within their magnetic bearings. The mechanical gimbal used in the five-wheel planar configuration is used for reconfiguration only. The large-angle magnetic bearing provides gimbaling for the purposes of attitude control.

TABLE 38.-ASSUMPTIONS FOR MAGNETIC BEARING STUDY

Parameter	Planar Configuration	
	Five Wheel	Six Wheel
Rotor mass (kg)	510	400
Rotor angular momentum (kNms)	140	120
Angular freedom required (degrees)	9	15
Force to accelerate rotor at 0.1 g (N)	500	390
Maximum control torque (Nm)	300	300
Torque to precess rotor at 0.065°/s (Nm)	160	140

Magnetic Bearing Options

Magnetic forces can be exerted either through the attraction of ferromagnetic bodies in a magnetic field, or the Lorentz force. The generation of force by these two mechanisms is discussed in detail below.

Ferromagnetic attraction forces are produced when the energy stored in a magnetic field is transformed into mechanical work through relative displacement of the bodies. This is stated mathematically as (refs. 83, 87, 90):

$$\bar{f} = (\bar{\nabla} W_m)$$

$$= \frac{\partial W_m}{\partial x}\,\underline{i} + \frac{\partial W_m}{\partial y}\,\underline{j} + \frac{\partial W_m}{\partial z}\,\underline{k}$$

where,

f = attractive force vector

W_m = magnetic energy

In well-designed magnetic circuits (little energy stored in non-useful paths) and where iron flux paths are not significantly saturated, a useful approximation can be made. All magnetic energy that can become available for performing useful mechanical work can be assumed to be resident in the air gap separating the magnetic suspension from the suspended body.

A particularly useful gap geometry (parallel surfaces) and its force (f) to flux density (B) relationships are shown in figure 36. These relationships assume that the air-gap length (G) is small compared to the other two system dimensions (t, w). μ_o is the permeability of free space (ref. 83).

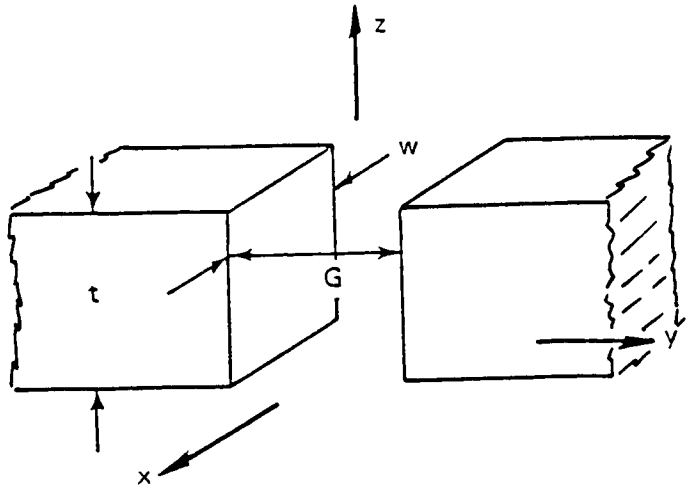

$$f_x = \frac{B^2}{2\mu_0}\,tG$$

$$f_y = \frac{B^2}{2\mu_0}\,wt$$

$$f_z = \frac{B^2}{2\mu_0}\,wG$$

Figure 36.- Forces of ferromagnetic attraction

The attraction forces result from the tendency of the bodies in the magnetic field to align themselves in such a way as to minimize stored energy. The primary attraction force (f_y in fig. 36) results from minimizing energy by closing the air gap. The secondary attraction forces (f_x, f_z) result from minimizing energy by aligning the pole faces (i.e., reducing fringing) (ref. 90).

Lorentz forces are generated by the interaction between an electrical current and a magnetic field. The Lorentz force is stated mathematically (ref. 90) as

$$\overline{f} = (\overline{J} \times \overline{B})\ V$$

where,

J = current density vector

B = flux density vector

V = volume where fields interact

Using attractive forces to suspend a rotor that is to have a fixed spin axis is the current state of the art for magnetic bearing designers in the United States, Europe, and Japan. The C. S. Draper Laboratory (CSDL) has employed a Lorentz force suspension with modest angular freedom in the design of a Combined Attitude, Reference, and Energy Storage (CARES) system for satellite applications (ref. 18).

The common denominator in conventional magnetic bearing designs is that forces are exerted in a pattern of cylindrical symmetry about the nominal spin axis (with a bias force usually along the spin axis to support the rotor weight in terrestrial applications). A large-angle magnetic bearing, however, requires that forces be exerted in a spherically symmetrical pattern about a point at the center of mass (CM) of the rotor. In order to exert these forces, several magnetic circuit and coil geometries suggest themselves. Among these, three alternatives (two attractive and one Lorentz) were studied. Schematic drawings of the three bearing alternatives are shown in figures 37, 38, and 39. All of the alternatives have the capability of providing five-degree-of-freedom actuation (force along all three axes and torques about the two radial axes).

The two attractive alternatives are similar in that they are both flux-biased bearing systems. This type of design has a higher gain than a non-biased design and is more nearly linear. Both employ two wound, four-pole disks on the stator. The two attractive alternatives, however, differ in the manner through which the biasing magnetic field is maintained. The first alternative utilizes a heteropolar field maintained by current in control coils wound on the salient poles. The second alternative utilizes a permanent magnet to produce the bias field. The permanent magnet is shown as part of the rotor, but it could also be incorporated in the stator structure if stresses due to rotation are a concern.

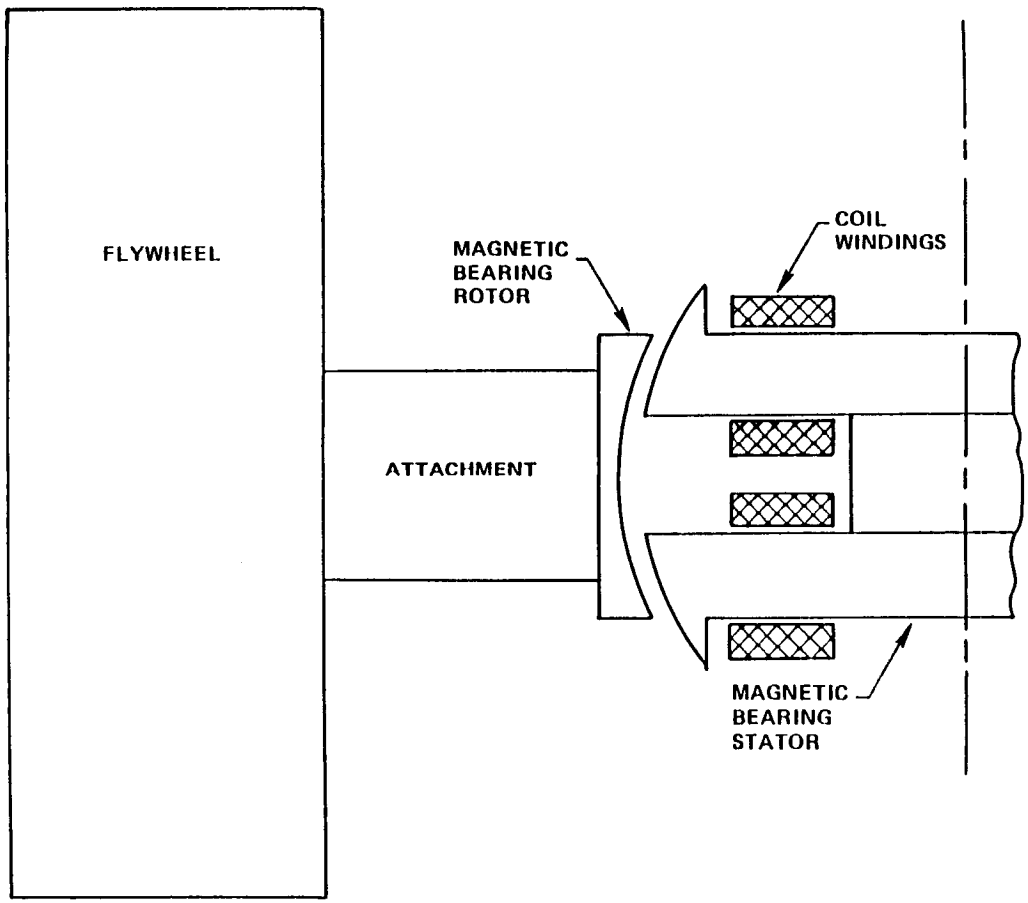

Figure 37.- Five-degree-of-freedom heteropolar attractive magnetic bearing

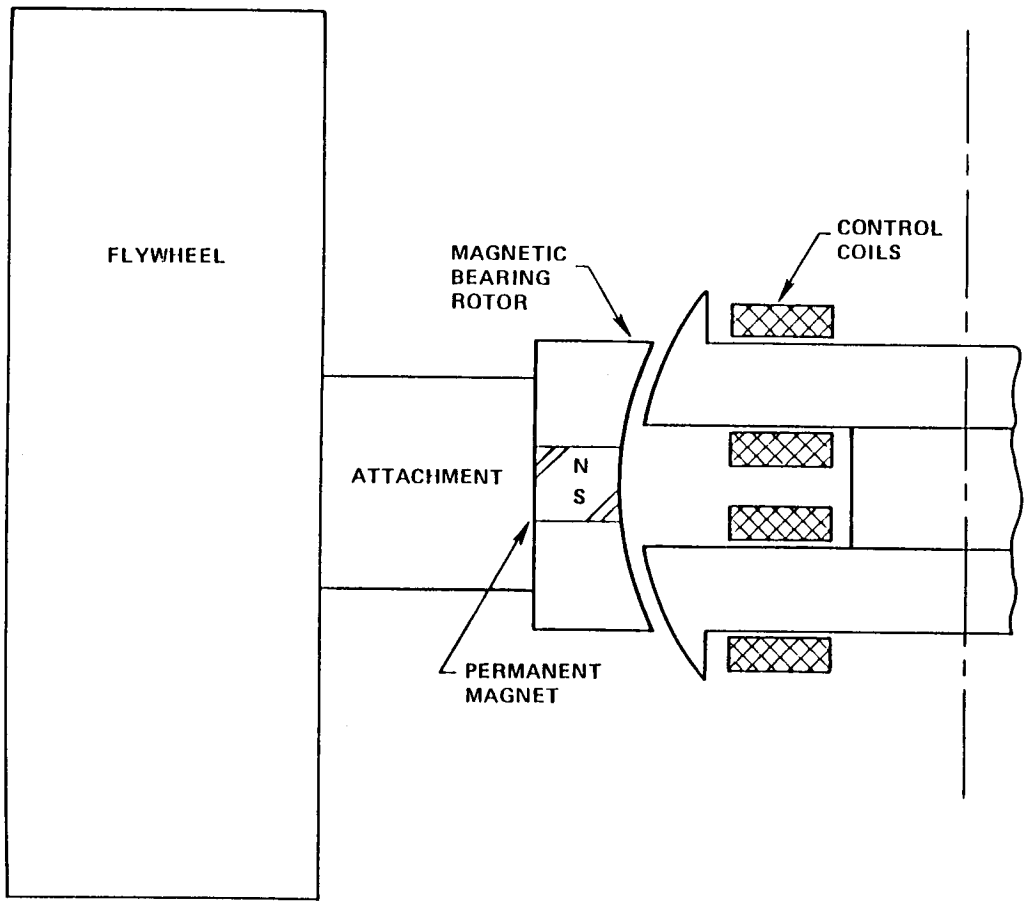

Figure 38.- Five-degree-of-freedom homopolar attractive magnetic bearing

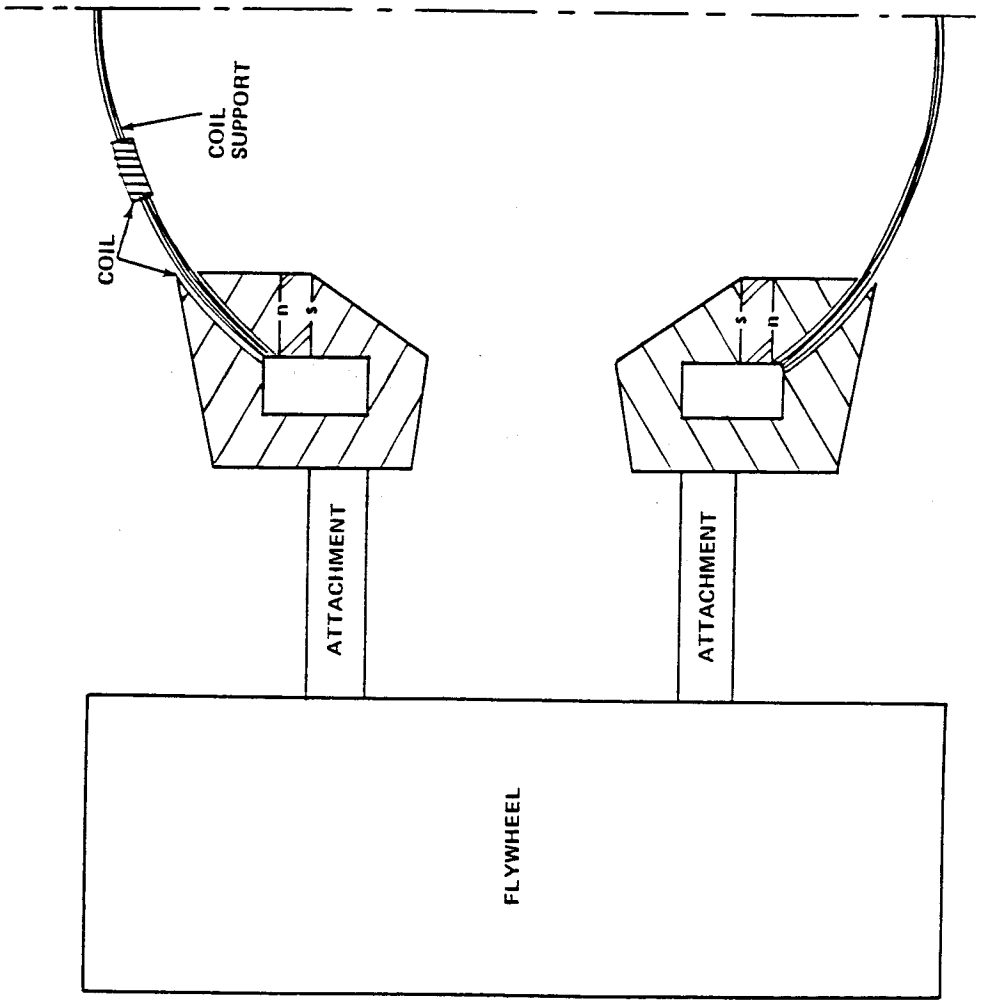

Figure 39.- Five-degree-of-freedom Lorentz force magnetic bearing

The Lorentz force alternative consists of two rotors that contain axially oriented permanent magnets and sufficient core material to yield approximately spherical magnetic fields in the air gaps. Each stator consists of a thin shell containing four control coils as is shown in figure 40.

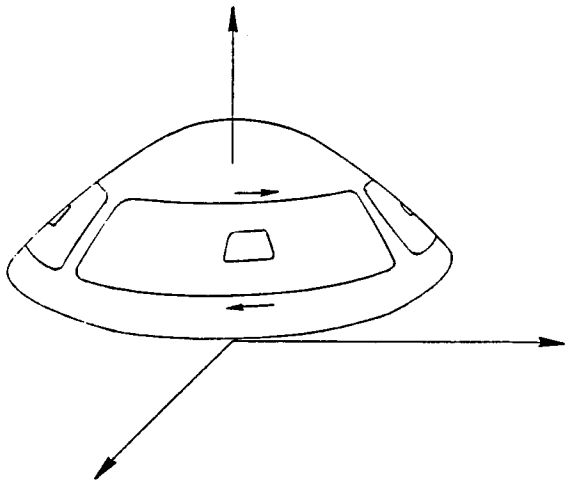

Figure 40.- Five-degree-of-freedom Lorentz force magnetic bearing stator

Study Methodology

The methodology employed in this study was to analyze the performance characteristics of each magnetic bearing type, and evaluate the weight and power scaling as the nominal spherical radius of the bearing varies. This approach shows the weight penalty that must be paid for decreased power consumption, or conversely, the power consumption penalty for reduced weight.

Attractive Bearings

A great deal of information regarding attractive magnetic bearings can be obtained through analysis of the case of a magnetic field with flux density (B_g), maintained between parallel opposed flat plates of cross-sectional area (A), separated by an air gap of length (G), which is small in comparison to other system dimensions. If leakage, fringing, and iron reluctance are ignored, these forces are given by the following (refs. 83, 86, 87):

$$f = \frac{B_g^2 A}{2\mu_0} = \frac{F^2}{2} \frac{P_g}{G}$$

where,

μ_o = permeability of free space

F = magneto-motive force (MMF) = Ni, where N = number of turns
i = current

P_g = gap permeance

$= \frac{\mu_o A}{G}$

The force equation may be linearized about some nominal air gap length (G_o) and flux density (B_o) as follows:

Since $f = f(i, G)$

$$\delta f = \frac{\partial f}{\partial i}\Big|_{\substack{G = G_o \\ B_g = B_o}} \delta i + \frac{\partial f}{\partial G}\Big|_{\substack{G = G_o \\ B_g = B_o}} \delta G$$

$$= K_s \delta i - K_u \delta G$$

where,

$$K_u = \frac{B_o^2 A}{\mu_o G_o}$$

$$K_s = \frac{N B_o A}{G_o}$$

Analysis of an actual bearing is accomplished by taking into account the number of attractive surfaces, as well as their direction and lumping these into equivalent bearing parameters (K_u, K_s).

$$\delta f = -K_u(\delta G) + K_s(\delta i)$$

$$= -\alpha K_u(\delta G) + \alpha K_s(\delta i)$$

where,

α = factor accounting for bearing geometry and is equal to 2 for most terrestrial application

When this bearing interacts with a rotor of mass (M), application of Newton's law produces the following differential equation for the position (x) of the rotor.

$$f = M \frac{d^2x}{dt^2}$$

The rotor position is defined as increasing as the air gap closes

$$\delta x = -\delta G$$

The linearized differential equation about a nominal rotor position (x_o) becomes

$$K_u(\delta x) + K_s(\delta i) = M \frac{d^2}{dt^2} (\delta x)$$

$$M \frac{d^2}{dt^2}(\delta x) - K_u(\delta x) = K_s(\delta i)$$

Taking the Laplace transform and rearranging shows that an unstable plant results such that

$$\frac{\delta x}{\delta i}(s) = \frac{K_s}{Ms^2 - K_u}$$

The stabilization of this plant implies a minimum closed-loop system bandwidth given by the following (ref. 84):

$$\omega_o^2 = \frac{K_u}{M} = \frac{\alpha B_o^2 A}{\mu_o M G_o}$$

The minimum bandwidth of a given piece of hardware is determined by the nominal (or bias) flux density. Selection of the bias flux density is, therefore, critical to the magnetic bearing design.

For terrestrial energy storage flywheels, where it is desired that the suspension consume zero power to support the weight of the flywheel rotor, the bias flux density is sized to support the rotor mass against gravity (refs. 84, 88)

$$Mg = \frac{B_o^2 A}{2\mu_o} \alpha$$

$$\omega_o^2 = 2g/G_o$$

The bias flux may then be provided by permanent magnets such that there is ideally no power consumed to support the rotor weight (ref. 88). The minimum bandwidth is then constrained by the air gap length.

In space, however, the minimum bias flux density is one-half of the maximum flux density (B_{max}). This is the flux density that is required to produce the maximum force for which the bearing is designed (f_{max}).

$$f_{max} = \frac{\alpha B_{max}^2 A}{2\mu_o}$$

$$B_o = \frac{B_{max}}{2} = \frac{1}{2}\sqrt{\frac{2\mu_o f_{max}}{\alpha A}}$$

$$K_u\Big|_{min} = \frac{f_{max}}{2 G_o}$$

Since the largest forces that the bearing must produce are typically those associated with the maximum required control torque (300 Nm), a larger bearing (and, therefore, lever arm) reduces the maximum force. The minimum bandwidth may then be made arbitrarily small. This increases robustness of the closed-loop system to uncertainties in the plant due to such effects as structural compliances and high-order suspension dynamics (e.g., unmodeled lags induced by iron losses, refs. 84, 89). A reduction in bandwidth, however, implies a reduction in performance in terms of command following and disturbance rejection. In flux-biased suspensions, the stabilizing and destabilizing constants are related as follows:

$$k_s^2 = N^2 k_u P_g$$

A reduction in minimum bandwidth, therefore, implies increased control effort (and, therefore, power consumption) for a given bearing or the use of a large bearing (increased performance) to maintain a given level of power consumption.

In order to use an attractive magnetic bearing in a large-angle configuration, the attractive surfaces on the rotor and stator can be shaped to approximate concentric spheres.

Figure 41 shows the forces acting on the rotor of a large-angle attractive magnetic bearing. The inward radial force (f_a) causes the unstable effect that was discussed above. The tangential force (f_b) results from the same mechanism as that which governs solenoids, reluctance motors, and passive magnetic bearings; that is, the tendency of magnetic systems toward a configuration of minimum reluctance. If the air-gap length is small in comparison to other physical dimensions, the forces may be approximated by assuming that the interacting surfaces are nearly parallel flat plates (refs. 80, 84). The previously discussed attraction force equations are evaluated for a spherical geometry.

$$f_a = \frac{B^2 A}{2\mu_o} = \frac{B^2 w_\theta w_\phi}{2\mu_o} = k_a B^2$$

$$f_b = \frac{B^2 w_\theta G}{2\mu_o} = k_b B^2$$

where

A = cross-sectional area of the bearing pole which is

$$= w_\theta w_\phi$$

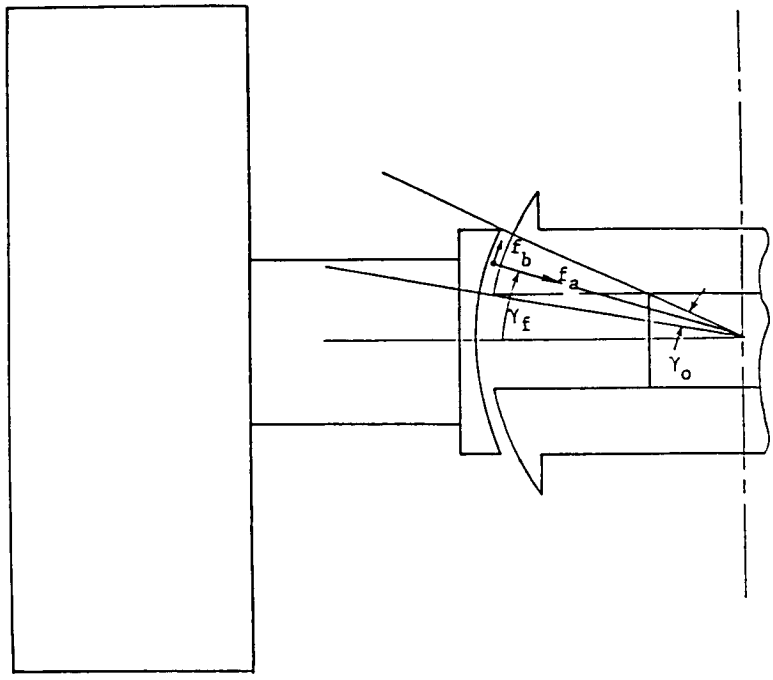

Figure 41.- Forces in a 5-DOF attractive magnetic bearing

w_θ = length of the pole in the azimuth direction which is

$$= \theta r_o \cos \gamma_f$$

θ = angular extent of the stator pole in the azimuth direction

w_ϕ = length of the air gap in the elevation direction, which is

$$= \gamma_o r_o$$

γ_o = angular extent of the air gap in the elevation direction

γ_f = angular location of the center of the air gap (see fig. 41)

r_o = nominal spherical radius

Figures 42 and 43 show how the coils wound on the salient poles should be excited to produce the required forces and torques for the alternatives shown in figures 37 and 38, respectively.

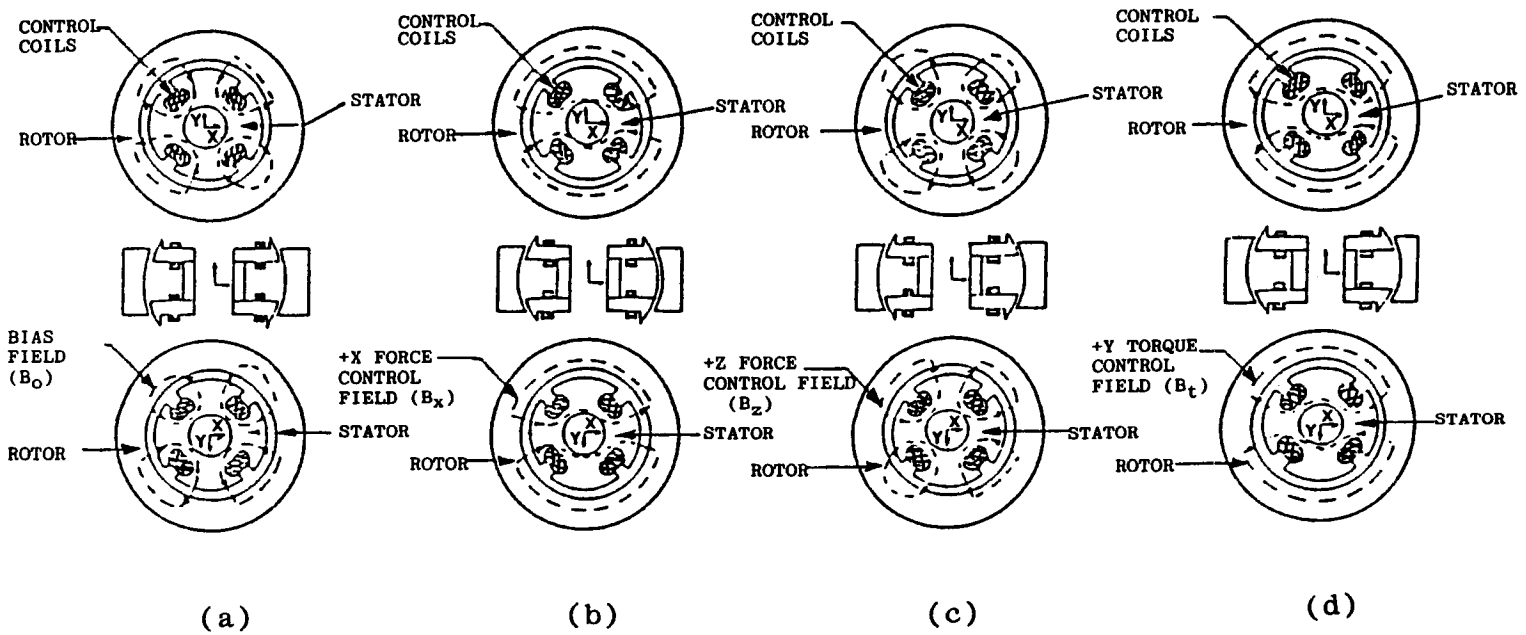

Figure 42. - Excitation of 5-DOF heteropolar attractive magnetic bearing

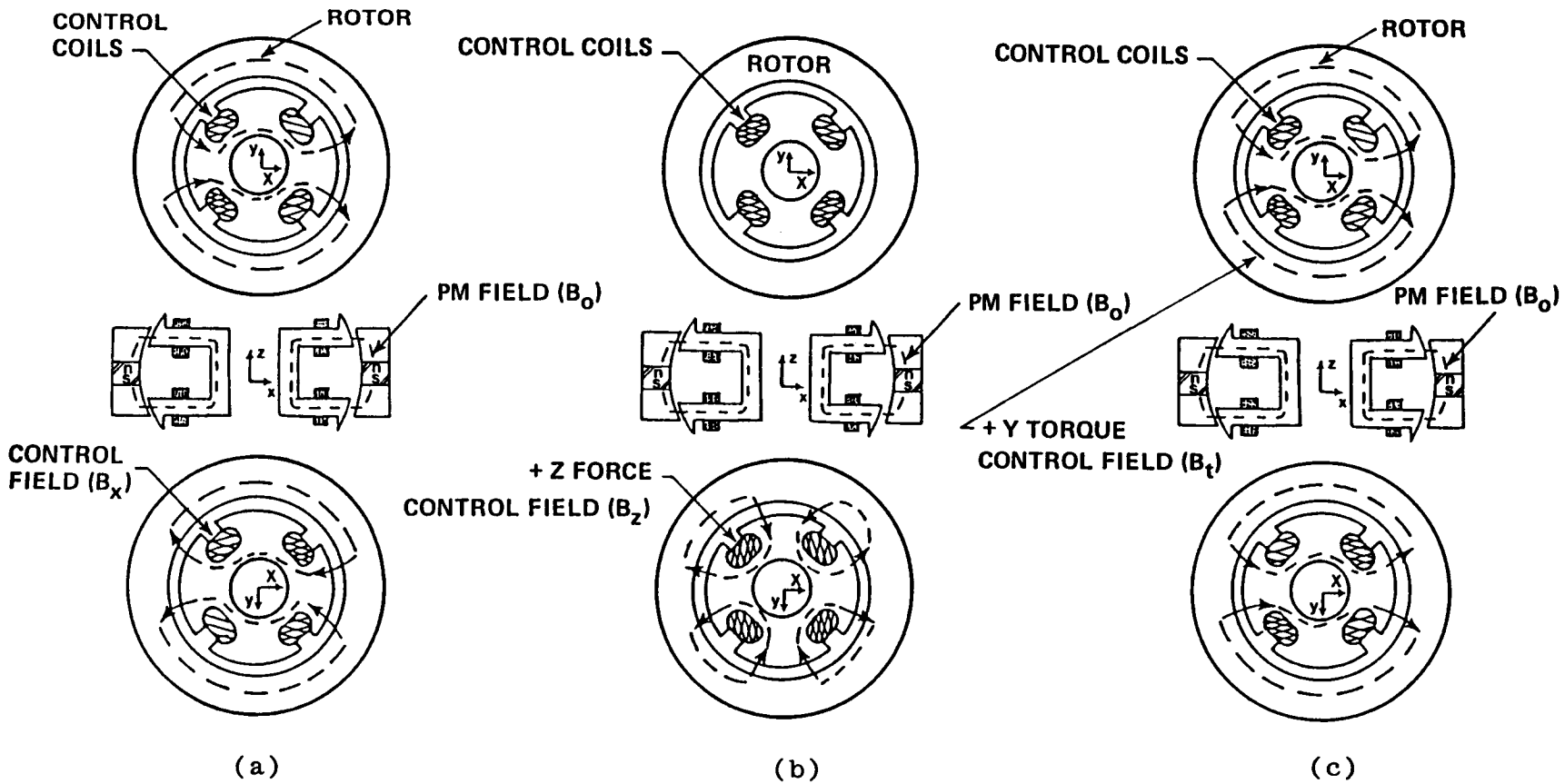

Figure 43.- Excitation of 5-DOF homopolar attractive magnetic bearing

Figure 42 (a) shows how the biasing field is produced by the heteropolar bearing.

Figures 42 (b) and 43 (a) show how a radial force (f_r) in the positive x-direction is exerted on the rotor. The poles on the "negative x-side" of the stator are excited to produce an increased flux density ($B_o + B_r$) while those on the "positive x-side" are excited to produce a reduced flux density ($B_o - B_r$) with all other poles having the bias flux density. By summing the force contributions of each of the magnetic bearing poles, the radial force is calculated.

$$f_r = 8(k_a \cos \gamma_f - k_b \sin \gamma_f)B_o B_r = K_r B_o B_r$$

Figures 42(c) and 43(b) show how an axial force (f_z) in the positive z-direction is exerted on the rotor. For the heteropolar bearing, the top poles are excited to produce a reduced flux density ($B_o - B_z$) while the lower poles are excited to produce an increased flux density ($B_o + B_z$). For the homopolar bearing, the poles are excited to produce alternately increased ($B_o + B_z$) and reduced ($B_o - B_z$) flux densities. By summing the force contributions of each of the eight magnetic bearing poles, the axial force is calculated.

$$f_z = 16(k_a \sin \gamma_f + k_b \cos \gamma_f)B_o B_z \quad \text{- heteropolar}$$

$$= K_{z1} B_o B_z$$

$$f_z = 4(k_a \sin \gamma_f + k_b \cos \gamma_f)B_z^2 \quad \text{- homopolar}$$

$$= K_{z2} B_z^2$$

Figures 42 (d) and 43 (c) show how a torque (τ) about the positive y-axis of the rotor is exerted. The poles on the top, negative x-side and bottom, positive x-side are excited to produce an enhanced flux density ($B_o + B_t$). The top, positive x-side pole and the bottom, negative x-side pole are excited to produce a reduced flux density ($B_o - B_t$). By summing the moment of the force contributions of each of the eight magnetic bearing poles, the torque is calculated.

$$\tau = 8k_b B_o B_r r_o = K_t B_o B_t r_o$$

Therefore, with the exception of the case of a homopolar magnetic bearing in axial force mode, the forces exerted by the flux-biased attractive magnetic bearing are linearly related to the changes in the air-gap flux density. The excitation in each coil (MMF) that is necessary to produce the required control flux densities are given by the following when iron permeability can be assumed to be large.

$$F_o = Ni_o = \frac{B_o G}{\mu_o} \qquad \text{(Heteropolar)}$$

$$F_r = Ni_r = \frac{B_r G}{\mu_o} \qquad \text{(Homopolar)}$$

$$F_r^+ = Ni_r^+ = \frac{(B_o + B_r)G}{\mu_o}$$

$$\text{(Heteropolar)}$$

$$F_r^- = Ni_r^- = \frac{(B_o - B_r)G}{\mu_o}$$

$$F_z = Ni_z = \frac{B_z G}{\mu_o} \qquad \text{(Homopolar)}$$

$$F_z^+ = Ni_z^+ = \frac{(B_o + B_z)G}{\mu_o}$$

$$\text{(Heteropolar)}$$

$$F_z^- = Ni_z^- = \frac{(B_o - B_z)G}{\mu_o}$$

$$F_t = Ni_t = \frac{B_t G}{\mu_o} \qquad \text{(Homopolar)}$$

$$F_t^+ = Ni_t^+ = \frac{(B_o + B_t)G}{\mu_o}$$

$$\text{(Heteropolar)}$$

$$F_t^- = Ni_t^- = \frac{(B_o - B_t)G}{\mu_o}$$

The power consumption of an attractive magnetic bearing is primarily composed of copper loss in the coil windings and core losses in the rotor. The copper loss is produced by the control currents in the windings; the core losses are produced by the changing magnetic field in the rotor as it spins.

The copper loss is readily calculated from the coil excitation. Each turn of wire has a cross-sectional area (A_w) and an average length (ℓ). The number of turns that can be fit into an area (A_c) is given by the fill factor (η_w).

$$NA_w = \eta_w A_c$$

The resistance of each coil (R_c) is given by

$$R_c = \frac{\rho N \ell}{A_w} = \frac{\rho \ell}{\eta_w A_c} N^2 = N^2 r_c$$

Physically, the variable r_c represents the result if all of the turns of the coil were in parallel rather than series (i.e., if a single turn of a Litz wire bundle were used).

The power consumed in the coil bundles to produce radial force (P_r), axial force (P_z), and torquing (P_t) can then be evaluated.

$$P_r = 4N^2 r_c i_r^2 = 4 r_c \left(\frac{G}{\mu_o K_r B_o} \right)^2 f_r^2$$

$$P_z = 4N^2 r_c i_z^2 = \frac{4 r_c}{K_{z_2}} \left(\frac{G}{\mu_o} \right)^2 f_z \quad \text{(Homopolar)}$$

$$P_z = 4 r_c \left(\frac{G}{\mu_o K_{z_1} B_o} \right)^2 f_z^2 \quad \text{(Heteropolar)}$$

$$P_t = 4N^2 r_c i_t^2 = 4 r_c \left(\frac{G}{\mu_o K_t B_o} \right)^2 \left(\frac{\tau}{r_o} \right)^2$$

In addition, the heteropolar magnetic bearing design has an additional copper loss due to the establishment of the bias field by current in the bearing windings. Since the fields producing the radial, axial, and torquing forces are fixed to the stator of the magnetic bearing, no core losses are produced in the stator as the rotor spins (in a centered position). However, the rotor core material sees an alternating magnetic field at the shaft rotational frequency for the case of the homopolar bearing used in either radial force or torquing mode, and at twice the shaft rotational frequency for the case of a homopolar bearing in axial force mode or the case of a heteropolar bearing in any mode. In addition, there are losses as the shaft spins for a heteropolar bearing. The additional copper and spinning losses of the heteropolar bearing were the eventual cause of its being dropped as a viable candidate. These core losses are not readily computed analytically, but they may be evaluated by using manufacturers data sheets or empirical relations derived from them (ref. 80). The total core loss for carbon steel, for instance, is estimated by the following emprical formula (ref. 80). Pure sinusoidal excitation is assumed.

$$P = 2.8\ \omega^{1.4}\ (\delta B)^{1.7}$$

where

P = total core lost (W/m^3)

ω = excitation frequency (r/s)

δB = peak flux density (T)

The weight of the five-degree-of-freedom attractive magnetic bearing does not lend itself to direct mathematical optimization because of the unique geometry involved. Weight reduction is most easily accomplished through the use of engineering judgment in terms of material selection and shaping. Less core material can be employed by selecting a material that has a relatively high saturation flux density, such as Vanadium Permendur. By removing unnecessary core areas (literally cutting corners) and operating the remaining core material near saturation for the largest excitation that is anticipated, a reduction in core material can be readily accomplished.

Permanent magnet selection is key to reducing this component of the bearing weight. To produce a given air-gap magnetic field, the amount of permanent magnet that is required is inversely proportional to the energy product of the magnet. To achieve maximum energy product, the length and cross-sectional area of the magnet must be chosen so as to provide the proper balance of magnetizing force and flux to the magnetic load (ref. 85).

The largest contribution to increased magnetic bearing weight is the large angle required to transfer angular momentum between the IPACS rotors and the spacecraft. While magnetic bearings of relatively modest angle capability can be made quite light, there is a weight penalty for shaping the magnetic bearing attractive surfaces into portions of concentric spheres with the required angular freedom.

Lorentz Bearings

As with attractive magnetic bearings, a simple model of a Lorentz force bearing can be used to gain a great deal of insight. Consider a loop containing N turns of a wire which is operating at a current density (J). Each turn has a uniform cross-sectional area (A_w) and an average length (ℓ). Along a portion of the coil of length (ℓ_u), a magnetic field with flux density (B) is perpendicular to the current flow. The magnitude of the resulting Lorentz force can be expressed as

$$f = NA_w \ell_u JB$$

The power (P) consumed in order to produce this force is given by

$$P = \rho NA_w \ell J^2$$

where,

ρ = resistivity of the wire

The number of turns is constrained by the fill factor (η_w) and the total available area for conductors (A_c).

After some manipulation, the relationship between the force capability and the power consumption of a Lorentz force bearing can be expressed as

$$\frac{f^2}{P} = \frac{\eta_w \ell_u^2 A_c}{\ell} \frac{B^2}{\rho} = \frac{V_{cu}^2}{V_c} \frac{B^2}{\rho}$$

$$= \left(\frac{\ell_u}{\ell}\right)^2 V_c \frac{B^2}{\rho}$$

where,

V_{cu} - useful conductor volume = $\eta_w A_c \ell_u$

V_c - total conductor volume = $\eta_w A_c \ell$.

This last equation gives a measure of the performance of a Lorentz force bearing. In designing a coil, the performance of the bearing is extremely sensitive to the fraction of the total copper volume that can produce useful force.

As with attractive magnetic bearings, the weight of the magnetic circuit required to produce the needed magnetic field must also be considered. The same engineering judgment regarding magnet circuit design applies to this bearing type as well. The Lorentz force design is less sensitive to the permanent magnet operating point than the attractive design, since higher air-gap flux density rather than optimum flux density is important to magnetic bearing performance.

Sizing Results

Through the use of the equations that were derived in the preceding pages, and through iterative tailoring of the magnetic bearing geometry, scaling studies were performed. The power consumption and mass properties of the magnetic bearing candidates were assessed as the size of the magnetic bearing (measured by the nominal spherical radius) was varied. The power consumption in each of the following magnetic bearing operational modes was evaluated: (1) radial force (maximum rotor linear acceleration); (2) axial force (maximum rotor linear acceleration); (3) torque (to precess rotor at orbit rate); and (4) torque (maximum control torque). The total bearing mass was also evaluated since this quantity will determine the acceptability of the bearing.

Based upon the results of these preliminary analyses, the heteropolar attractive magnetic bearing was dropped from further consideration due to excessive rotor core losses. The two surviving designs were examined for each of the IPACS configurations of interest (5- and 6-wheel planar). The Lorentz

and homopolar attractive magnetic bearings were found to have roughly comparable weights and power consumption for the relatively modest 9° angle required for the five-wheel planar configuration. For the six-wheel planar configuration, however, the 15° of required rotor angular freedom places a severe penalty on the attractive bearing (roughly, a factor of two over the Lorentz-type bearing).

Lorentz Force Bearing.-Figures 44 (a) and (b) show the manner in which the power consumption and mass of a Lorentz force magnetic bearing for the five-wheel configuration scale with the nominal spherical radius of the bearing. Since the power consumed to exert the maximum required control torque is large in comparison to other power consumption components, it was used in the power versus bearing mass tradeoff that is shown in figure 44(c). Figures 45 (a), (b), and (c) present the equivalent information for the six-wheel configuration.

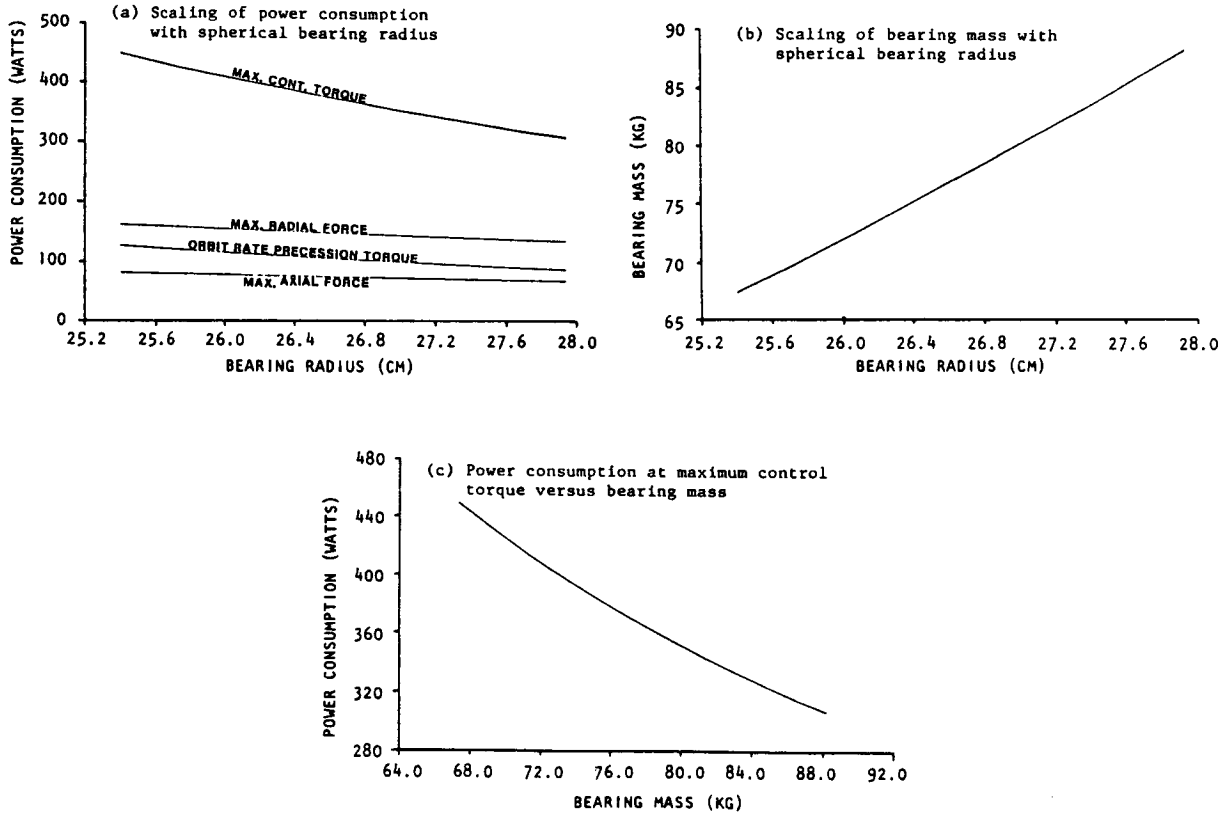

Figure 44.- Lorentz force magnetic bearing sizing (5-wheel planar configuration)

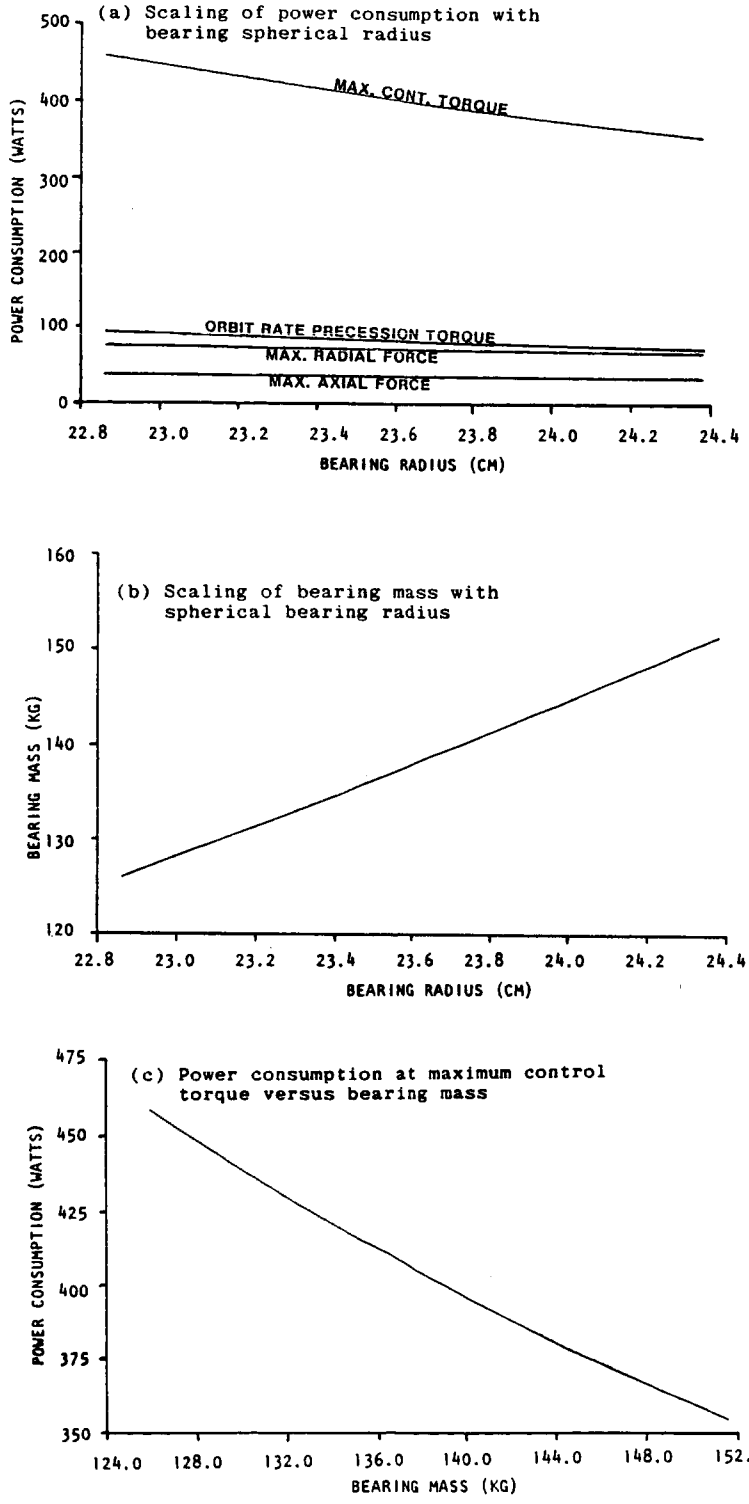

Figure 45.- Lorentz force magnetic bearing sizing (6-wheel planar configuration)

In order to determine the overall efficiency of the IPACS energy storage function, some measure of the standby power consumption of the magnetic bearings must be determined. For the Lorentz force magnetic bearings the standy loss consists of joule (i^2R) losses only. The joule losses result from exerting sufficient torque to precess the angular momentum of the IPACS rotor at orbital rate. Figures 46 (a) and (b) show that even this severe definition of standby loss results in losses of less than one percent of the normal power delivered by each rotor; (c) and (d) of this figure show the tradeoff between standby losses and bearing mass.

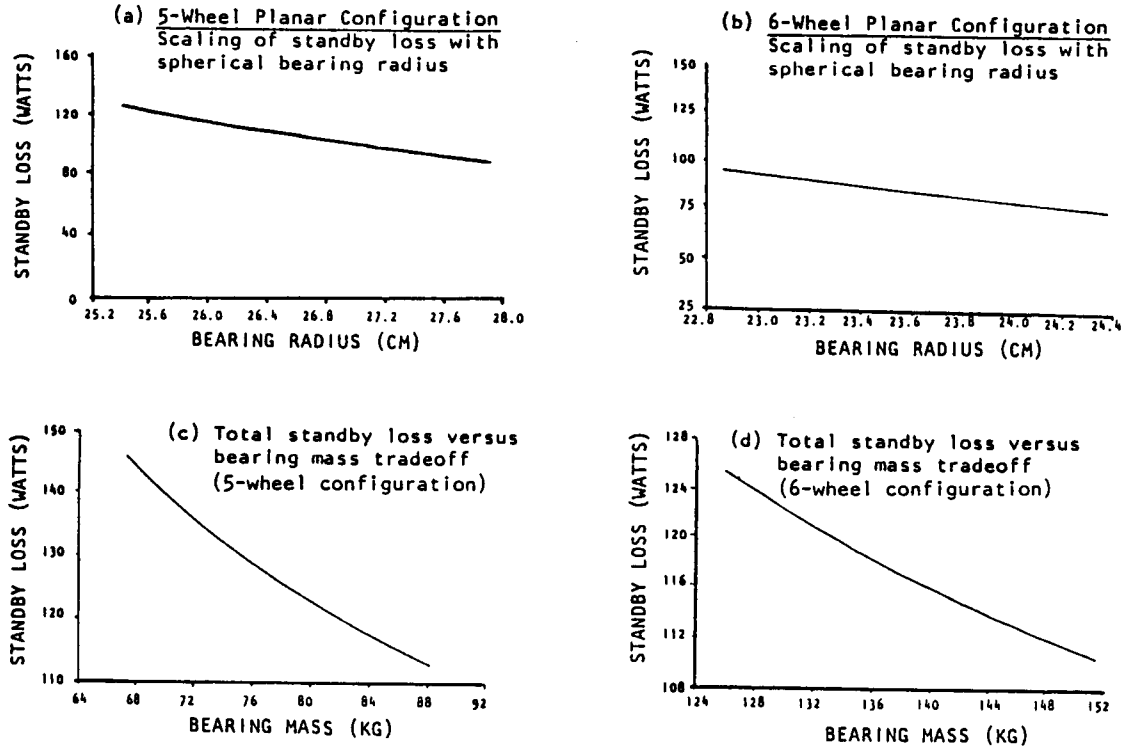

Figure 46.- Lorentz force bearing standby losses

Table 39 shows the baseline designs for Lorentz force magnetic bearings for the two IPACS configurations of interest. For roughly equivalent power consumption during maximum control torquing, a six-wheel configuration magnetic bearing has a mass that is 64 kg (141 lb) greater than that of a five-wheel configuration bearing.

Attractive Bearing.-In a large-angle attractive magnetic bearing, the air-gap length is readily used as an optimization parameter. For small air gaps the rotor core losses will dominate because of the high flux density components that are required to perform torquing. At large air gaps, the large excitations in the stator windings to drive flux across the gap will result in large copper losses. There is a minimum, as is shown in figure 47. In all subsequent calculations, the air-gap length of all attractive magnetic bearings has been optimized for minimum power consumption during maximum control torquing.

TABLE 39.-BASELINE LORENTZ FORCE MAGNETIC BEARING

FIVE-WHEEL PLANAR CONFIGURATION			SIX-WHEEL PLANAR CONFIGURATION		
TOTAL WHEELS		5	TOTAL WHEELS		6
WHEELS IN FAIL-OPERATIONAL MODE		4	WHEELS IN FAIL-OPERATIONAL MODE		5
AVAILABLE ENERGY PER WHEEL (KWH)		14.8	AVAILABLE ENERGY PER WHEEL (KWH)		11.8
ROTOR PARAMETERS			ROTOR PARAMETERS		
ROTOR MASS (KG)		511	ROTOR MASS (KG		386
MAXIMUM ANGULAR VELOCITY (RPM)		10,000	MAXIMUM ANGULAR VELOCITY (RPM)		8,700
MAXIMUM ANGULAR MOMENTUM (NMS)		140,000	MAXIMUM ANGULAR MOMENTUM (NMS)		120,000
ANGULAR FREEDOM REQUIRED (DEGREES)		9.0	ANGULAR FREEDOM REQUIRED (DEGREES)		15.0
LORENTZ FORCE FIVE-DEGREE-OF-FREEDOM BEARING WITH 9.0 DEGREES OF ANGULAR FREEDOM			LORENTZ FORCE FIVE-DEGREE-OF-FREEDOM BEARING WITH 15.0 DEGREES OF ANGULAR FREEDOM		
NEODYMIUM-IRON-BORN PERMANENT MAGNET			NEODYMIUM-IRON-BORON PERMANENT MAGNET		
MAXIMUM ENERGY PRODUCT (KJ/KG)		280	MAXIMUM ENERGY PRODUCE (KJ/KG)		280
SPECIFIC GRAVITY		7.47	SPECIFIC GRAVITY		7.47
PERMEANCE COEFFICIENT		1.1	PERMEANCE COEFFICIENT		1.1
DIMENSIONS OF MAGNETIC SUSPENSION (CM)			DIMENSIONS OF MAGNETIC SUSPENSION		
NOMINAL SPHERICAL RADIUS		26.2	NOMINAL SPHERICAL RADIUS		23.6
AIR GAP LENGTH		1.27	AIR GAP LENGTH		1.27
ROTOR SPHERICAL RADIUS		26.8	ROTOR SPHERICAL RADIUS		24.3
STATOR SPHERICAL RADIUS		25.5	STATOR SPHERICAL RADIUS		23.0
BEARING LEVER ARM		52.3	BEARING LEVER ARM		47.2
PERMANENT MAGNET OUTER RADIUS		19.4	PERMANENT MAGNET OUTER RADIUS		18.2
PERMANENT MAGNET INNER RADIUS		22.8	PERMANENT MAGNET INNER RADIUS		22.4
PERMANENT MAGNET LENGTH		5.1	PERMANENT MAGNET LENGTH		5.5
BEARING MASS (KG)			BEARING MASS (KG)		
ROTOR IRON	83		ROTOR IRON	36	
PERMANENT MAGNET	36		PERMANENT MAGNET	25	
ROTOR TOTAL		119	ROTOR TOTAL		61
STATOR IRON	0		STATOR IRON	0	
WINDINGS (8 COILS)	20		WINDINGS (8 COILS)	13	
NONMAGNETIC STRUCTURE	0		NONMAGNETIC STRUCTURE	0	
STATOR TOTAL		20	STATOR TOTAL		13
TOTAL BEARING		138	TOTAL BEARING		74
LOADS ON MAGNETIC SUSPENSION			LOADS ON MAGNETIC SUSPENSION		
FORCE (N)			FORCE (N)		
MAX. ACCELERATION		500	MAX. ACCELERATION		378
TORQUES (NM)			TORQUES (NM)		
NOMINAL PRECESSION TORQUE		136	NOMINAL PRECESSION TORQUE		159
REQUIRED TORQUE ON SPACECRAFT		300	REQUIRED TORQUE ON SPACECRAFT		300
AIR GAP FLUX DENSITY (TESLA)		0.70	AIR GAP FLUX DENSITY (TESLA)		0.70
POWER CONSUMPTION DURING VARIOUS SCENARIOS (WATTS)			POWER CONSUMPTION DURING VARIOUS SCENARIOS (WATTS)		
RADIAL POWER (MAX. ACCELERATION)		71.3	RADIAL POWER (MAX. ACCELERATION)		152.0
AXIAL POWER (MAX. ACCELERATION)		35.6	AXIAL POWER (MAX. ACCELERATION)		76.0
TORQUING POWER			TORQUING POWER		
(NOM. PRECESSION RATE)		82.8	(NOM. PRECESSION RATE)		111.8
TORQUING POWER (REQUIRED TORQUE)		402.1	TORQUING POWER (REQUIRED TORQUE)		399.0

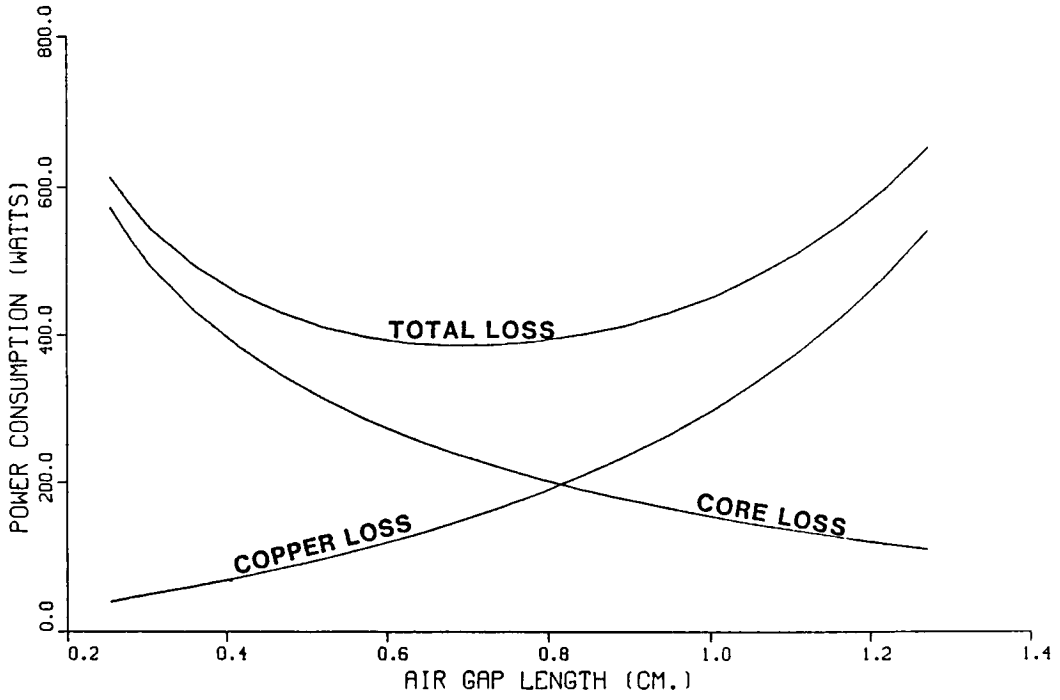

Figure 47.-Attractive magnetic bearing scaling of power consumption with bearing air-gap length (Five-wheel planar configuration)

Figures 48 (a), (b), and (c) show the scaling of power consumption and bearing mass, as well as the tradeoff between maximum control torquing power consumption and bearing mass for the five-wheel planar configuration. However, when a design study is attempted for a six-wheel planar configuration, it becomes obvious that acceptable bearing mass and power consumption are not attainable. Figure 49 shows how the mass of a large-angle attractive magnetic bearing scales with the amount of required angular freedom. Even for bearings with only 12 degrees of angular freedom, the bearing mass is much larger than for the Lorentz bearing.

The standby losses for an attractive magnetic bearing consist of the copper and core losses that occur in precessing the rotor at orbit rate and the additional core losses due to constantly magnetizing and demagnitizing a part of the rotor as it spins at an extreme angle of tip. The standby losses are shown in figure 50. They are somewhat higher than the Lorentz force bearing, but still only about 1.1% of the total nominal rotor power output.

Consideration must also be given to the control of an attractive magnetic bearing. The minimum bandwidths of the bearings examined for the five-wheel planar configuration are shown in figure 51. These frequencies are all probably in a range where flexible modes of the Space Station are present and will, therefore, make control of the bearing difficult. Figure 52 (a) presents the classical lead-lag solution for controlling an attractive magnetic bearing plant. A poor design in terms of gain and phase margin

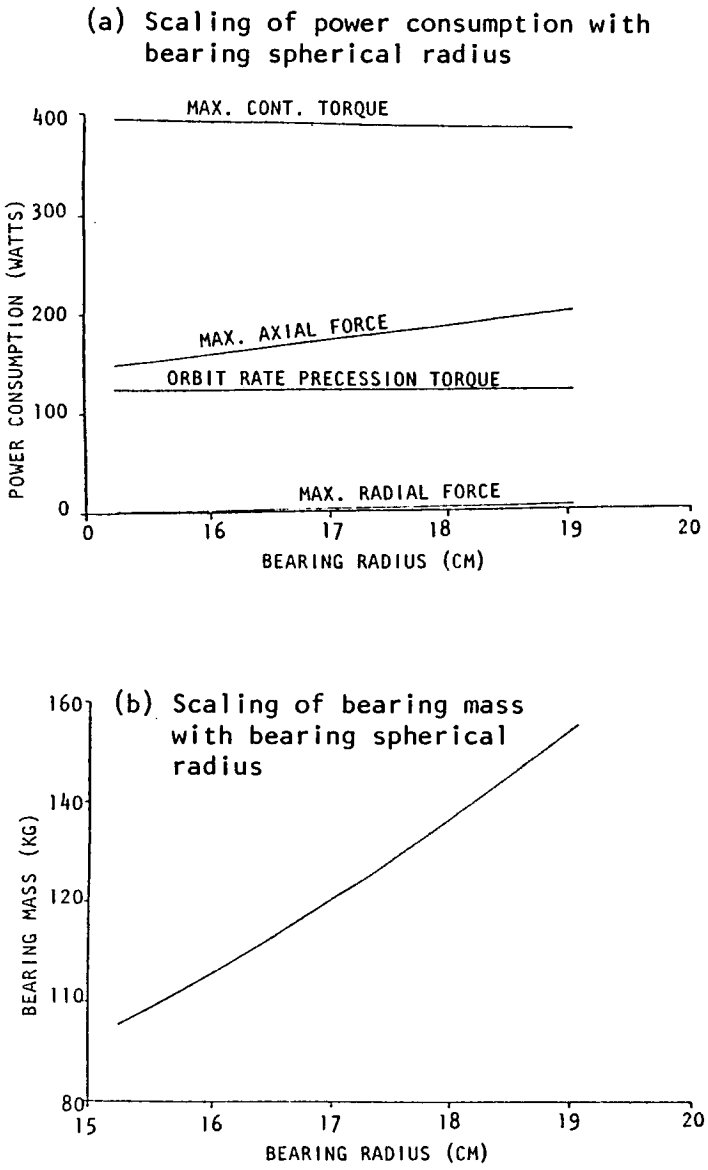

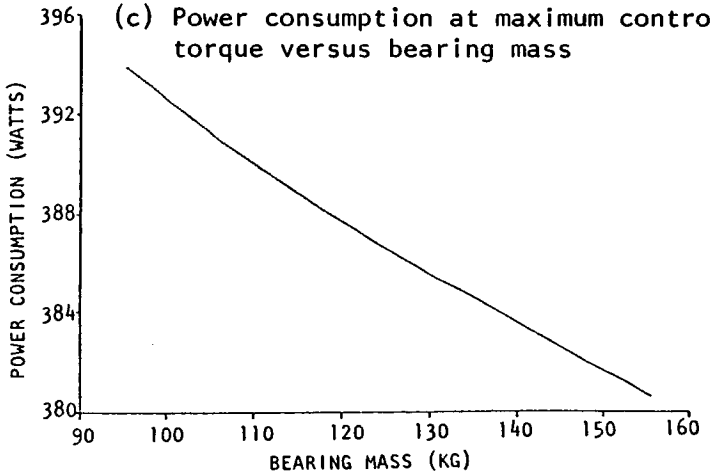

Figure 48.- Attractive magnetic bearing scaling trades (Five-wheel planar configuration)

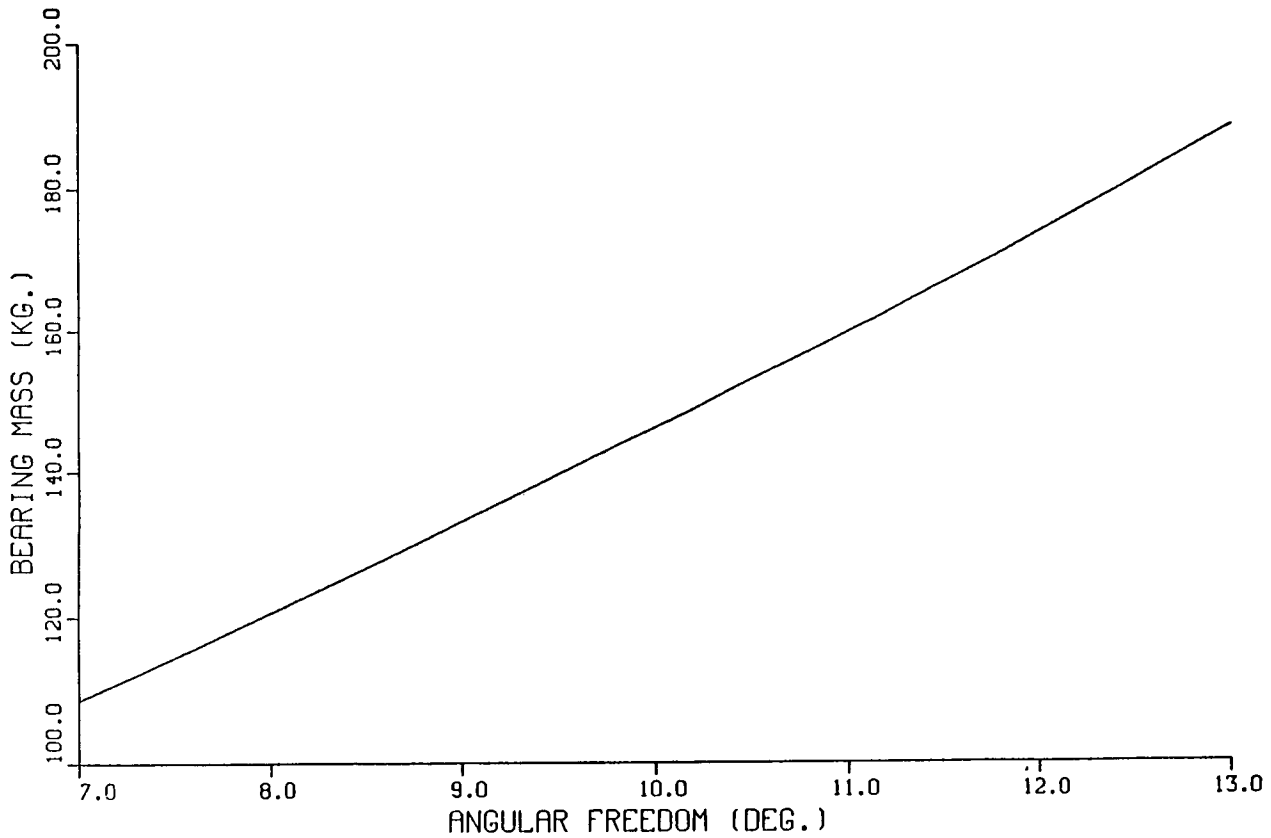

Figure 49.- Attractive magnetic bearing scaling of bearing mass with required bearing angular freedom

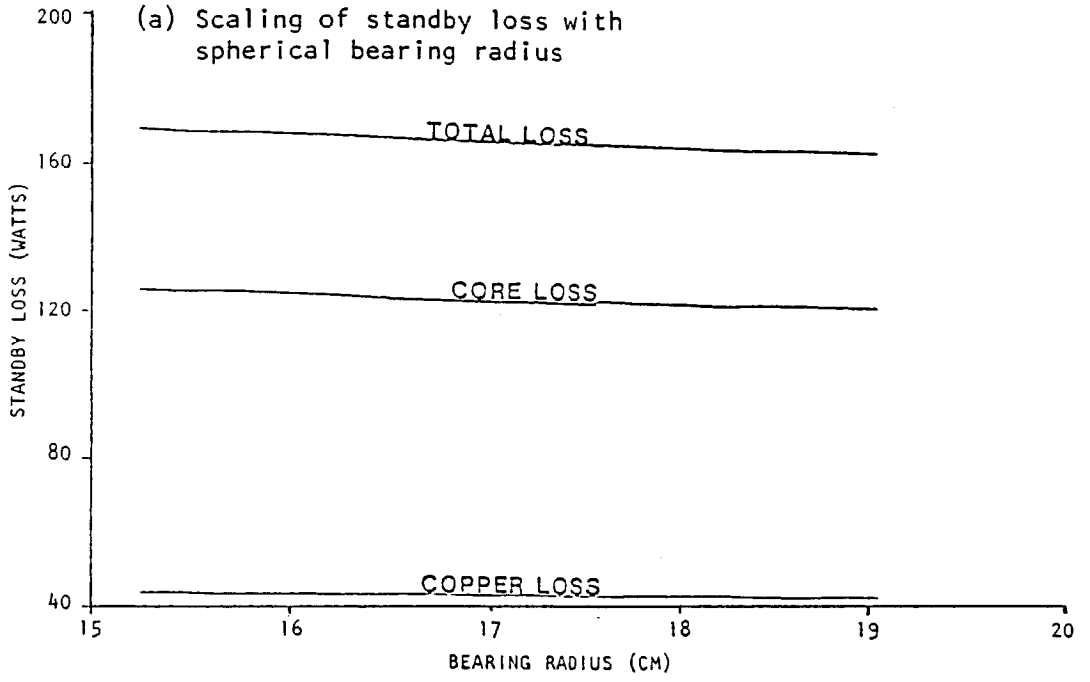

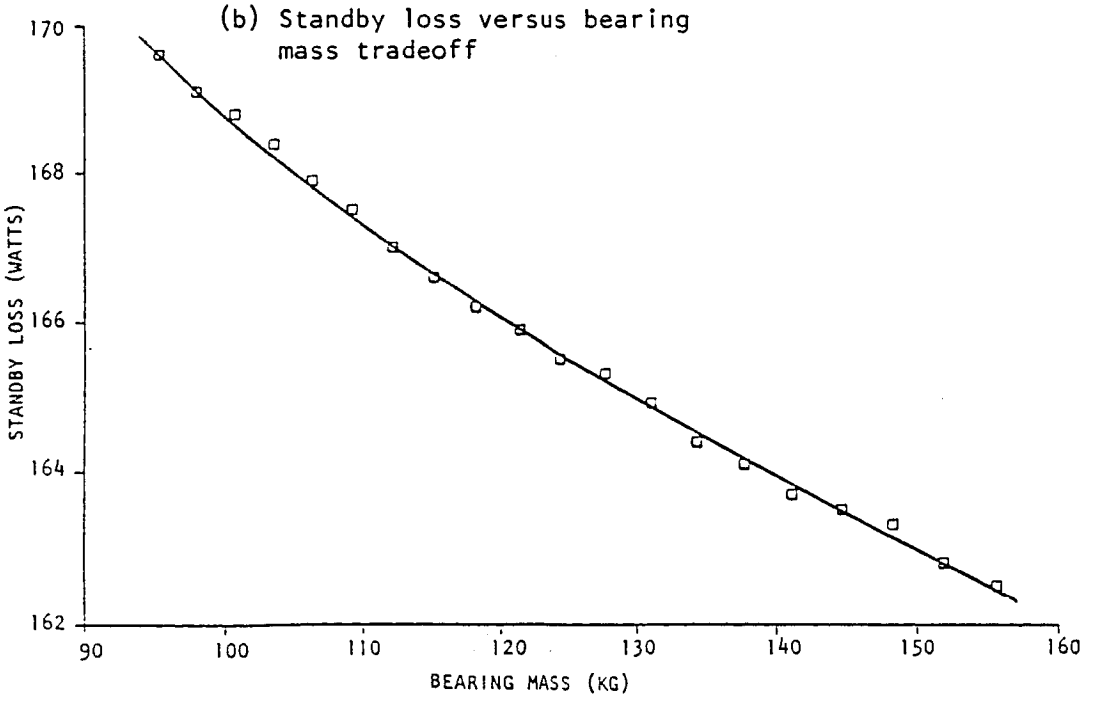

Figure 50.- Attractive magnetic bearing scaling of standby loss with spherical bearing radius (Five-wheel planar configuration)

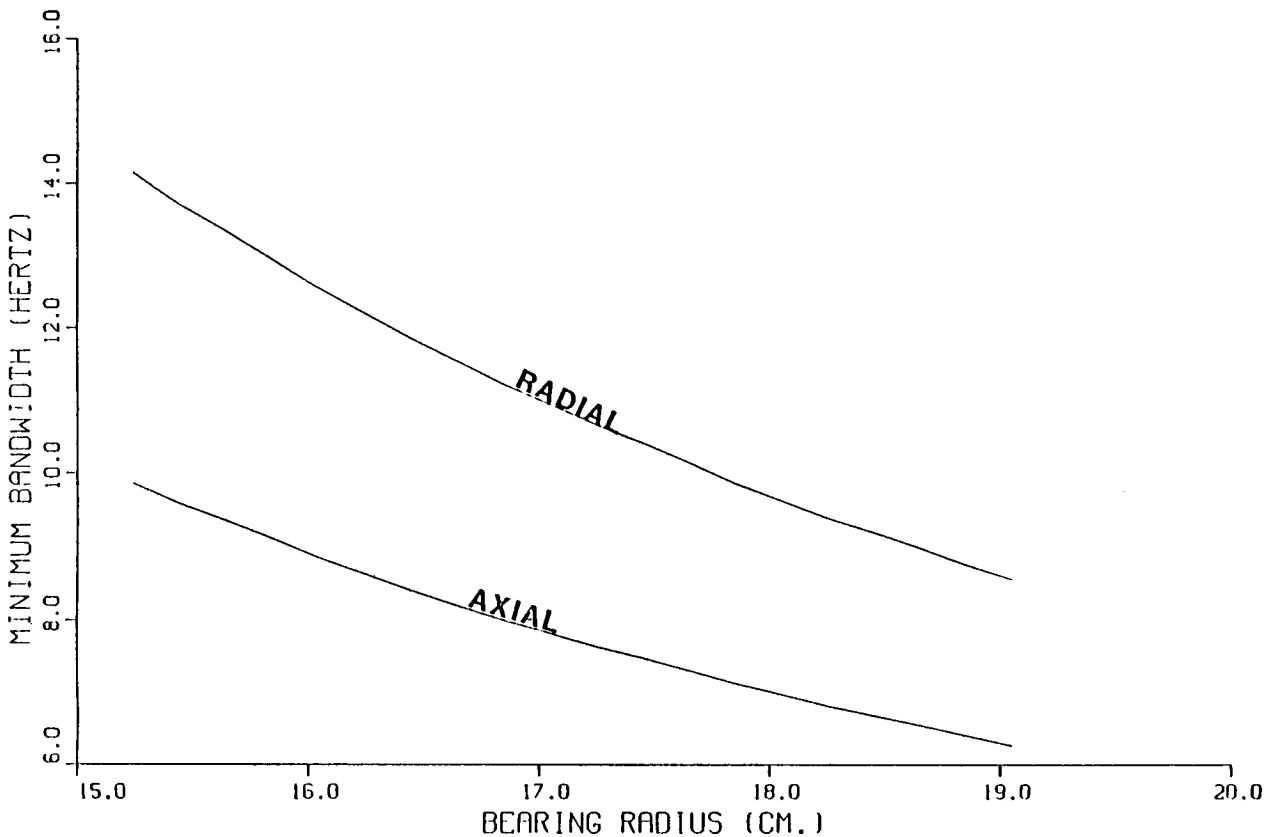

Figure 51.- Attractive magnetic bearing scaling of minimum bandwidth with spherical bearing radius (Five-wheel planar configuration)

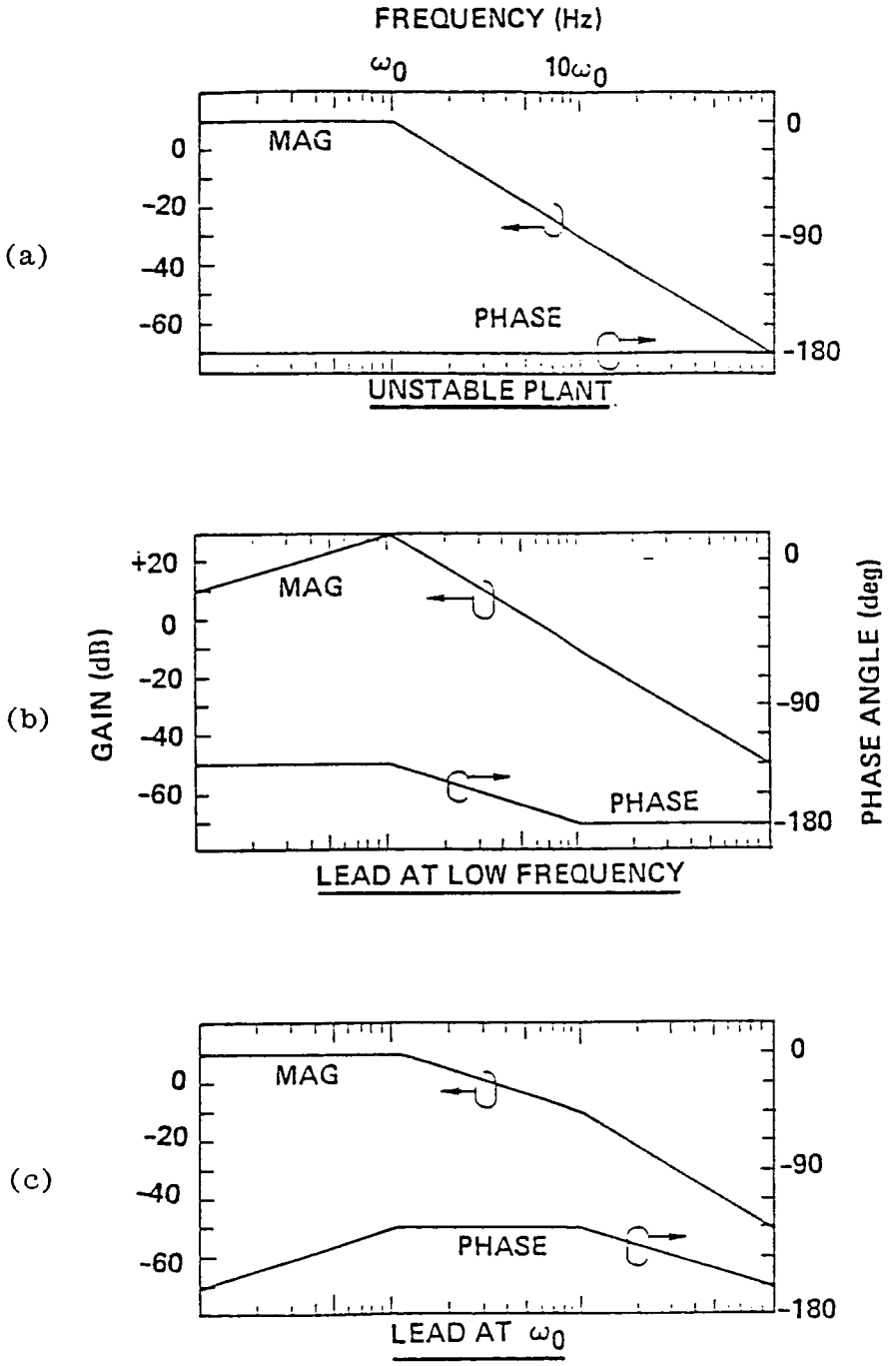

Figure 52.- Classical lead-lag compensation of magnetic bearing

results from trying to cross the system over below the minimum bandwidth frequency as is shown by figure 52 (b). A properly compensated plant is shown in figure 52 (c). Additional problems can result from such effects as structural resonances and unmodeled lags. The manner in which each of these effects can compromise system stability is shown in figures 53 and 54, respectively (ref. 84). By examining the way that minimum bandwidth and high frequency

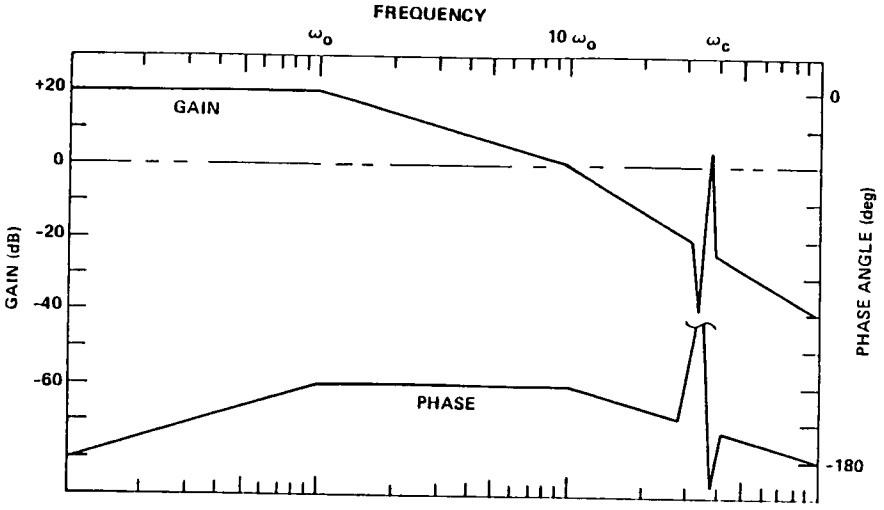

Figure 53.- Performance reduced by structural flexibility

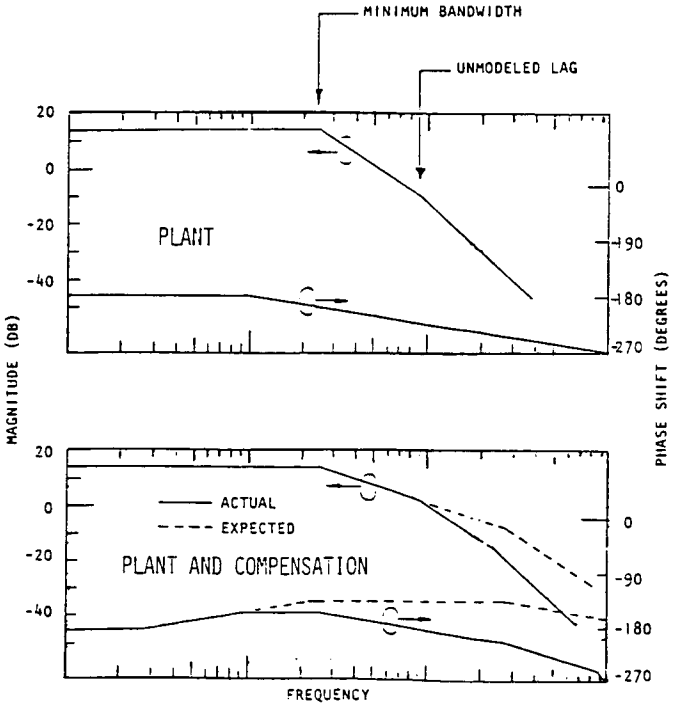

Figure 54.- Stability compromised by unmodeled lag

attenuation scale with flux density and bearing permeance, it can be shown that an octave lowering of the minimum bandwidth and a 10 dB increase in attenuation at high frequency can be obtained only at the expense of a tenfold increase in power consumption.

Conclusions and Recommendations

The large-angle attractive magnetic bearings are competitive in terms of mass and power consumption with large-angle Lorentz force magnetic bearings for an angular freedom less than about 10^{o}. However, the difficulties involved with controlling the inherent instability of the attractive bearing plant swing the design decision in favor of the large-angle Lorentz force bearings. For bearings requiring large amounts of angular freedom, the Lorentz force bearing is the preferred candidate due to its lower weight and power consumption.

The large-angle magnetic bearing design concept developed herein represents a significant departure from existing magnetic bearing design practice, and it is recommended that its development be pursued through further design study and laboratory validation.

APPENDIX D

POWER CONVERSION DESIGN ANALYSIS

by
Richard Hockney and Laura Larkin

The power conversion system is the interface between the flywheel rotor and the spacecraft power bus. As such, it must perform the following functions:

- Bidirectional energy conversion
- Flywheel speed control
- Power bus regulation

For flywheel systems to be viable, the efficiency of the first of these functions must be extremely high. This level of efficiency has recently been made possible by technology improvements in both machines and semiconductors. The other parameters which impact the selection of the candidate system are weight, reliability, and feasibility. Electronics weight is primarily a function of dissipated power, so that it will be minimal for a high-efficiency system. Also, since the power conversion system weight will be on the order of 10% of total system weight, a machine which carries a moderate weight penalty for its higher efficiency will have negligible impact on net energy density. Machine reliability is not considered an issue in the selection process and electronics reliability is discussed when appropriate. The tradeoffs leading to selection of the system with the highest efficiency are described, and the overall efficiency calculated. Finally, the technological advancements required for feasibility are assessed.

The following approach was taken to achieve this task:

1. A baseline configuration was chosen, including voltage and power levels.
2. The electronics configuration options were studied and analyzed to determine the maximum efficiency option and the constraints it imposed on the machine interface.
3. The machine types were traded off against one another under the constraints of the rotor/bearing interface.

The above results were then combined to produce the candidate system.

Baseline Configuration

The power conversion system must perform the interface between the spacecraft's fixed voltage dc bus and the variable speed flywheel rotor. There is a class of machines which operate over variable speeds with fixed

frequency and/or fixed voltage excitation; wound field synchronous and doubly fed machines are examples. The field losses in these machines are known to become prohibitive when they are operated over the 2:1 speed range required here (ref. 72). In addition to their detrimental impact on system efficiency, these losses typically occur on the rotor and creat problems in both heat transfer and power transfer across a high-speed rotating inerface. The remaining machine classes will require variable frequency, variable voltage excitation, and the options for the electronics are limited to two. The excitation can be produced in a two-step process, variable voltage from a dc-to-dc converter, and variable frequency from a square-wave interter as in figure 55 (a); or a single-step pulse-width modulated (PWM) inverter as in figure 55 (b) can be utilized. The fundamental differences are twofold: first, the square-wave inverter requires a machine with square-wave back EMF, and the PWM inverter requires sinusoidal back EMF; second, the dc-to-dc converter can have only low-bandwidth control over net inverter current, whereas the PWM inverter can have very high bandwidth control of each phase current. The latter is seen as the distinction which dictates the choice of configuration: if the system is to be insensitive to commutation faults due to noise, loss of synchronization, or line transients, it must have rapid control of machine phase currents. Thus, PWM is the logical choice.

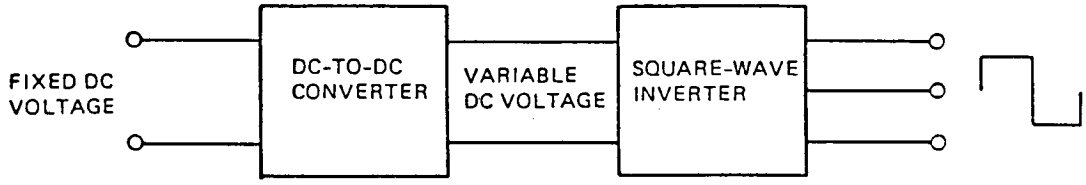

(a) Two-Stage Interface

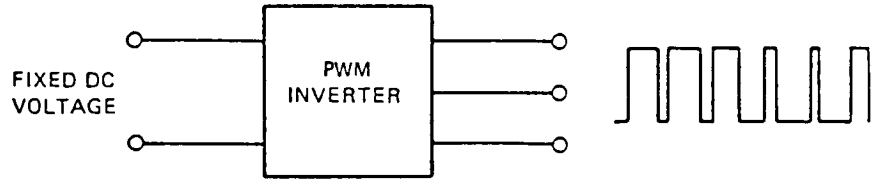

(b) Single-Stage Interface

Figure 55.- Electronics options

Also required for the loss and sizing calculations were the baseline power and voltage levels. The preliminary estimates of 75 kW power and five storage units resulted in a delivered power-level baseline of 15 kW. The rough bounds on bus voltage (150 V < V_{BUS} < 400 V) led to a baseline choice of 300 volts.

Electronics

The goal of this analysis was to determine the most efficient semiconductor device configuration for a PWM machine drive system. Losses in semiconductors employed in this type of system are of two types: switching loss, which is a result of the finite transition time from the on state to the off state; and conduction loss, which is generated by the finite voltage drop in the on state. The devices eligible for inclusion in this study are shown in Table 40, along with their salient characteristics (ref. 73). Since it was known apriori that the switching losses of MOSFET's would be significantly lower than either bipolar junction transistors (BJT) or silicon controlled rectifiers (SCR) (ref. 74), the conduction or on-state losses were calculated first.

TABLE 40.-SEMICONDUCTOR TYPES

CHARACTERISTICS	SCR	BJT	FET
"ON" LOSS	$I \times V_D$	$I \times V_D$	$I^2 \times R_D$
SPEED	SLOW	FAST	VERY FAST
DRIVE	LATCH	CURRENT	VOLTAGE
POWER CAPACITY	VERY HIGH	HIGH	MEDIUM

The model used to calculate per phase conduction losses is shown in figure 56. An interesting result of this system configuration is that there is a value of machine inductance (L_ϕ) above which the machine cannot deliver 15 kW to the bus. This is true because as the machine inductance increases, the increased voltage drop across it requires that the phase voltage (V_ϕ) decrease. This, in turn, requires an increase in the phase current (I_ϕ) and produces a larger voltage drop across the inductance and so on. Eventually,

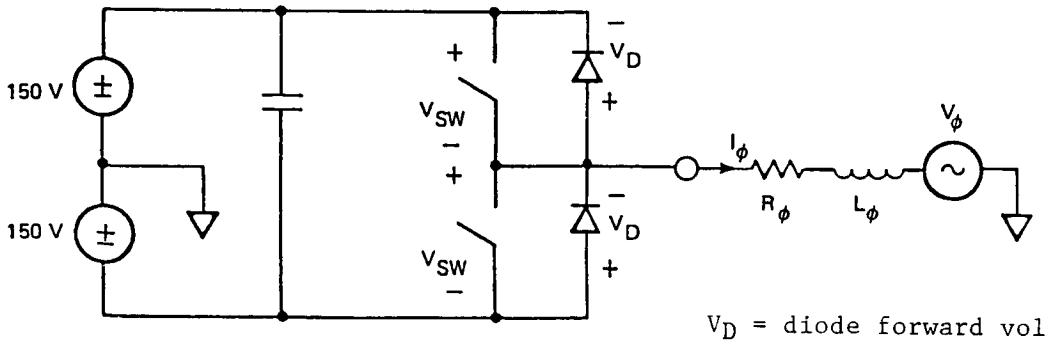

$V_\phi = K\omega_m \sin \omega_m t$

$\bar{I}_\phi = A \sin \omega_m t$

V_D = diode forward voltage drop

V_{SW} = switch forward voltage drop

K = back-EMF constant

ω_m = machine angular frequency

A = peak phase current

Figure 56.- Loss model

Kirchoff's voltage law can no longer be satisfied, and the machine output power must drop off. Curves of maximum machine inductance are shown in figure 57 as a function of bus voltage and full speed of the machine.

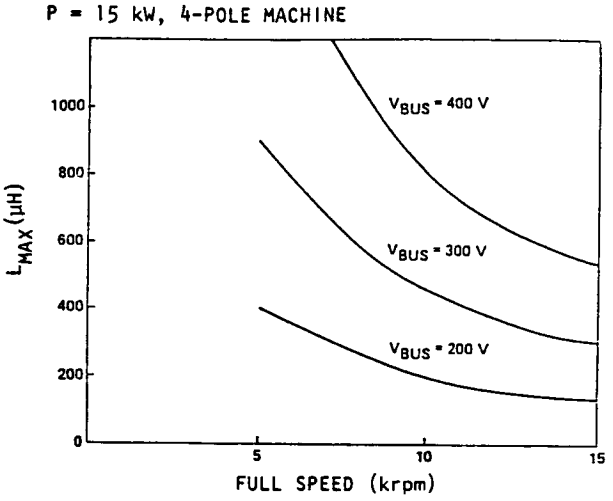

Figure 57.- Maximum machine inductance vs. full speed and bus voltage

The conduction loss is found by multiplying the current in each device times the voltage across the devices times the duty cycle of its conduction (δ_{SW} or δ_D).

$$P_C = 2(V_{SW}I_\phi\delta_{SW} + V_DI_\phi\delta_D)$$

The models used to find V_{SW} and V_D for each device are shown in figure 58. This loss was computed over an entire charge or discharge cycle as a function of machine inductance. The results for the zero inductance case are listed in Table 41 as a percentage of per-phase power.

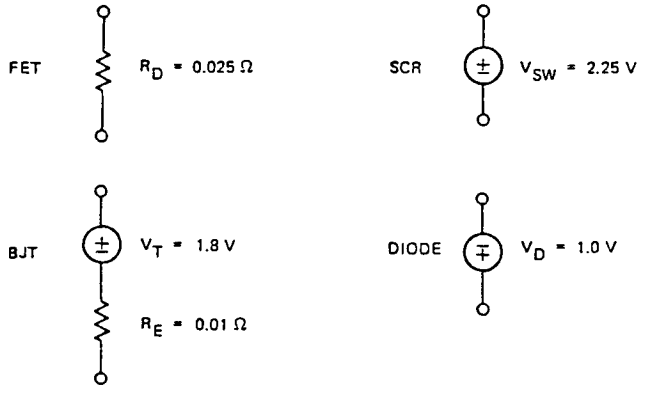

Figure 58.- Device models

TABLE 41.-TOTAL CONDUCTION LOSSES
WITH $L\phi = 0$

	FET	BJT	SCR
Motor	2.1%	2.5%	2.4%
Generator	1.3%	1.6%	1.5%

As is apparent, the losses are comparable. Unfortunately, the number of devices per switch for each type is not. At this power level only one SCR is required, three BJT's are required, and 15 FET's are required to carry the per-phase current. The ramifications of this fact will be discussed later. It should be noted that properly implemented paralleling will actually lead to a reliability improvement, since each switch will be capable of withstanding a single-device failure with only minor degradation of its derating factor.

The switching loss calculations were performed on the basis of approximation shown in figure 59 (ref. 75). Thus,

$$P_S = V_{CC} I_C t_{VI} f_{SW}$$

where f_{SW} is the PWM switching frequency. This frequency is determined by the machine inductance such that the peak high-frequency current ripple is 10% of the low-frequency, per-phase RMS value. This loss as a percentage of per-phase power, integrated over an entire charge and discharge cycle, is plotted in figures 60 and 61 for the FET case, along with the conduction loss and total

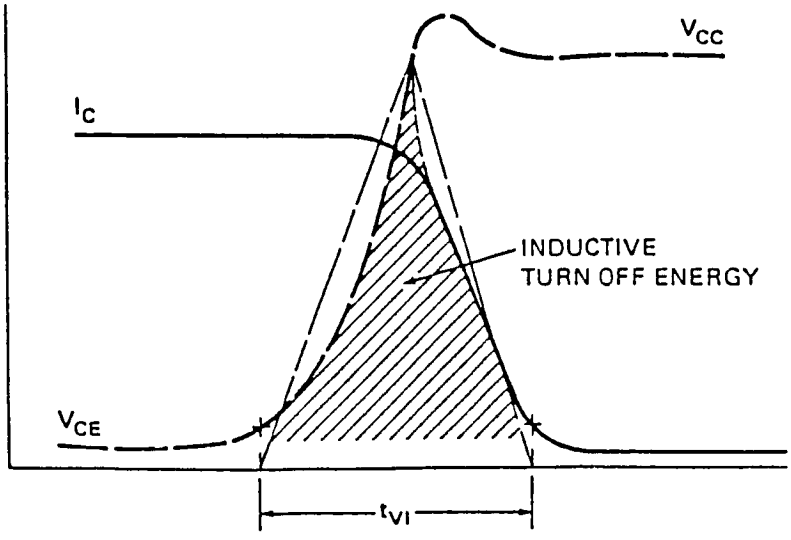

V_{CC} = off-state voltage
V_{CE} = on-state voltage
I_C = on-state current
t_{VI} = on-to-off transition time

Figure 59.- Inductive turn-off energy approximation

loss as a function of machine inductance; t_{VI} was taken as 600 ns. Since a BJT can be expected to be three to five times slower, the total loss in the generator mode would be at least 15%; clearly too high to be considered further. The SCR would be even slower. Thus, the semiconductor of choice is the MOSFET with a total loss in the generator mode of approximately 5% and in the motor mode of 3%. As is apparent from the figures, the optimal machine inductance is approximately 250 μH; this dictates a switching frequency of 19 kHz by the peak current-ripple relationship stated above.

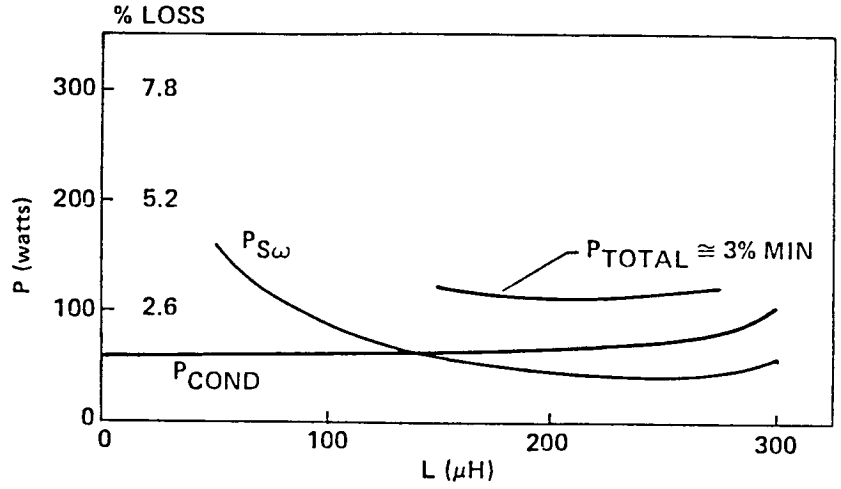

Figure 60.- Per-phase electronics loss
(Motor, P = 11.4 kW)

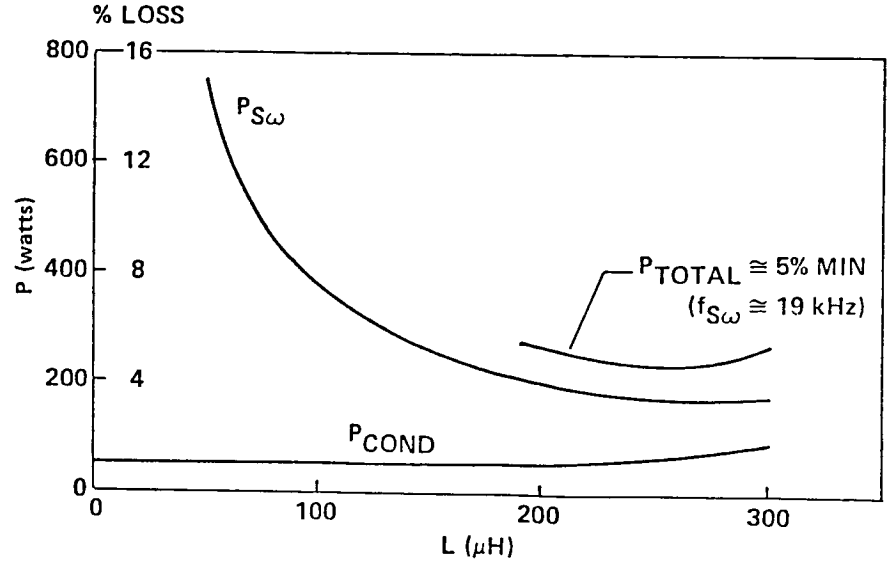

Figure 61.- Per-phase electronics loss
(Generator, P = 15 kW)

Motor/Generator

A flywheel energy storage system requires a very high efficiency motor/generator to transfer energy bidirectionally between the spinning flywheel and the electrical bus to be advantageous over a battery system. This machine must operate as both a motor and a generator over the anticipated 2:1 speed range of the flywheel. For spacecraft applications, weight and volume of system components are critical factors to allow lightweight and relatively small (launchable) satellites. For a motor/generator, this translates into a high-efficiency machine.

This selection analysis assumed parameters compatible with Space Station specifications. The primary considerations in the choice of machine type were copper loss, iron loss, and side-loading forces (acting to pull the rotor toward the stator) which would act as disturbances to the magnetic suspension. Of secondary concern were level of integration with other system components and machine complexity. Current and advanced motor/generator technology was reviewed and evaluated for this application. This thorough literature search yielded the original candidate machines which are listed below along with a qualitative description of attributes.

Type	Advantages	Disadvantages
• PM reluctance	• No field windings. PM's are stationary.	• Potential large side forces. Voltage is a function of speed only.
• Wound-field synchronous	• Can control voltage by changing field strength.	• Power used to generate field is lost. Rotor and stator copper loss.
• Induction	• Has simple, rugged design.	• Inherent rotor losses. Hard to remove heat from rotor. Large side forces. Rotor and stator copper loss.
• Conventional synchronous permanent magnet (PM)	• No field windings.	• Magnets typically rotate; potential large side forces. Voltage is a function of speed only
• Ironless/ rotating backiron	• Minimizes hysteresis and eddy current losses. Low side force. Readily available high-energy product magnets.	• More complex mechanically. Voltage is a function of speed only. Expensive magnets.

The permanent magnet (PM) reluctance machine is a synchronous device that uses the generated electrical force to align the rotor axis with that of the stator. The rotor typically consists of teeth and slots for windings while the stator contains PM's or windings to induce a magnetic field. Iron losses occur in the rotor along with eddy current and copper losses in the windings. This type of machine is mainly used for low output devices such as phonographs and was dropped from further consideration due to, in general, a low power factor and relatively low efficiency (ref. 72).

The wound-field synchronous machine works on the principle of Faraday's law of electromagnetic induction, and generates electromotive force (emf) through the relative motion of conductors and magnetic flux. A synchronous machine is comprised of a magnetic field structure carrying a dc excited winding and the armature, often a three-phase winding. Almost all modern machines have stationary armatures and a rotating field structure. The rotating field is connected to an external source through slip-rings (or brushes), or brushless excitation provided by rotating diodes. The wound-field synchronous machine is capable of providing good voltage regulation, but was discarded due to the high flywheel speed required (>20,000 rpm) for a satellite application. At this speed, slip-rings would not be reliable and the excitation frequency for rotating diodes would be too high.

The induction machine operates on the basis of the interaction between the induced rotor currents and the air-gap fields. It generally consists of a rotor mounted on bearings and a stator separated by an air gap. The stator consists of a core made up of punchings (or laminations) carrying slot-embedded conductors (armature windings). Alternating current is supplied to the stator windings and the currents in the rotor windings are induced by the stator currents. Copper losses occur in both the rotor and stator. To reduce core losses, the working flux density must be kept small. This imposes a conflicting requirement on the load current since the torque is directly proportional to the flux density. However, because of its simple and rugged design, the induction machine is the most common machine in use today (ref. 76).

The conventional (or synchronous) PM machine is similar to the wound-field machine except that the field is generated by PM's. The efficiency is higher than a wound-field synchronous machine due to the elimination of the field electrical loss. Also, with the advances in PM technology, such as the improved availability of high-energy density product Samarium Cobalt (SmCO), high field fluxes resulting in a small machine are now readily obtainable. Loss mechanisms include core (hysteresis) loss and winding copper and eddy current losses.

The ironless stator/rotating back-iron PM machine utilizes the large air gaps and high field fluxes available from high-energy product magnetic materials. In this type of machine, the magnetic portions of the magnetic circuit are on the rotor (all rotate); the stator contains only copper and structural/thermal support. Thus, the "ironless" refers to the stator. This eliminates the hysteresis and eddy current losses in the iron portions of a conventional synchronous brushless PM machine and results in a higher efficiency motor/generator (refs. 77, 78).

The five machine candidates described above were pared down to those shown in Table 42. This table shows the three machines chosen for further evaluation along with qualitative information on machine losses, side-loading forces, complexity in fabrication, torque values, and type of feedback control.

TABLE 42.-MACHINE TYPES

		PM BRUSHLESS	PM "IRONLESS"	INDUCTION
TORQUE		KI	KI	KI^2
LOSS	IRON	MED	VERY LOW	LOW
	COPPER	I^2R_W	I^2R_W	$I^2(R_S + R_R)$
SIDE-LOAD		YES	NEGLIGIBLE	YES
FEEDBACK		POSITION	POSITION	SPEED
COMPLEXITY		MED	HIGH	LOW

K = TORQUE CONSTANT

I = PER-PHASE CURRENT

R_W = PER-PHASE RESISTANCE

R_S = STATOR RESISTANCE

R_R = ROTOR RESISTANCE

Machine choices were to be further reduced by calculating the side-force negative spring constant for each machine. This is the force which acts to pull the rotor toward the stator and is, therefore, unstable and must be counteracted by the magnetic suspension.

Motor side-loading forces are radial forces due to the radial flux between two cylinders. The radial force, F_R, is described by (ref. 76):

$$F_R = \frac{1}{2} F_a^2 \frac{dP}{dx}$$

where

F_a = magnetomotive force

$\frac{dP}{dx}$ = spatial derivative of the permeance between the inner and outer cylinders (rotor and stator)

The permeance of two cylinders of differing radii wholly within on another and eccentric is described (ref. 79) as:

$$P = \frac{2\pi\mu\ell}{\log_e[1 + a(1 + \sqrt{\frac{2}{a} + 1})]}$$

where

$a = (g^2 - x^2(/[2r(r + g)]$

ℓ = axial length

g = nominal gap

r = inner radius of larger cylinder

x = offset from nominal gap

The magnetomotive force, F_a, can be expressed in terms of the flux in the radial gap, ϕ.

$$F_a = \frac{\phi}{P}$$

and the flux may be expressed in terms of gap flux density, B, and gap area, A.

$$\phi = BA$$

Substituting the derivative of the permeance and the expression for the magnetomotive force into the original equation allow evaluation of the radial force.

Once the radial force is found, the equivalent radial spring constant, k_r, is calculated by differentiating this radial force with respect to x,

$$k_r = \frac{dF_R}{dx}$$

Analysis of this permeance and magnetomotive force produced the following equation for the spring constant:

$$k_r = \frac{\pi B^2 l (2r + g)}{2\mu_0 g}$$

where

B = air gap flux density (Tesla)

l = machine axial length (m)

r = radial distance to the air gap (m)

g = air gap length (m)

μ_0 = permeability constant of free space (N/A^2)

The results of this analysis, using parameters from existing machines and assuming a 455-kg flywheel (compatible with Space Station requirements), are shown in Table 43. An unstable frequency of 150 rad/s is sufficiently high to rule out the indiction machine since it would place a bandwidth restriction on the magnetic suspension system which is much greater than that dictated by momentum control considerations (ref. 81). While techniques exist to stabilize the side-force of an induction machine, they have been shown to require operation in the high-slip region; i.e., the low efficiency region of operation for this type of machine (ref. 82).

TABLE 43.-MACHINE SIDE-LOAD (15 kW)

	Spring Constant	Natural Freq. (m = 455 kgm)
Induction Machine	11 x 10^6 N/m	154 rad/s
PM "Ironless"	Negligible	<0.1 rad/s
Conventional PM	285 x 10^3 N/m	25 rad/s

The losses in both the rotating back-iron (ironless) PM and conventional PM machines must now be evaluated. Thus, the copper volume and I^2R loss as a function of current density were calculated for an ironless machine given the interface requirements (voltage, speed, etc.). Using the volume of copper, the eddy-current loss (P_e) was calculated through the derivation presented in ref. 80.

$$P_e = (\pi f B_p \tau)^2 \frac{V}{6\rho}$$

where,

B_p = peak flux density

f = electrical frequency

τ = copper wire diameter

V = copper volume

ρ = copper resistivity

These losses were integrated over a full charge and discharge cycle, and the total results are shown as a percentage of total power in figures 62 (A) and (B), respectively, for a machine whose minimum speed (ω_{min}) is 6,000 rpm. The total loss for the conventional PM machine was then calculated by adding the eddy-current and hysteresis losses of the iron to those of the copper. These data are also shown in figures 62 (A) and (B). As is evident, the loss of the conventional machine is approaching that of an ironless machine at 10^7 A/m^2; however, for high-reliability, long-life applications, the recommended limit on current density is about 8 x 10^6 A/m^2 (ref. 76). There, the conventional machine losses are significantly higher (5.0% versus 3.4%, and 5.5% versus 3.8%). Despite the fact the "ironless" machine has thermal and mechanical characteristics which are inferior to those of the conventional machines, the 50% higher losses of the latter dictate that it occupy the "fall-back" position should developmental problems occur with the higher efficiency "ironless" machine.

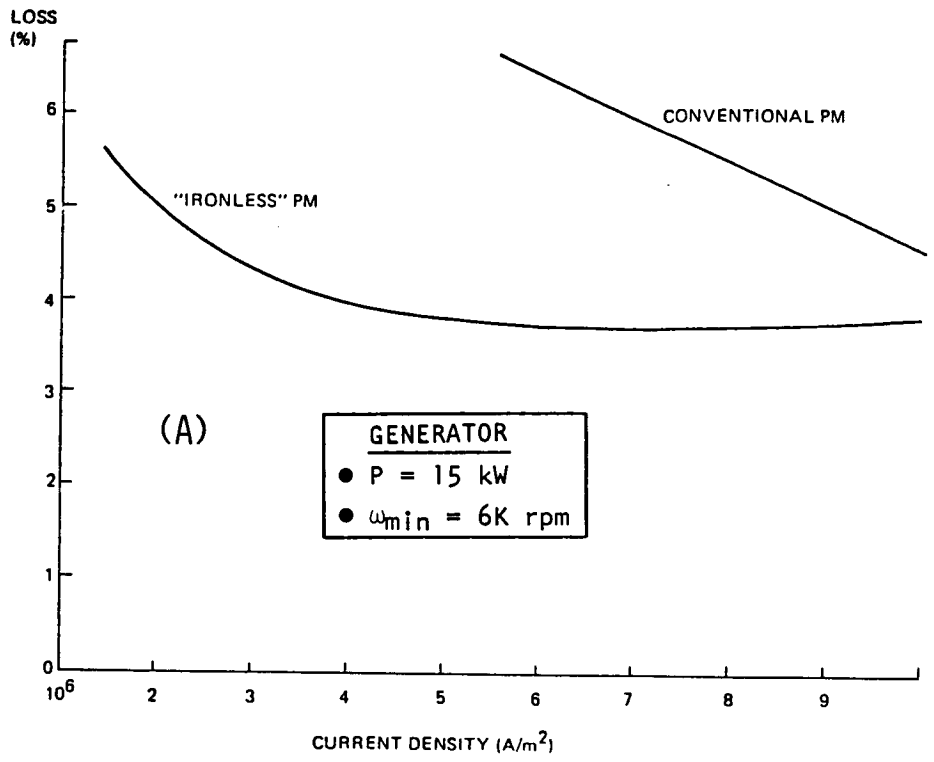

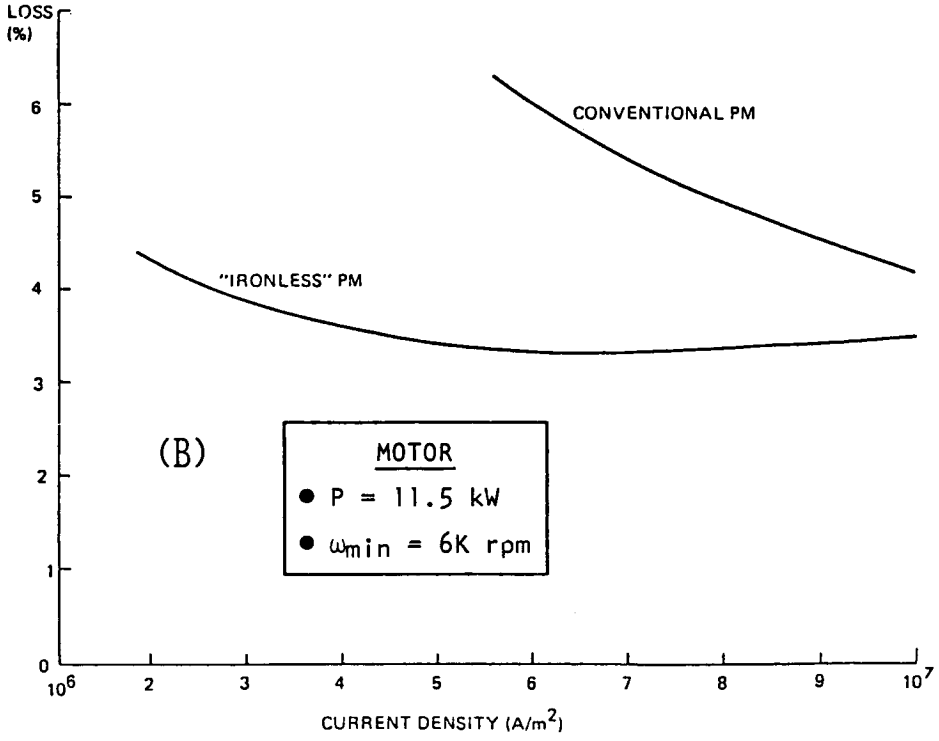

Figure 62.- Cycle loss vs. current density

The design of a 15-kW, 6K-rpm-minimum-speed rotor is shown in figure 63; its weight is calculated at 26.4 kg. The ironless stator would fit in the air gap. Removing excess back-iron material can reduce the overall machine weight by "cutting corners" on the back-iron. In figure 63, this would mean removing a triangular section from the lower-right and -left corners of the back-iron. This area is shown as lightly shaded in the fiture. This reduces the weight to 23.2 kg. Further weight reduction could be achieved through future magnetic materials development. This study assumed the use of samarium-cobalt magnets. Neodymium-iron-boron ("Crumax") magnets, with twice the maximum energy product of samarium cobalt, could reduce machine weight by an additional 10%.

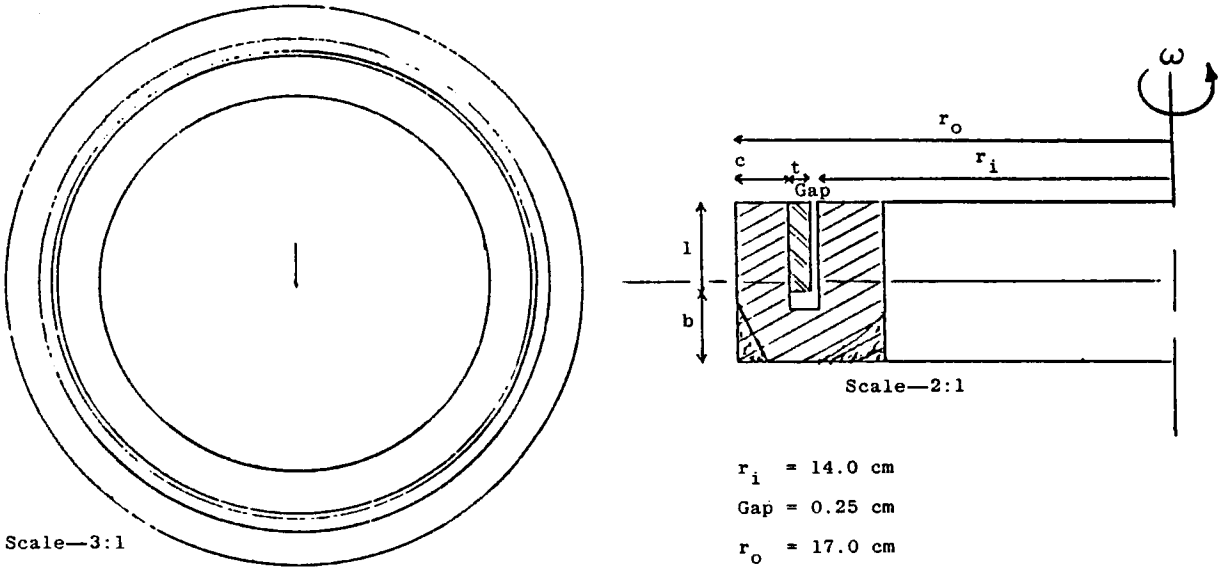

Mass = 26.4 kg
Current density (assumed) = 6×10^6 A/m^2
Magnets = Samarium Cobalt
ω_{min} = 6,000 rpm
P = 15 kW

r_i = 14.0 cm
Gap = 0.25 cm
r_o = 17.0 cm
b = 3.0 cm
l = 3.7 cm
t = 0.76 cm
c = 2.1 cm

Figure 63.- Design case—PM "ironless"/rotating back-iron motor/generator

This design could be modified to allow magnetic suspension gimbaling. A sketch of a spherical air-gap, ironless stator, PM motor/genrator is shown in figure 64. Dimensions would be similar to the above design, but the copper losses would be slightly higher due to the increased stator active length.

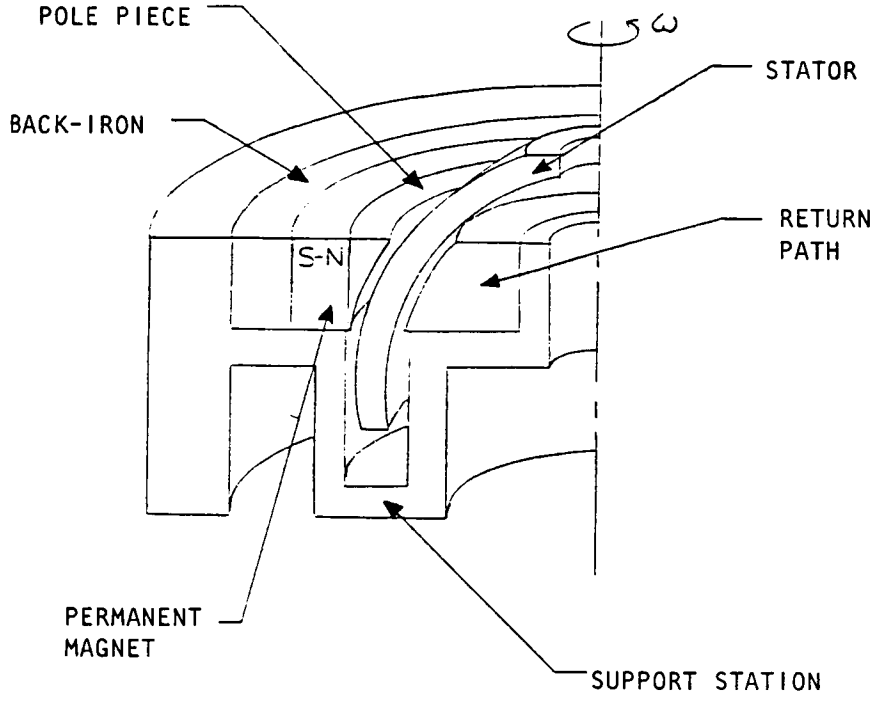

Figure 64.- Spherical air-gap, ironless stator, PM motor/generator concept

Conclusions

The results of the preceding analyses may now be combined to produce the baseline power conversion system and determine its efficiency. The power semiconductor type is the MOSFET since it has the lowest switching loss and comparable conduction loss. An added benefit is the minimal power required to drive the device. The machine type is PM rotating back-iron since its lack of iron losses makes it the more efficient of the low side-force devices. The added benefit here is that the side-force is negligible, and represents no interference with the magnetic bearing system. The system configuration is the PWM inverter shown in figure 65, since this allows high-bandwidth control of each phase current—a capability necessary for maintaining high power factor commutation fault recovery. This approach also offers the advantage of a single power stage, which simplifies system architecture and thermal design.

The PWM frequency should be about 20 kHz for minimum semiconductor loss, and the machine inductance should be about 250 μH for reasonable current ripple and quadrature foltage component.

The cycle loss summary for this configuration is shown in Table 44. The miscellaneous losses include power for the logic and drive electronics, and stray machine and interconnect losses. The magnetic bearing losses and power

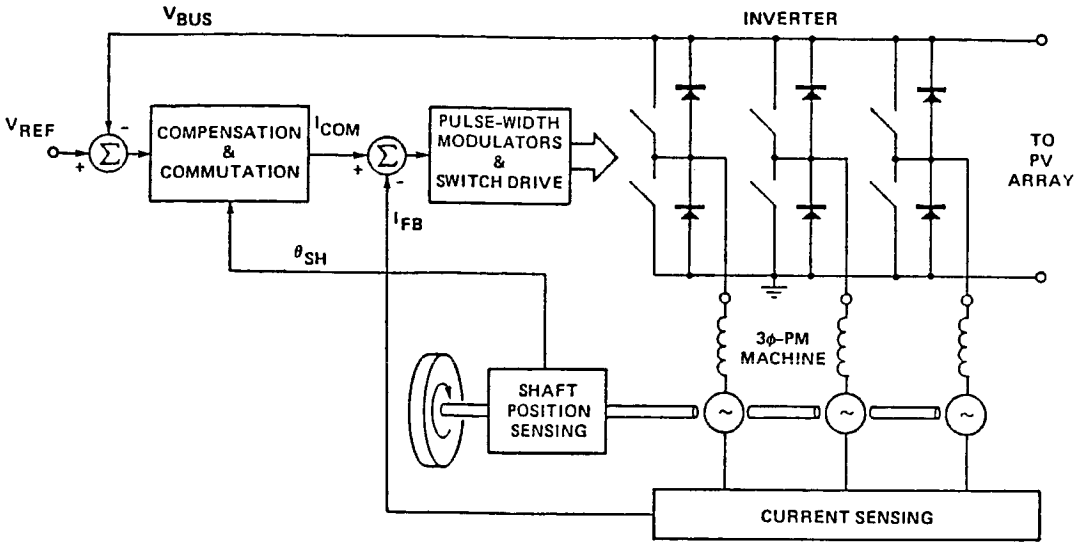

Figure 65.- Baseline power conversion system

for orbit-rate precession are also included, so that the loss quotes are representative of the complete energy storage system. The projected round-trip efficiency of 85% substantially exceeds that of completing energy storage systems and is a viable technology.

TABLE 44.-LOSS SUMMARY,
MOSFET-PWM DRIVEN PM-IRONLESS MACHINE

Loss Item	Motor	Generator
Semiconductor	2.7%	4.6%
Machine	3.4%	3.8%
Magnetic bearing	0.5%	0.4%
Miscellaneous	0.3%	0.3%
Total Loss	6.7%	8.9%
Total round-trip efficiency = 85%.		

Recommendations

There are two areas in which technology advancement would improve the feasibility of the proposed power conversion system. The first is in techniques for paralleling power MOSFET's. While discrete circuits have been built which parallel up to ten MOSFET's, these typically have switching frequencies in the vicinity of 1 to 2 kHz; an order of magnitude below what is required here. While the operational degradation in these circuits at higher frequencies may not be severe, it would be preferable to employ power circuit hybridization techniques to parallel the devices in order to reduce

parasitic effects. Commercial devices currently exist (Motorola MTE 100N06) which parallel three devices in a power hybrid. The extension of this technology to six or even ten devices would certainly improve the chances for success in utilizing so many devices per switch in the proposed system.

The second area in which there is a perceived weakness is in cooling the copper in an "ironless" PM machine running in a vacuum. (A 26-kW axial air-gap ironless stator PM motor/generator built by AiResearch in 1983 (ref. 77) ran into thermal problems. The machine required the manufacture of four stators due to shorting caused by excessive heat.). Since the stator of this device has no iron in it, the normal thermal conduction paths are nonexistent, and other thermal control methods must be investigated.

APPENDIX E

INTEGRATED COMPONENT DESIGN TRADE

by
Stephen R. O'Dea

The purpose of Appendix E is to use the parametric results of the preceding appendices to design an overall IPACS unit that meets the Space Station system requirements in a relatively optimized fashion. Appendix E is, therefore, organized into: (1) a description of the requirements, design drivers, and their impact on system design; and (2) a description of the scaling and trade-offs that lead to design optimization.

IPACS Component-Level Requirements and Design Drivers

The overall IPACS system-level requirements are developed in the "IPACS System Configuration Definition" section, and were summarized in Table 2. In this same section the component-level requirements are developed for four-, five- and six-wheel versions of the baseline planar array wheel configuration, and were summarized in Table 14. They are predicated on the energy-balance diagram efficiencies given in figure 19.

The most fundamental requirements that are design drivers in influencing the IPACS component sizing and design are energy storage, bus power level, momentum transfer, and redundancy. By considering the array configuration and the redundancy requirement, the minimum number of wheels can be determined. Although a four-wheel system meets the requirements, the selection of a five- or six-wheel system seems better when other factors are included. Factors favoring the minimum number of wheels include:

- Potential for lower manufacturing cost
- Potential for more momentum storage
- Less complex control law
- Fewer wheels required in the growth Station

Factors favoring a greater number of wheels include:

- Less oversizing for redundancy, especially for the initial Station
- Less design risk for smaller wheels, motors, and electronics
- Potential to accomplish attitude control in fail-operational (FO) mode using only a magnetic bearing for systems of six or more wheels

A major design driver is the combination of momentum storage requirements and body rate. These requirements combine to increase bearing weight and power consumption. That is because the momentum transfer requirement leads to large wheel momentum and/or large bearing angles (which increases bearing weight). Large momentum and body angular rates lead to high power requirements to precess the wheels. If body rates were reduced by 30%, the control torque requirement would then become the driver for bearing power.

The interpretation of the FO requirement affects system efficiency. Current calculation of efficiency is based on a 75% depth of discharge (DOD), which will occur only under a failure condition. This is because the system is sized to provide rated energy storage with one wheel failure. Under normal conditions, a five-wheel system will have a DOD of 60% (62.5% for six wheels). Storage efficiency would increase if it were calculated based on 60% DOD. In addition, slightly higher energy density could be realized by changing the cyclic stress levels. Alternatively, the remaining operational wheels could allow 10% higher speed under failure conditions.

Finally, the maximum voltage impacts efficiency since the motor/generator and the electronics losses are largely related to current.

Safety Considerations

The large amount of kinetic energy stored in a Space Station IPACS warrants some consideration of the hazard associated with a rotor structural failure. Some composite materials have been shown to fail much more gracefully than some of the metallic materials; however, a failed rotor can still impose substantial hazard. Although safety was not considered to be a major concern in the current study, it is prudent to assess any design penalties associated with the achievement of satisfactory safety. The approach employed herein for this purpose is twofold: (1) to survey the results of the recent DOE contracts and determine if any techniques were identified that were appropriate to the current application; and (2) to try to conceive other safety techniques that might be more appropriate to space application which was not considered in the DOE effort.

The DOE studies focused on terrestrial application of energy storage wheels, and considered rotor failure containment as the primary safety approach. The rotor failure containment approach requires a containment vessel whose mass is large relative to the rotor mass, and would severely penalize the IPACS energy density. "Fail-safe" and "limited-failure" design concepts were also proposed and tested by at least one of the contractors (refs. 68 or 69). Unfortunately, these rotor design concepts are not readily adaptable to the thin-wall annular rotor design concept selected in this study.

The safety design approach selected for this effort employs two techniques. The first is to use conservative design margins so as to avoid all but the most remote of failure mechanisms (such as a collision or meteoroid strike on a wheel unit). Thorough ground testing of each IPACS unit is used to detect conventional structural flaws. In addition, composite rotors generally manifest a balance shift prior to failure, which is detectable with the magnetic bearing instrumentation. The second safety design approach is to arrange the wheel array, and its location, so that the shrapnel path from a failed rotor (approximately in a plane perpendicular to the spin vector) does not intersect habitable modules or critical structure. For the current Space Station concept (figure 3), this is made somewhat easier by its large size which permits the IPACS equipment to be located at a reasonably large distance from the habitable modules.

Component Tradeoffs and Integration

To meet the IPACS requirements in some optimized (efficiency, weight) fashion requires consideration of the characteristics of each of the previously discussed subsystems (rotor, bearing, and power conversion). In many instances, performance requirements or technology limitations dictated the form of the solution (such as the type of motor and electronics), and the necessary tradeoffs could be done almost entirely within the subsystem design task. These tradeoffs were discussed in the preceding appendices. Other areas, most notably the rotor and bearing integration, required significant tradeoffs to achieve a design that met often conflicting requirements, was lightweight and with low losses. In addition, the attachment of the rotor to the bearing/motor has associated tradeoffs. This appendix will be broken into three main parts dealing with scaling of the subsystems for system optimization, system-level model/optimization, and rotor attachment. Each of these parts will be further divided into more specific tradeoff areas.

Subsystem Scaling.-This section of the appendix describes the process of taking the scaling results of the previous appendices and putting them in a form suitable for use in the overall system model. The areas covered include rotor and motor scaling and, in the case of bearing scaling, some tradeoff issues as well.

Rotor Scaling.-It was decided to look at annular rotors with inside-to-outside radius ratios (α) in the range from 0.75 to 0.85. The lower value (0.75) was chosen because that is the point at which the flywheel stress limit can safely be considered to be tangential stress. This is important because tangential properties are better known and more easily controlled than radial properties. The upper value (0.85) was somewhat arbitrarily assumed, but represents greater than 95% of the "ideal" ($\alpha = 0.99$) energy density. Values of $\alpha > 0.85$ will increase system volume and case weight. By examining both figures 29 and 30 (Appendix A), this can be verified. Additionally, the energy density at $\alpha = 0.85$ is less than 8% greater than at $\alpha = 0.75$. For the purpose of the design trades, the flywheel was assumed to be a constant mass with an energy density of that of an $\alpha = 0.80$ rotor. At the conclusion of the design trades this assumption will again be examined. Small changes in shape (conical, flared) do impact energy density, but these changes involve studies wholly within the rotor design task. The important parameters at system level are speed (ratio of energy to momentum storage) and α. Changes in these affect the radius-to-height ratio. Boron/epoxy was chosen as the rotor material because of :

- High energy density potential (18.6 Wh/lb) for the derated rotor.
- A relatively safe failure mechanism is predicted (compared to isotropics). Failure mechanisms for metal matrix composites (MMC) are not well known.
- Acceptable radial growth (40% less growth than graphite/epoxy, yet only 10% less energy density).

Motor Scaling.-As the rotor speed increases, the mass decreases because less torque is required to deliver the power. The motor mass increases with increasing bearing tilt-angle because more iron and copper must be used in a motor which sweeps through a large (>5°) angle. This suggests a model of the form

$$M_{motor} = a = b\theta + C/\omega$$

where θ is the gimbal angle in degrees, and ω is the rotational speed in rpm.

For the design discussed earlier, the equation reduces to

$$M_{motor\ (kg)} = 2 \cdot \theta + 3.6 \times 10^5/\omega.$$

Bearing Scaling and Dependence on Rotor Design.-The design of the rotor has a very strong impact on the design of the magnetic bearing. It is obviously critical to design the rotor so that it operates very close to its maximum energy density. However, within this constraint, considerable variation in speed and height/radius ratio (and, therefore, angular momentum) is possible. The impact of rotor angular momentum on the bearing is large because: (1) high angular momentum allows small gimbal angles, substantially reducing bearing weight; and (2) low angular momentum allows lower precession torques and, therefore, a much smaller power consumption requirement to precess the wheels.

To address these issues quantitatively, the power versus mass characteristic was plotted for two Space Station attitude rates, assuming a five-wheel configuration. The curves are shown in figure 66. The left-hand curve shows the intuitively obvious trends that, for a relatively fixed torque requirement (control torque dominated), bearing mass increases with both increasing

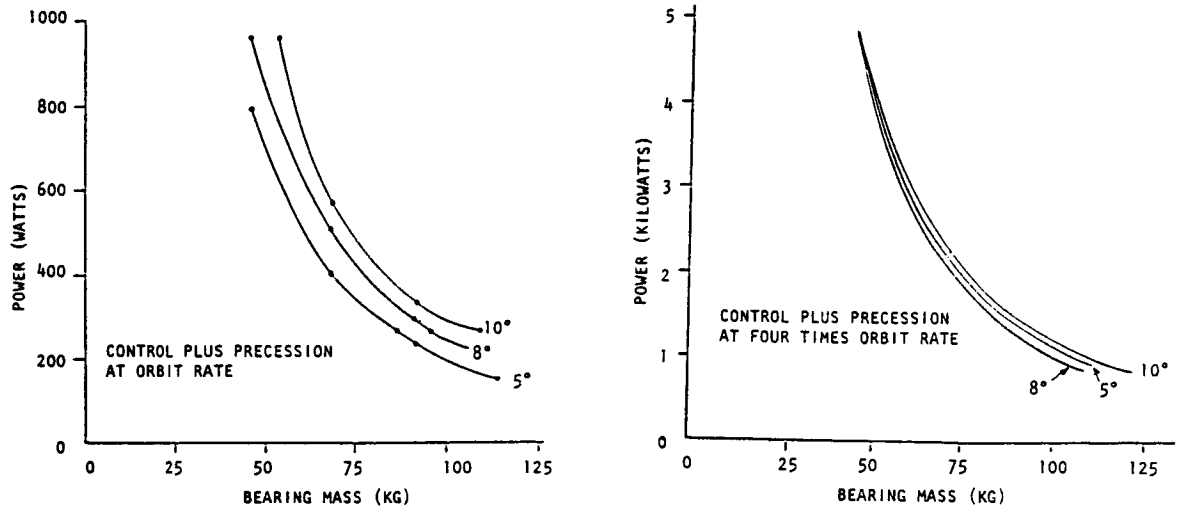

Figure 66.-Power vs. weight tradeoff for different Space Station attitude rates

angular travel and decreasing power consumption as shown in Appendix C. The results of the right-hand curve require some explanation. When precessing at four times orbit rate, the precession torque for high angular momentum wheels (that need only small bearing tilt angles) can exceed the control torque requirement, and thus become a major power/mass driver. In this case, there is a tradeoff between bearing mass penalties cause by attempts to reduce power consumption at fixed torque and those caused by the physically larger bearing resulting from increasing angular travel. This tradeoff shows that there is a minimum bearing mass configuration, which occurs with a bearing/rotor system designed for 8° of tilt. In order to show how bearing mass scales with bearing angle, figure 66 was replotted to yield figure 67.

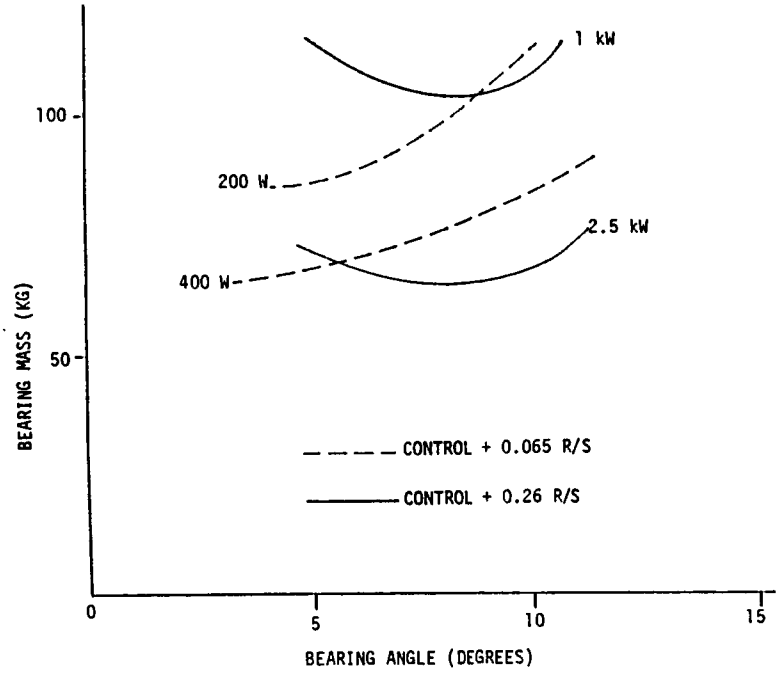

Figure 67.- Bearing mass vs. angular freedom trade

System Integration/Optimization

Bearing/Motor Integration.-There are several types of both motors and bearings, which were discussed in their respective appendices. The selection of an ironless PM motor and Lorengtz bearing was made partially based on the interaction between the motor and bearing. The most important interaction is the effect of motor side loading on bearing stiffness, power consumption, and bearing control bandwidth. The use of a conventional induction motor was ruled out based on these considerations. The conventional PM machine would have been acceptable from a bearing viewpoint, but was less efficient than the "ironless" machine. Another possibility which was investigated was to integrate the bearing and motor into a single subsystem. This, in theory, could be accomplished with either a PM or wound field and appropriate control coils, or with an induction machine driven so as to control side loading. Since the "ironless" motor is the least massive subsystem, little was seen to be gained

by the first approach. The use of a controlled induction machine would typically require more slip than would be desirable from an efficiency standpoint, although weight reductions would be possible. This is an area where technology advancements may make the concept attractive.

Rotor/Motor Integration.-As was discussed earlier, a rotor design for a minimum radius/maximum speed would result in the lightest motor. Thus, in finding the "optimum" described later in this section, the effect of speed on motor weight was included.

Depth of Discharge (DOD).-In this study, DOD was taken as 75%. Given the momentum transfer requirement and the emphasis on minimum system mass, this choice is appropriate. For other applications, or for a Space Station with different requirements, a different DOD may be appropriate. Qualitatively, the considerations affecting DOD are listed below. The advantage of higher DOD is:

- Minimum rotor mass which, given the charge/discharge characteristics of Space Station, would also reduce system mass

The potential advantages of lower DOD are:

- More momentum available at the "discharged" condition
- Smaller motor mass, which in a system with higher relative power levels would reduce system mass
- Greater charge/discharge cycle efficiency

Overall System Optimization.-To determine the optimum wheel momentum/speed operating point requires knowing:

- Basic system concept
- Bearing power vs. momentum
- Bearing weight vs. torque capability/power
- Bearing weight vs. "gimbal" angle
- Locus of maximum energy density for the rotor
- Other factors, including effect on rotor critical speeds, manufacturing, rotor radial growth, effect on motor weight
- Location of various constraint boundaries, since many "optimal" solutions are determined by constraints

The designs for the five- and six-wheel systems illustrate the importance of the last point above, given the basic system concept reviewed below. The design of the six-wheel system is driven almost entirely by the in-plane momentum transfer and FO requirements, as the bearings must use their freedom for both reconfiguration and momentum transfer. Since the designs for the five- and six-wheel systems have significantly different results, they will be described in separate sections that follow.

IPACS Overall System Concept.-The basic concept is to use a large-scale magnetic suspension as a limited 2-DOF gimbal. The reasons for baselining a system that does not use traditional 2-DOF gimbals are:

- Gimbal structure and torque motors add substantial mass.
- If unlimited gimbal travel were used, the problems of transferring power and heat in/out of the flywheel motor/generator and electronics would be significant.
- Volume swept by the tangential velocity vectors is limited by the "gimbal" travel, so the wheels could potentially be oriented such that even if a rotor fractured, containment may not be necessary.

Because of the limited "gimbal" travel, only a fraction of the total wheel angular momentum can be transferred along various Space Station axes. Flywheel angular momentum requirements are, therefore, inversely related to available magnetic bearing "gimbal" angle capability. Figures 68 and 69 relate the angular momentum to rotational speed and bearing angle, respectively. These figures are discussed further below.

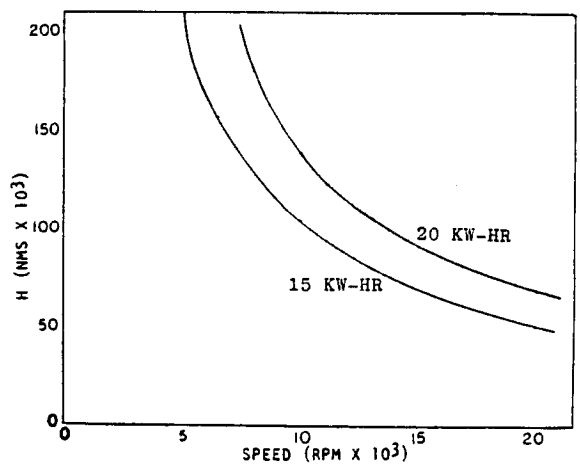

Figure 68.- Rotor angular momentum at full speed vs. maximum operating speed

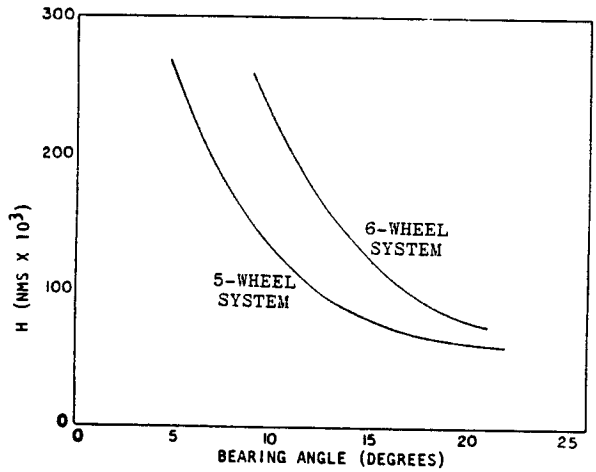

Figure 69.- Rotor angular momentum required to meet momentum transfer requirements vs. bearing tilt angle

Six-Wheel System.-The conceptual advantage of the six-wheel system over the five-wheel system is that it is possible to do both reconfiguration, after a wheel failure, and subsequent momentum transfer using only the angular freedom of the magnetic bearing. The reconfiguration step uses approximately 5.7° of bearing travel. The impact of using this 5.7° for reconfiguration is that it is a substantial reduction in the available travel and, therefore, drives the rotor design to one of much higher momentum (lower speed). Figure 68 shows the momentum versus wheel speed for two cases: 15 kWh (6-wheel), and 20 kWh (5-wheel). Figure 69 shows the momentum required versus angle capability of

the magnetic bearing. The actual magnetic bearing design is limited to about 15° of travel. Just to meet the momentum transfer requirement will require a wheel angular momentum of 120K Nms, which results in a wheel speed of 8500 rpm. The end result is a flywheel system that is slower (and heavier) than the "optimum," but still potentially higher than a system requiring crude gimbals for reconfiguration.

Five-Wheel System.-In the five-wheel system, reconfiguration after failure is accomplished by a crude gimbal system, leaving the entire bearing travel available for momentum transfer. In addition, because of the larger energy storage per wheel, each wheel has more angular momentum at a given speed than in the six-wheel case. For the five-wheel (failing to four) case, the equations for rotor geometry, bearing mass, and motor mass can be combined to plot total system mass versus speed. The results of these calculations are shown in figure 70. The IPACS component mass is broken down more accurately in Table 45, based on a system operating at 10,000 rpm. This value was chosen as a reasonable compromise between the high- and low-penalty design. The five-wheel system is selected as the baseline reference configuration for the purpose of this report, primarily because it has fewer wheels and because the smaller gimbal travel presents lower development risk.

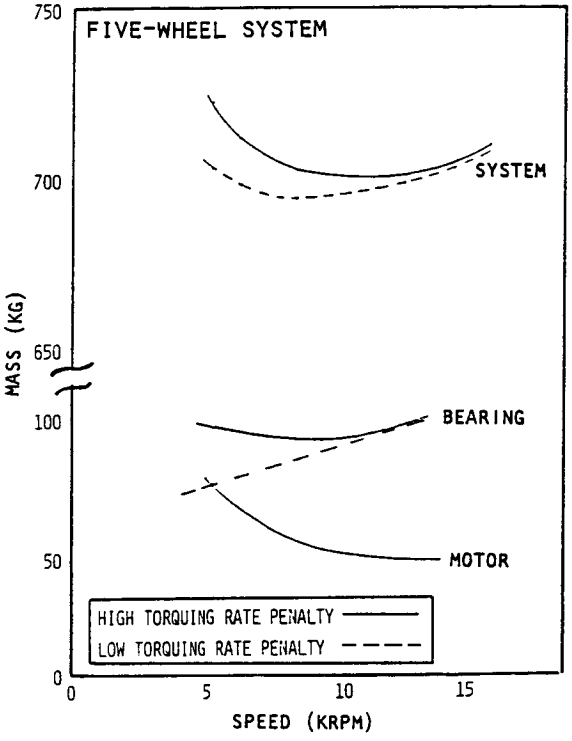

Figure 70.-Mass vs. maximum operating speed for different power penalties on rotor precession

For the particular IPACS component design reflected in Table 45, the rotor energy storage capacity is 18.5 kWh. The total energy storage capacity including the bearing and hub structure is 19.2 kWh. The usable capacity considering the 75% DOD is 14.4 kWh. At $\alpha = 0.8$, the height/radius ratio equals 1.0, which is reasonably consistent with the initial assumptions and trade studies. For $\alpha = 0.85$, the rotor mass would decrease by nearly 20 kg, but the height/radius ratio would increase to 1.3, causing a comparable increase in case weight. The energy density based on the usable energy and the total mass of the system is 18.3 Wh/kg (8.3 Wh/lb). It should be noted that this energy density value is derived on a very conservative basis and includes a 64% stress derating factor, 10^6 fatigue cycle derating, and a conservative estimate of the stress bearing capacity of the selected born-epoxy composite material. After a thorough examination of the performance data, it is concluded that system energy densities in the range of 22 to 33 Wh/kg are feasible using the technology that exists at this time. The use of new composite materials that are now becoming available (approximately 50% improved stress-bearing capacity) will permit the achievment of energy densities as high as 33 to 50 Wh/kg.

TABLE 45.-IPACS COMPONENT MASS SUMMARY
(FIVE-WHEEL SYSTEM)

Item	Mass (kg)
• Rotor	470
• Bearing	73
• Motor/generator	50
• Electronics	35
• Rotor Attachment	45
• Levitation Magnet (for ground test)	20
• Case	95
Total	788

Rotor Attachment.-It is necessary to design a structure that is intermediate between the rotor and the motor/bearing structure. The reasons for this include:

- Momentum requirements demand a large rotor radius, while weight considerations demand a small motor/bearing radius.
- The rotor and the motor/bearing materials have different stiffnesses, strengths, and thermal expansion coefficients.

There are many requirements associated with this intermediate structure, including:

- Stiffness sufficiently high to avoid, or at least minimize, structural resonances in radial, axial, and tipping directions.
- Low enough interfacial pressure to avoid overstressing the rotor.
- Providing stable interfaces to materials with significantly different thermal expansion coefficients and mechanical properties.
- Minimizing or eliminating changes in the position of the center of mass.
- Sufficient stiffness to effect momentum transfers at the required control bandwidth.

For the system described in the previous sections, some simple calculations will indicate the difficulty of meeting the requirements. First, for the resonant frequency to be above the frequency associated with rotor speed, the spring constant, k, must follow:

$$k > \omega^2 M$$

$$k > 430 \times 10^6 \text{ N/m}$$

where ω is the natural frequency and M is the rotor mass, for the 20-kWh wheel operating at 10,000 rpm. The interfacial stresses, especially at the rotor boundary, must operate safely below their fatigue limits. This implies a maximum force

$$F < \sigma_c A < \sigma_c (2\pi r_i h)$$

which, for the wheel described above and for a maximum stress times usable area of 70 MPa, yields

$$F < 7.0 \times 10^6 \text{ N}$$

which must be further reduced into effective force along each axis. The 70 MPa is an estimate based on a range of epoxy yield strengths (300-1000 MPa) and fractions of rotor area over which a good bond could be obtained (5%-20%). For the differences in radial growth expected, about 1.5 cm, it appears these constraints could be met, in theory. In practice, such a design would be extremely difficult. A structure such as the one shown in the next section might accomplish the attachment requirements. Whether or not it is necessary (or even desirable) to have a magnetically suspended wheel operate below critical speed, requires further study. Lastly, a boron/aluminum wheel could easily be designed to have critical rotor speeds above the operating speeds, but there would be a significant reduction (50%) in rotor energy density.

System Concept Definition

This section combines the results of the previous sections to present a picture of the overall component concept. This is accomplished by creating a drawing that represents one way that the subsystems could be arranged to form the overall system. This concept is shown in figure 71, and is representative of either a five-wheel (with the addition of a crude gimbal instead of the fixed base) or six-wheel system. The five-wheel configuration is the selected baseline system. Its rotor has a diameter of 1.15 m (3.77 ft), and a height of 0.573 m (1.88 ft). The maximum case diameter if 1.65 m. In this design, the motor and bearing would have to be assembled in segments to form a roughly cylindrical hub-like structure. The details of the attachment of the "spoke" structure to this hub and the rotor were not considered. The ground testing requirement would be met using an attractive-type magnetic suspension, which could be of small enough mass (less than 20 kg) that it would remain with the flywheel system permanently. The inner surface of the motor would provide bearing area for touchdown bearings. The touchdown bearings were not examined in detail and do represent a significant design challenge.

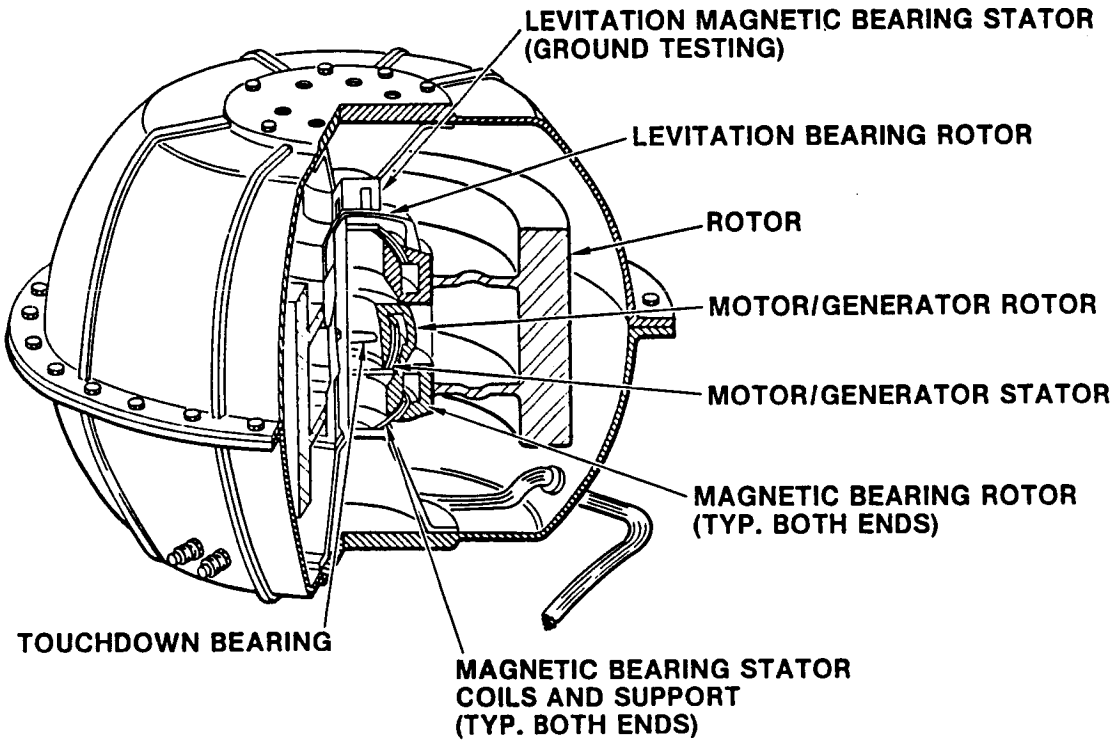

Figure 71.- Advanced IPACS unit design concept

This overall concept definition meets both the energy and momentum storage requirements of the Space Station, with an electrical storage efficiency of 85% and energy storage density of 18.3 Wh/kg (21 Wh/kg excluding case).

APPENDIX F

IPACS SIZING ALGORITHMS

by
Ronald E. Oglevie

The purpose of this appendix is to present IPACS sizing algorithms suitable for incorporation in the NASA LaRC Model Synthesis Program, which is used for mission/system tradeoff studies. These relationships provide estimates of the IPACS component mass and volume requirements, and are suitable for system-level trade studies. They are applicable to the baseline design concept presented in this report, and the Space Station type application. Caution should be employed in extending them to other applications.

The IPACS mass is given approximately by the expression

$$m = (K_E E + K_P P + K_T T)\, R \qquad \text{(F1)}$$

The first term reflects the mass of the items that scale as a function of rotor size. The second term includes the mass items that are associated with the motor/generator and electronics. The third term includes the additional mass of the magnetic bearing required for control torquing. The numerical values may be obtained from the following:

R = Redundancy factor (5/4 for the baseline system)

E = Deliverable energy storage required

P = Rated deliverable power

T = Maximum control torque required (300 N-m per unit for the baseline system

K_P = 4.53 kg/kW

K_T = 0.243 kg/N-m

K_E = 1/ED

ED = Energy density of the rotor and remaining mass items that scale as a function of rotor size

$$= (ED)_o \left(\frac{\sigma}{\sigma_o}\right)\left(\frac{\rho_o}{\rho}\right)\left(\frac{F_f}{F_{fo}}\right)\left(\frac{F_s}{F_{so}}\right) \qquad \text{(F2)}$$

$( )_o$ = Denotes value used in baseline system

σ = Rotor yield limit, σ_o = 1062 MPa

ρ = Rotor material density, ρ_o = 2020 kg/m^3

F_f = Fatigue stress derating factor, F_{fo} = 0.802

F_s = 1/Safety Factor, F_{so} = 0.64

$(ED)_o$ = 22.5 Wh/kg

The last two terms in equation (F1) are very sensitive to a number of design parameters and assumptions, and are not appropriate for scaling over large ranges, nor for designs or applications that are substantially different than the ones described in this report. To avoid this difficulty, the second and third terms of equation (F1) may be assumed to scale linearly with E, and be lumped into the first term, which is clearly the dominant term. The resulting equations are:

$$m = \left(\frac{R}{ED}\right) E \qquad \text{(F3)}$$

where ED is defined as before, equation (F2), but with $(ED)_o$ = 18.1 Wh/kg.

The above expressions and numerical values yield the desired sizing for IPACS mass. The simplified one [equation (F3)] is almost as accurate as equation (F1), and avoids potential errors in the latter two terms of (F1). The mass includes all hardware, including the rotor, bearing, motor/generator/electronics, levitation magnet, case, and mounting structure. It also includes the mass items necessary to perform the attitude control function (replace the control moment gyros).

These algorithms may be used for parametric studies by varying the different terms. Improved energy density through use of newer materials may be estimated by varying the σ, ρ, F_f and F_s factors. More optimistic performance can also be achieved by less conservative F_f and F_s factors. The stress design margins provided by these factors can realistically be reduced through the improved confidence provided by laboratory testing, and more experience working with the material. In addition, the $(ED)_o$ can be adjusted for different system assumptions using more fundamental data given in other appendices of this report.

The volume requirements for the baseline IPACS are given by

$$V = K_v E$$

where V = the rectangular volume containing the largest overall dimensions of the IPACS unit, and

K_v = 0.177 m^3/kWh of deliverable energy.

The above algorithms will provide IPACS sizing data that are valid for preliminary design trades, and for systems that are similar to the one developed herein for the Space Station. They contain the same levels of conservatism that are embodied throughout the report, and are felt to be representative of systems that are achievable with state-of-the-art engineering practices.

REFERENCES

1. Anderson, W. W.; and Keckler, C. R.: **An Integrated Power/Attitude Control System (IPACS) for Space Application.** Paper presented at the Fifth IFAC Symposium on Automatic Control in Space; Genoa, Italy; June 1973.

2. Cormack, A. III: **Three Axis Flywheel Energy and Control Systems.** North American Rockwell Corporation, Guidance and Control TN-73-G&C-8; 1973.

3. Will, R. W.; Keckler, C. R.; and Jacobs, K. L.: **Description and Simulation of an Integrated Power and Attitude Control System Concept for Space-Vehicle Application.** NASA TN D-7459, 1974.

4. Notti, J. E.; Cormack, A., III; and Schmill, W. C.: **Integrated Power/ Attitude Control System (IPACS) Study. Vol. I - Feasibility Studies.** NASA CR-2383, 1974.

5. Notti, J. E.; Cormack, A., III; Schmill, W. C.; and Klein, W. J.: **Integrated Power/Attitude Control System (IPACS) Study. Vol. 2 - Conceptual Designs.** NASA CR-2384, April 1974.

6. Keckler, C. R.; and Jacobs, K. L.: **A Spacecraft Integrated Power/ Attitude Control System.** Paper presented at the Ninth Intersociety Energy Conversion Engineering Conference; San Francisco, California; August 26-30, 1974.

7. Cormack, A., III; and Notti, J. E.: **Design Report for the Rotating Assembly for an Integrated Power/Attitude Control System.** NASA CR-172317, September 1974.

8. Cormack, A., III; and Ruiz, M. L.: **Energy-Momentum Unit Standardization Study.** North American Rockwell Corporation, Space Division; Guidance and Control TN-74-G&C-3, September 1974.

9. Cormack, A., III; and Murphy R. S.: **IPACS Electronics Improvements: IPACS Application to Extended Duration Orbiter and Space Base.** Rockwell International, Space Division; Guidance and Control TN-77-IPACS-1; 1977.

10. Kulkarni, S. V.: **Flywheel Rotor and Containment Technology Development Program of the U.S. Department of Energy.** Paper presented at the Third International Conference on Composite Materials; 1980.

11. Slifer, L. W. Jr.: **Initial Guidelines & Estimates For a Power System With Inertial (Flywheel) Energy Storage.** NASA, TM-82134, 1980.

12. Studer, P. A.; and Evans, H. E.: **In-Space Inertial Energy Storage Design.** ASME proceedings of the 16th Intersociety Energy Conversion Engineering Conference, Vol. 1, 1981, pp.74-79.

13. Jarvinen, P. O.: **Advanced Flywheel Storage System.** Paper presented at the Mechanical, Magnetic, and Underground Energy Storage, Annual Contractors Review. DOE/FT 20279-157, 1981.

14. Rodriguez, G. E.; Studer, P. A.; and Bour, D. A.: **Assessment of Flywheel Energy Storage For Spacecraft Power Systems.** NASA TM-85061, May 1983.

15. Keckler, C. R.; Rodriguez, G. E.; and Groom, N. J., eds.: **Integrated Flywheel Technology.** NASA CP-2290, December 1983.

16. Keckler, C. R.: **Integrated Power/Attitude Control System (IPACS).** Integrated Flywheel Technology 1983, NASA CP-2290, December 1983, PP. 5-23.

17. Keckler, C. R.; and Groom, N. J.: **Advanced Control and Power System (ACAPS) Technology Program.** Integrated Flywheel Technology 1983, NASA CP-2290, December 1983, pp.. 141-157.

18. Eisenhaure, D. B., Downer, J. R., Bliamptis, T., and Hendrie, S., **A Combined Attitude, Reference, and Energy Storage System For Satellite Applications,** C. S. Draper Laboratory, Report CSDL-P-1754 (1984).

19. Eisenhaure, D. B.; Downer, J. R.; Hockney, R. L.; and O'Dea, S. R.: **Multiple Function Utilization of Inertial Energy Storage Wheels in Spacecraft Application.** AIAA Paper 84-1837, 1984.

20. Gross, S.: **Study of Flywheel Energy Storage For Space Stations.** Boeing Aerospace Co. Report D180-29751-1, February 1984.

21. Keckler, C. R.; and Groom, N. J.: NAS9-16151, MOD 75: **Advances in Flywheel Energy Storage Systems.** Presented at the 1984 Power Sources Workshop; Los Angeles, California, May 8-9, 1984.

22. Keckler, C. R.; Bechtel, R. T.; and Groom, N. J., eds.: **An Assessment of Integrated Flywheel System Technology.** NASA CP-2346, December 1984.

23. Giudici, R. J.; **Comparative Energy Storage Assessment Item.** An Assessment of Integrated Flywheel System Technology, NASA CP-2346, December 1984, pp. 91-99.

24. Oglevie, R. E.; and Eisenhaure, D. B.: **Integrated Power & Attitude Control Systems For Space Station.** AIAA Paper 85-0358; January 16, 1985.

25. Anderson, W. W.; and Groom, N. J.: **The Annular Momentum Control Device (AMCD) and Potential Applications.** NASA TN D-7866, March 1975.

26. Ball Brothers Research Corporation: **Annular Momentum Control Device (AMCD),** Volumes I and II. NASA CR-144917, 1976.

27. Groom, N. J; and Terray, D. E.: **Evaluation of a Laboratory Test Model Annular Momentum Control Device.** NASA TP-1142, March 1978.

28. Groom, N. J.: **The Rim Inertial Measuring System (RIMS).** NASA TM-80100, August 1979.

29. Anderson, W. W.; Groom, N. J.; and Woolley, C. T.: **The Annular Suspension and Pointing System.** AIAA Journal of Guidance and Control, Volume 2, Number 5, pp. 367-373, September-October 1979.

30. Groom, N. J.: **Annular Momentum Control Device (AMCD). Integrated Flywheel Technology.** NASA CP-2290, 1983, pp. 123-132.

31. Groom, N. J.: **Description of A Laboratory Model Annular Momentum Control Device (AMCD). An Assessment of Integrated Flywheel System Technology.** NASA CP-2346, 1984, pp. 157-167.

32. Groom, N. J.: **Overview of Magnetic Bearing Control and Linearization Approaches For Annular Magnetically Suspended Devices.** An Assessment of Integrated Flywheel System Technology, NASA CP-2346, 1984, pp. 297-306.

33. Oglevie, R. E.: **Space Station Attitude Control - Challenges and Options.** AAS Paper 83-066, 5 February 1983.

34. Barrows, D.; Bedell, H.; Hahn, E. H.; Kaczynski, R.; and Levinthal, J.: **Momentum Management For the Space Platform.** AAS Paper 83-004, 30 January 1983.

35. O'Connor, B. J.; and Morine, L. A.: **A Description of the CMG and Its Application to Space Vehicle Control.** AIAA Paper No. 67-589; August 1967.

36. Auclair, G. F.; and Wells, R. C.: **Control Moment Gyro Selection and Design Criteria.** AIAA Paper No. 70-976, August 1970.

37. Oglevie, R. E.: **Attitude Stabilization and Control System Synthesis For Future Spacecraft.** North American Rockwell Space Division; Technical Note 73-G&C-5; August 1973.

38. Phillips, J. P.: **Control Moment Gyro Characteristics and Their Effects on Control System Performance.** AIAA Paper No. 68-875, August 1968.

39. Powell, B. K.; et al: **Synthesis of Double Gimbal Control Moment Gyro Systems for Spacecraft Attitude Control.** AIAA Paper No. 71-937, August 1971.

40. Ross, C. H.; and Worley, E.: **Optimized Momentum and Attitude Control System (MACS) for Skylab.** AIAA Paper No. 71-938, August 1971.

41. Kennel, H. F.: **Steering Law for Parallel Mounted Double-Gimbaled Control Moment Gyros - Revision A.** NASA TM-82390, January 1981.

42. Davis, L. P.: **Optimization of Control Moment Gyroscope Design.** Sperry Phoenix Co. Publication LJ-1252-0765, May 1967.

43. Chubb, C. H.; Kennel, H. F.; Rupp, C. C.; and Seltzer, S. M.: **Flight Performance of Skylab Attitude and Pointing Control System.** AIAA Paper No. 74-900, August 1974.

44. **Power Extension Package Solar Array.** LMSC-D665479, Final Report, September 1979.

45. Hoberecht, M. A.; et al: **Design Considerations for a 10-kw Integrated Hydrogen-Oxygen Regenerative Fuel Cell System.** Proceedings of the 19th Intersociety Energy Conversion Engineering Conference, 1984, pp. 240-246.

46. Miller, L.: **The Nickel-Hydrogen Battery System - an Historical Overview.** 16th Intersociety Energy Conversion Engineering Conference proceedings, 1981, pp. 220-223.

47. Ritterman, P. F.: **Characteristics of Nickel-Hydrogen Cells Under a Daily Energy Balance Low Altitude Orbit Cycling Regime.** 17th Intersociety of Energy Conversion Engineering Conference proceedings, 1982, pp. 765-768.

48. Levy, E. Jr.: **Life Engineering, and Acceptance/Qualification Test Data on Air Force Design Nickel Hydrogen Batteries.** 19th Intersociety Energy Conversion Engineering Conference proceedings, 1984, pp. 85-88.

49. Dunlop, J. D.; et al: **Status of Comsat/Intelsat Nickel-Hydrogen Battery Technology.** 15th Intersociety Energy Conversion Engineering Conference proceedings, 1980, pp 1878-1884.

50. Archer, J.; and Winters, W.: **Composite Structures for Space Systems.** TRW/DSSG/Quest, Spring 1980, pp. 43-65.

51. **Introduction to Metal Matrix Composites,** Tutorial Series. DoD Metal Matrix Composite Information Analysis Center (MMCIAC); Santa Barbara, CA; MMC No. 272; June 1982.

52. Clauser, H.: **Advanced Composite Materials.** Scientific American, Volume 229, No. 1, July 1973, pp. 36-44.

53. Kreider, K.: **Introduction to Metal-Matrix Composites.** Composite Materials, Vol. 4, Academic Press, New York, 1974.

54. Zweben, C.: **Advanced Composites - A Revolution for the Designer.** AIAA-81-0894, May 1981.

55. Irving, R.: **Metal Matrix Composites Pose a Big Challenge to Conventional Alloys.** Iron Age, 12 January 1983, pp. 35-39.

56. Riley, W.: **Future Trends in Metal Matrix Composites.** MMCIAC No. 000436, June 1983.

57. Schoutens, J.: **Particulate, Whisker, and Fiber-Reinforced Metals: A Comparison and Discussion.** Special Technical Report prepared for American Cyanamid Co., November 1981.

58. Hagen, D.; and Erdman, A.: **Flywheels for Energy Storage: A Review With Bibliography.** ASME Publication 76-DET-96, 1976.

59. Post, R.; and Post, S.: **Flywheels.** Scientific American, Volume 229, No. 6, December 1973, pp. 17-23.

60. Toland, R.: **Current Status of Composite Flywheel Development.** Lawrence Livermore Laboratory preprint UCRL-80604, 17 January 1984.

61. Chiao, T.; and Stone, R.: **Program for Composite Flywheels.** Proceedings of the 1975 Flywheel Technology Symposium, 10-12 November 1975, pp. 53-55.

62. Smith, P.; and Froes, F.: **Developments in Titanium Metal Matrix Composites.** Journal of Metals, March 1984, pp. 19-25.

63. Chamis, C.; and Lark, R.: **Non-Metallic Hybrid Composites: Analysis, Design, Application, and Fabrication.** Hybrid and Select Metal Matrix Composites; Chapter 2, AIAA publication, New York, 1977.

64. **Advanced Composites Design Guide,** First Edition DoD/NASA, July 1983.

65. Chamis, C.; and Kiraly, L.: **Rim-Spoke Composite Flywheels - Stress and Vibration Analysis.** NASA TN D-8339, November 1976.

66. Kulkarni, S.; et al: **Prototype Development of an Optimized Tapered-Thickness, Graphite/Epoxy Composite Flywheel.** Lawrence Livermore Laboratory, Report UCRL-52623, November 1978.

67. Reedy, E. Jr.: **A Composite-Rim Flywheel Design.** SAMPE Quarterly, pp. 1-6, April 1978.

68. Davis, D.; Csomor, A.; and Ginsburg, B.: **From Vehicles to Satellites: The Technology Revolution in High-Performance Wheels.** Paper presented at 1980 Flywheel Technology Conference, 26 October 1980.

69. Zachary, A. T.; and Ginsburg, B. R.: **Flywheel Power Module.** Paper presented at 17th IECEC, 8 August 1982.

70. Timoshenko, S.; and Goodier, J.: **Theory of Elasticity,** third edition; McGraw-Hill, New York, 1970.

71. Beer, F.; and Johnston, E. Jr.: **Mechanics for Engineers/Statics;** third edition; McGraw-Hill, New York, 1976.

72. Nassar, S. A.; and Unnewehr, L. E.: **Electromechanics and Electric Machines.** John Wiley & Sons, 1979.

73. Wood, P.: **Switching Power Converters.** Van Nostrand Reinhold Co., 1981, pp. 286-312.

74. Eisenhaure, D.; Stanton, W.; and Hockney, R.: **MOSFET-Based Power Converters for High-Speed Flywheels.** Proceedings of the 1980 Flywheel Technology Symposium, ASME, Vol I, pp. 380-391.

75. Hnatek, E. R.: **Design of Solid-State Power Supplies.** Van Nostrand Reinhold Co., 1981, pp. 226-227.

76. Alger, P. L.: **Induction Machines.** Gordon & Breach Science Publishers, 1970.

77. Beauchamp, E. D.; Hadfield, J. R.; and Wuertz, K. L.: **Advanced Single Permanent Magnet Axipolar Ironless Stator AC Motor for Electric Passenger Vehicles.** AiResearch Manufacturing Company, the Garrett Corporation, NASA CR-167974, August 1983.

78. Millner, A. R.: **High Efficiency Permanent Magnet Motor-Generator.** Proceedings of the International Workshop on Rare Earth-Cobalt Permanent Magnets and Their Applications, 3rd, June 27-30, 1978.

79. Roters, H. C.: **Electromagnetic Devices.** John Wiley & Sons, 1941.

80. **Magnetic Circuits and Transformers.** Members of the Staff of the Department of Electrical Engineering at MIT, John Wiley & Sons, 1958.

81. Downer, J. R.: **Design of Lorentz-force, Large-angle Magnetic Suspension Systems.** Ph.D. Dissertation, Massachusetts Institute of Technology, December 1985.

82. Basore, P. A.: **Passive Stabilization of Flywheel Magnetic Bearings.** Ph.D. Dissertation, Massachusetts Institute of Technology, February 1980.

83. Frazier, R.; Gilinson, P.; and Oberbeck, G.: **Magnetic and Electric Suspensions.** The MIT Press, 1974.

84. Eisenhaure, D.; Downer, J.; and Hockney, R.: **Factors Affecting the Control of a Magnetically Suspended Flywheel.** Proceedings of the 1980 Flywheel Technology Symposium, ASME, Vol I.

85. McCraig, M.: **Permanent Magnets in Theory and Practice.** John Wiley & Sons, 1977.

86. Eisenhaure, D.; Downer, J.; and Savarino, T.: **Technical and Economic Considerations in the Design of Low Loss Flywheel Electromagnetic Bearings.** R-1474, the Charles Stark Draper Laboratory, Cambridge, MA, June 1981.

87. Oberbeck, G.: **Energy Storage Components Used as Signal and Force Devices.** E-1565, Massachusetts Institute of Technology Instrumentation Laboratory (now the Charles Stark Draper Laboratory), Cambridge, MA, May 1964.

88. Eisenhaure, D.; Oberbeck, G.; and Downer, J.: **Development of a Low Loss Flywheel Magnetic Suspension System.** Proceedings of the 14th Intersociety Energy Conversion Engineering Conference, August 1979.

89. Downer, J.: **Analysis of a Single Axis Magnetic Suspension System.** S. M. Thesis, Massachusetts Institute of Technology, Mechanical Engineering Department, January 1980.

90. Woodsen, H.; and Melcher, J.: Electrical/Mechanical Dynamics, Part I, **Discrete Systems.** John Wiley & Sons, Inc., 1968.